MALT1 phosphorylation controls activation of T lymphocytes

Dissertation der Fakultät für Biologie

der Ludwig-Maximilians-Universität München

angefertigt am

Helmholtz Zentrum München

Deutsches Forschungszentrum für Gesundheit und Umwelt

Institut für Molekulare Toxikologie und Pharmakologie

Abteilung Zelluläre Signalintegration

vorgelegt von

Torben Gehring

München, den 25.09.2018

Table of content

List of figures

List of tables

1 Summary

Recognition of pathogens by antigen receptors expressed on T and B lymphocytes represents the initiating step in the adaptive immune response. Engagement of the T cell receptor (TCR) by specific antigens induces several signaling pathways culminating in T cell activation, differentiation and proliferation. Thereby, the CARD11-BCL10-MALT1 (CBM) complex bridges proximal TCR signaling to MALT1 protease activation and canonical NF-κB signaling. MALT1 exerts a dual function in the CBM complex upon TCR stimulation: MALT1 scaffold recruits the E3 ligase TRAF6 to the CBM complex resulting in activation of the canonical NF-κB pathway and JNK signaling. In addition, MALT1 has a proteolytic activity, which modulates T cell activation by cleaving several signaling and post-transcriptional regulators. To date, regulation of MALT1 function was shown to be mainly mediated by mono- or poly-ubiquitination. In this study, multiple novel phosphorylation sites in the C-terminus of MALT1 were identified upon T cell activation supporting the MALT1 scaffolding function.

In mass spectrometry experiments, three phosphorylated MALT1 peptides were identified, covering a total of five phosphorylated serine residues (MALT1B S559, S562, S645, S649 and S803). Generation of phospho-specific antibodies allowed detection of MALT1 phosphorylation in Jurkat T cells over a time course, revealing that MALT1 is transiently hyper-phosphorylated upon TCR stimulation. Rescue experiments of MALT1-deficient Jurkat and primary CD4 T cells with phospho-defective MALT1 variants showed for the first time that MALT1 phosphorylation augments IκBα degradation and NF-κB activation. In contrast, MALT1 protease activity was not altered by phospho-defective MALT1 mutants, indicating that C-terminal phosphorylation does not affect all MALT1 downstream functions, but is selectively required to channel CBM signaling to IκBα degradation and the canonical NF-κB pathway. In addition, it could be shown that MALT1 is prone to chronic phosphorylation in activated B cell-like diffuse large B cell lymphoma (ABC DLBCL) cell lines, indicating that constitutive CBM complex assembly, as a result of chronic BCR signaling or oncogenic CARD11 mutations, is sufficient to induce MALT1 phosphorylation. Furthermore, CK1α was identified as a MALT1 protein kinase catalyzing the phosphorylation on S562 as identified in *in vitro* kinase assays using a phospho-specific antibody. Indeed, CK1α could be shown to be essential for CBM assembly and NF-κB activation. In rescue experiments of CK1α-deficient Jurkat T cells, CK1α catalytic activity and CARD11 binding were not only required for its recruitment to CARD11, BCL10 and MALT1, but were also essential for the formation of the entire CBM complex. Additionally, constitutive NF-κB activation in Jurkat T cells expressing the oncogenic CARD11 L225LI variant, which resulted in constitutive CBM assembly, still relied on CK1α activity, indicating an additional, kinase-dependent function of CK1α downstream of the CBM assembly.

Collectively, identification of MALT1 phosphorylations after TCR signaling and in chronic activation has revealed a new level in the regulation of the CBM-mediated NF-κB pathway and potentially opens new avenues for therapeutic treatments of immune diseases or malignant lymphoma.

1 Zusammenfassung

Die Erkennung von Pathogenen durch Antigen-Rezeptoren auf T- und B-Lymphozyten stellt den ersten Schritt in der Aktivierung des adaptiven Immunsystems dar. Durch die Bindung spezifischer Antigene an den T-Zell Rezeptor (TZR) werden verschiedene Signalwege induziert, die zur Aktivierung, Differenzierung und Proliferation von T-Zellen führen. Dabei spielt der CARD11-BCL10-MALT1 (CBM) Proteinkomplex eine entscheidende Rolle und verbindet proximale TZR-Signale mit der MALT1 Proteaseaktivität und dem kanonischen NF-κB Signalweg. Eine zentrale Komponente des CBM Komplexes stellt MALT1 dar, welches sowohl als Gerüstprotein als auch als Protease fungiert und somit eine Doppelfunktion ausübt. Die Gerüstfunktion von MALT1 führt zur Rekrutierung der E3 Ligase TRAF6 und ermöglicht dadurch die Aktivierung des kanonischen NF-κB und des JNK Signalweges. Durch die proteolytische Aktivität werden verschiedene Signalmoleküle und post-transkriptionelle Regulatoren gespalten und somit die T-Zellantwort moduliert. Bisher konnte gezeigt werden, dass beide MALT1 Funktionen hauptsächlich durch Mono- und Poly-Ubiquitinierungen reguliert werden. In der vorliegenden Arbeit wurden neue Phosphorylierungsstellen in MALT1 identifiziert, die die Gerüstfunktion von MALT1 unterstützen.

In Massenspektrometrie-Experimenten konnten insgesamt fünf stimulationsabhängig phosphorylierte Serine identifiziert werden (MALT1B S559, S562, S645, S649 und S803). Durch die Herstellung phospho-spezifischer Antikörper konnten diese MALT1-Phosphorylierungen in Jurkat T-Zellen in einem zeitlichen Verlauf verfolgt werden. Zudem konnte mit Hilfe der Antikörper gezeigt werden, dass MALT1 nach T-Zell Aktivierung vorrübergehend hyper-phosphoryliert ist. Die Rekonstitution MALT1-defizienter Jurkat T-Zellen und primärer CD4 T-Zellen mit phospho-defekten MALT1-Mutanten zeigte zum ersten Mal, dass MALT1 Phosphorylierungen die Degradation von IκBα und die Aktivierung von NF-κB verstärken. Die MALT1 Proteasefunktion dagegen wurde nicht beeinträchtigt, was darauf hinweist, dass nicht alle nachgelagerten MALT1 Funktionen beeinflusst werden. Außerdem konnte gezeigt werden, dass MALT1 in Zelllinien des aktivierten B-Zell-Typ von diffus großzelligen B-Zell-Lymphomen chronisch phosphoryliert vorliegt. Diese Zelllinien weisen eine chronische Aktivierung des B-Zell Rezeptors oder onkogene CARD11 Mutationen auf, welche zu einer konstitutiven Bildung des CBM Komplexes führen. Somit konnte gezeigt werden, dass diese dauerhafte CBM Komplexbildung ausreichend ist, um MALT1 Phosphorylierungen zu induzieren. Weiterhin konnte gezeigt werden, dass CK1α die Phosphorylierung an MALT1B S562 *in vitro* katalysiert und somit eine Kinase für MALT1 darstellt. Zudem konnte bewiesen werden, dass CK1α für die Assemblierung des CBM Komplexes und die Aktivierung des NF-κB Signalweges essentiell ist. Die Rekonstitution CK1α-defizienter Jurkat T-Zellen zeigte, dass sowohl die katalytische Aktivität als auch die Bindung von CK1α an CARD11 für die CBM-Komplexbildung benötigt werden. Zusätzlich wird die konstitutive CBM Komplexbildung und chronische NF-κB-Aktivierung onkogen-aktiver CARD11 Varianten auch durch CK1α Aktivität gesteuert. Dies deutet auf eine zusätzliche Kinase-abhängige Funktion von CK1α unterhalb des CBM Komplexes hin.

Die Identifizierung von stimulationsabhängigen MALT1 Phosphorylierungen offenbart eine neue Regulierungsebene der CBM-vermittelten Aktivierung des NF-κB Signalweges und eröffnet neue potentielle Angriffspunkte zur Bekämpfung von Immunkrankheiten und bösartigen Lymphomen.

2 Introduction

The human body is continuously challenged by pathogenic organisms and thus, the integrity of the immune system determines whether these organisms invade the host and cause disease or are effectively opposed and eliminated. The immune system is composed of several cell types, which collectively work to rapidly detect and combat a variety of invading organisms. The immune system can be divided into two distinct parts: the innate and the adaptive immune system. If the immune system is deregulated, disorders of the immune system, such as autoimmune diseases, inflammation and cancer, can result.

2.1 Innate Immunity

The innate component of the immune system is the first line of defense against pathogens and is highly conserved. The innate immune system responds rapidly, but unspecifically, to pathogenic insult [1]. The cellular compartment comprises so-called phagocytes, such as macrophages, neutrophils and dendritic cells. Phagocytes engulf pathogens, a process termed phagocytosis. The intracellular degradation of pathogens takes place in lysosomes or endosomes that contain specific enzymes, acids or toxic oxygen metabolites, such as hydrogen peroxide or hydroxyl radicals. The recognition of pathogens by phagocytes occurs via cell surface pattern-recognition receptors (PRRs), such as Toll-like receptors (TLR), Scavenger receptors or C-type lectin receptors. These receptors recognize specific structures termed pathogen-associated molecular patterns (PAMPs), which are components of microbes but not of host cells. PAMPs are conserved structures of bacterial surfaces constituents, including lipopolysaccharide (LPS), lipotechoic acid, mannose or DNA as well as RNA [2-4]. Phagocytes process the engulfed pathogens by intracellular degradation into small peptide fragments and then display those peptides, bound to major histocompatibility complex class II (MHC class II), on their cell surface. Thereby, T cells can recognize and interact with presented peptides leading to their activation and differentiation (see Section 2.2.2).

The ingestion and degradation of pathogens by phagocytes is increased 100-fold if the particle/pathogen is first opsonized with specific antibodies or complement. The complement system is the second major component of the innate immune system. It consists of at least 20 serum glycoproteins and is activated in cascades with numerous amplification steps. There are three major pathways of complement activation, which are all driven by different foreign substances: the classical, the alternative, and the mannose-binding lectin pathways. All three pathways converge with the activation of the central component molecule C3 and a common final pathway leading to pathogen lysis through forming transmembrane pores (C5 - C9), opsonisation of microbes through C3b and the recruitment and activation of other immune cells (C5b) [1, 3]. As well as being directed to sites of infection by complement proteins, innate immune cells can also be guided to these sites by cytokines and chemokines. These signaling molecules can be secreted by all immune cells and act in an autocrine, paracrine or endocrine manner. Cytokines and chemokines mediate intracellular signaling events in immune cells by binding to specific surface receptors found on all

leucocytes that affect cell activation, division, apoptosis or movement. On the one hand, cytokines induce the local upregulation of specific adhesion molecules in the vascular endothelium, thereby increasing the potency of homing of immune cells. And on the other hand, they establish a chemical gradient and induce the migration of cells along it [1, 5, 6]. Furthermore, the composition of secreted cytokines can drive the adaptive immune response appropriate to the type of infection by supporting activation and inducing differentiation in different cell subtypes, such as T_H1, T_H2, T_H17 and regulatory T (T_{reg}) cells.

2.2 Adaptive Immunity

In addition to responding to and eliminating pathogens directly, the innate response is also crucial for the activation of the adaptive immune response. The adaptive immune response is the second part of the immune system in higher animals. In contrast to the innate response, the adaptive immune system acts in a highly specific manner that also generates long-lasting protection against pathogens. The cellular compartment of the adaptive immune response comprises B and T lymphocytes. To recognize specific antigens, T and B cells express on their cell surface T cell receptors (TCR) and B cell receptors (BCR), respectively. Because of the broad range of foreign antigens, their specificity needs to be highly diverse. Therefore, T and B lymphocytes evolved a unique genetic mechanism that enables the generation of an almost unlimited number of antigen-binding sites. This is achieved by the formation of respective sites by variable regions of both the light and the heavy chain of antibodies. Furthermore, variable regions undergo somatic recombination of different gene regions before they are transcribed. This leads to the potential formation of more than 10^{12} different antibody molecules [7-9]. Recognition of a pathogen through the binding of pathogenic antigens to antigen-receptor (AgR) induces cell activation and differentiation in specialized lymphoid tissues, and triggers specific effector responses associated with the two branches of the adaptive immune response: the humoral immune response and the cell-mediated immune response. Cell-mediated immunity is defined through the local effects of T cells, which directly eliminate infected host cells and support innate immune cells in eliminating invaded pathogens. In contrast, the main cellular component of the humoral immune response are B cells, which secrete antibodies that then bind to extracellular pathogens and their toxins and aid in their recognition and removal [1, 10].

2.2.1 B lymphocytes

B lymphocytes are activated by soluble and cell-bound antigens, and thereby differentiate into antibody-secreting cells. Secreted antibodies help in the neutralization of pathogens, the induction of phagocytosis and the activation of the complement system (See section 2.1) [1, 7]. B cells develop from hematopoietic stem cells (HSC) in the bone marrow (BM). Their development in the BM comprises different stages such as pro- and pre-B cell. In these phases, the sequential rearrangement of the BCR segments occurs. To complete the development process, immature B cells undergo selection for self-tolerance and then migrate from the BM into the peripheral lymphoid organs, where they mature and

differentiate into follicular (FO) or marginal zone (MZ) B lymphocytes [11]. Both are able to secrete several types of immunoglobulin and they mostly remain in secondary lymphoid organs, such as the spleen and lymph nodes. FO B cells constitute the main fraction of B lymphocytes and generate the majority of high-affinity antibodies during an infection. They require T cell-dependent activation in order to acquire full functionality. MZ B cells are mainly found in the marginal zone of the spleen and constitute the first line of defense against blood-borne pathogens, in a predominantly T cell-independent manner [8, 11]. A minor fraction of the MZ B lymphocytes expand and differentiate into plasma cells or long-lived memory cells. These cells often return to the BM. As a consequence of reinfection with known pathogens, antigen presenting cells (APCs) such as macrophages or dendritic cells and also T cells are able to activate these plasma cells to produce specific antibodies [12-14].

In addition, the B cell compartment comprises the distinct B1 B cell population. B1 B lymphocytes arise from B1 progenitors in the fetal liver and persist as a self-renewing population. They are predominantly found in the peritoneal cavity [15, 16] and play an important role in the early T cell-independent immune response to most pathogens invading the gut epithelium. B cell receptors of B1 B lymphocytes show a higher poly-specificity because of the usage of variable gene segments lacking N-region additions [17]. Furthermore, B1 B cells are the main source of natural IgM in serum [18, 19].

2.2.2 T lymphocytes

T lymphocytes define cell-mediated adaptive immunity. They directly induce the death of phagocytes that have engulfed pathogens as well as infected host cells [7, 20], but also act more indirectly to support the immune cells of the innate immune system in eliminating invaded pathogens [21]. Furthermore, T cells can secrete cytokines that support to shape adaptive immune response by promoting differentiation of T cells and activation of B cells.

Foreign antigens are detected via the TCR (see Section 1.2), which consists of an extracellular N-terminal domain, followed by a transmembrane segment and a very short cytoplasmic tail. In addition, CD3 molecules associate with to the C-terminal domain of the TCR via hydrophobic interactions, and possess cytoplasmic ends that contain one or several immunoreceptor tyrosine-based activation motifs (ITAMs). The TCR-CD3 complex can only detect foreign antigens that are presented by major histocompatibility complex (MHC) receptors, which are expressed on APCs [22, 23]. There are two classes of MHCs known: MHC class I and class II. They are divided based on the presentation of intracellular (class I) or extracellular (class II) proteins. Both MHC classes can present self-peptides as well as foreign peptides [24].

There are two major subpopulations of T lymphocytes known: the CD4 or T helper (T_H) and the CD8 or cytotoxic T cells. CD4 and CD8 molecules are co-receptors that assist the TCR and they differ in their selectivity in binding to MHC classes. While CD8 T cells recognize peptides presented by MHC class I receptors, which are present on the surface of all nucleated cells, CD4 T cells are selective for MHC class II-bound antigens. Typically, these

MHC class II-presenting cells belong to the compartment of dendritic cells, macrophages and B cells (see Section 1.1) [23, 24]. Binding of CD4 T cells to these MHC class II molecules leads to T cell activation and differentiation as well as rapid proliferation (Figure 2-1). Activated CD4 T cells then secrete cytokines that facilitate different types of immune responses including activation of B cells or macrophages. In contrast, CD8 T cells are involved in the killing of cells infected with intracellular pathogens like viruses or cytoplasmic bacteria. Healthy nucleated cells mainly present self-peptides on their MHC class I molecules, but pathogen-specific peptides are presented and are recognized by CD8 T cells following infection. This leads to the secretion of perforin and granzymes that induce apoptosis in the pathogen-infected cell [21].

2.3 TCR/CD28 co-engagement triggers T cell activation

TCR engagement by an antigen bound to the MHC elicits several cascades of intracellular events that are critical for T cell activation (Figure 2-1). The recognition of an antigen triggers conformational changes in the cytoplasmic portion of the CD4 or CD8 co-receptors. This leads to the activation of the associated protein tyrosine kinase Lck, which in turn phosphorylates the CD3 ITAMs and results in the recruitment of ZAP-70 (zeta-associated protein-70) via its SH2 domains. ZAP-70 specifically binds to phosphor-tyrosine residues on the ITAMs [25, 26]. This binding in turn triggers the phosphorylation and activation of ZAP-70 by Lck (lymphocyte-specific protein tyrosine kinase) which again phosphorylates the adaptor proteins LAT (linker for the activation of T cells) and SLP-76 (SH2 containing leukocyte phosphoprotein of 76 kDa) that nucleate the assembly of a multiprotein complex [27-29]. Through phosphorylation of LAT and SLP-76, several SH2 domain-bearing proteins like PLCγ1 (phospho lipase Cγ1), Grb2 (growth factor receptor-bound protein 2) and Gads (Grb2-related adapter downstream of Shc) are recruited and activate several downstream proteins [30]. A key event in the initiation of distal signaling is the activation of PLCγ1. Activated PLCγ1 hydrolyzes membrane-bound PIP$_2$ (phosphatidylinositol-4, 5-bisphosphate) into the two essential second messenger IP$_3$ (inositol-3-phosphate) and DAG (diacylglycerol). Thereby, PLCγ1 mediates the induction of several signaling pathways that collectively result in cytokine production, differentiation, proliferation and survival of T lymphocytes. Several signaling pathways are activated after TCR engagement, such as the ERK (extracellular signal-regulated kinase) - AP1 (activator protein-1), the Calcineurin-NFAT (nuclear factor of activated T cells), the JNK (c-Jun N-terminal kinase) as well as the NF-κB (nuclear factor kappa B) signaling pathways (Figure 2-1).

Formation of IP$_3$ and DAG in turn trigger the activation of Ca^{2+}-dependent Calcineurin-NFAT signaling pathway via IP$_3$ as well as other major signaling pathways, including RasGRP1 (Ras guanyl nucleotide-releasing protein 1)-, PKCθ (protein kinase C θ)- and PDK1 (phosphoinositide-dependent kinase 1)-mediated pathways via DAG (Figure 2-1) [31, 32]. IP$_3$ binds to its receptor on the endoplasmic reticulum and triggers the release of intracellular calcium into the cytosol. Ca^{2+} directly activates the protein phosphatase Calcineurin, which dephosphorylates NFAT leading to its translocation into the nucleus. NFAT, together with the

transcription factor AP-1 (Jun/Fos), binds to specific DNA response elements and induces the expression of genes involved in T cell activation [33]. AP-1 is, in turn, activated by the RasGRP1-ERK1/2 as well as the JNK-mediated pathways. While RasGRPF1 is directly activated by DAG, JNK activation is triggered by CBM complex formation and further downstream events (Figure 2-1). However, exclusive activation of the Ca^{2+}-Calcineurin-NFAT pathway leads to T cell anergy, which is a state where cells remain inactive following TCR engagement instead of becoming activated [34, 35].
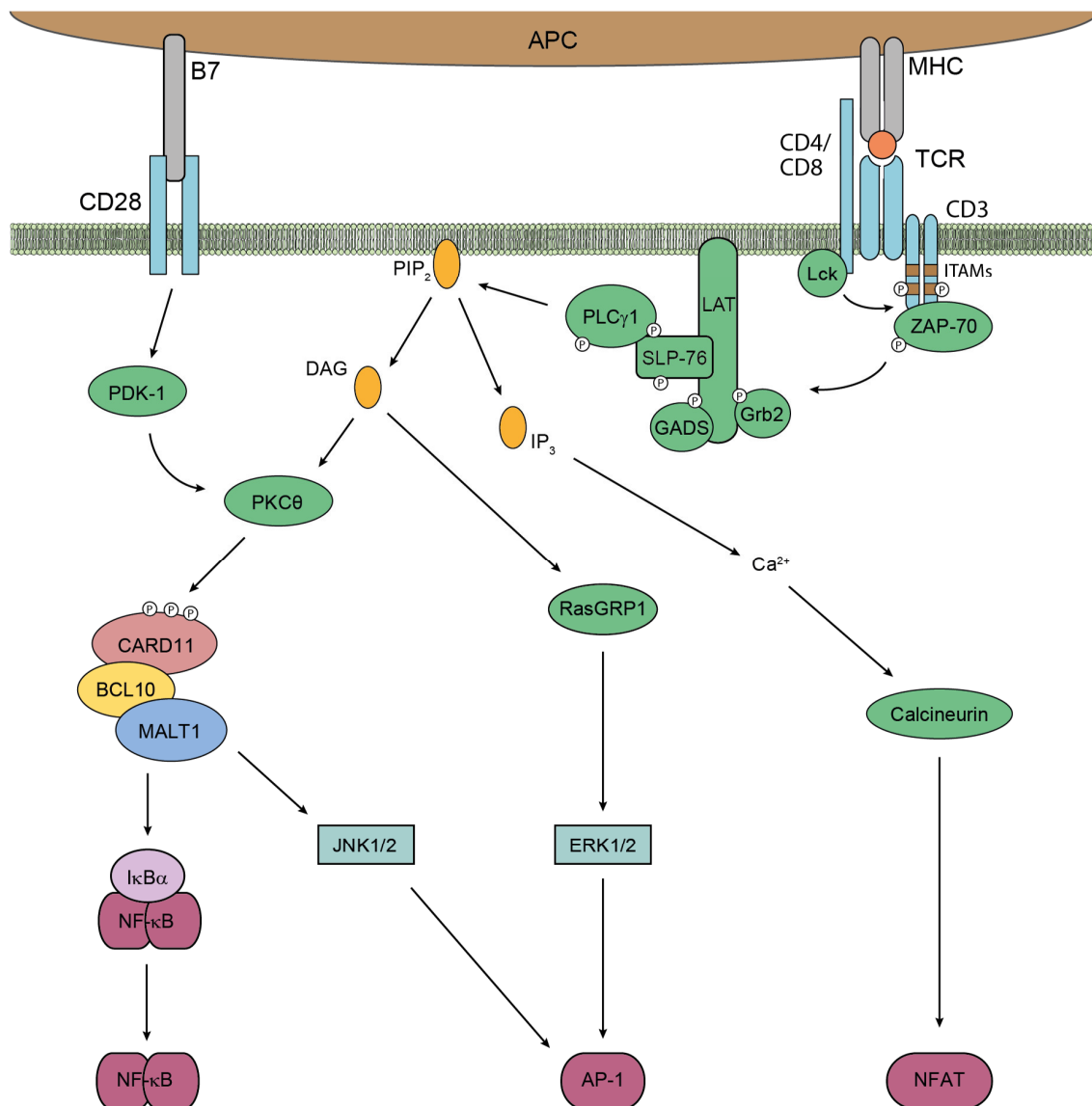
Figure 2-1: Proximal T cell receptor signaling. Activation of the TCR and its co-receptors CD4/CD8 and CD28 leads to a cascade of intracellular events resulting in activation of several transcription factors. Upon activation, Lck phosphorylates the CD3 ITAMs leading to the recruitment of ZAP-70, which in turn initiates the formation of a multi-protein complex by phosphorylation of LAT and SLP-76. This leads to the activation of PLCγ1, which hydrolyzes PIP_2 into IP_3 and DAG. This allows the initiation of the Calcineurin-NFAT, the ERK1/2-AP-1, the JNK and the NF-κB pathways.

DAG-mediated activation of PKCθ leads to the initiation of the NF-κB pathway. In addition, APCs express the surface protein B7, which binds to the co-receptor CD28 expressed by T lymphocytes and results in the activation of PDK1. In turn, PDK1 binds to and phosphorylates PKCθ supporting its DAG-mediated initiation [36]. Activated PKCθ phosphorylates the adaptor protein CARD11, which recruits BCL10/MALT1 heterodimers leading to the formation of the high molecular weight CBM complex, consisting of CARD11, BCL10 and MALT1 (Figure 2-1) [37, 38]. The CBM complex in turn serves as an essential regulator in bridging proximal antigen-receptor signaling events to downstream IKK (inhibitor of κB kinase)/NF-κB signaling. Recruitment of the IKK and the TAB (TAK1 binding protein)/TAK1 (transforming growth factor beta activated kinase) complexes to the CBM complex leads to the degradation of the regulatory protein IKKγ, also known as NF-κB essential modifier (NEMO), and the activation of the catalytic subunits IKKα and IKKβ. These in turn phosphorylate the protein IκBα (inhibitor of κBα) leading to its proteasomal degradation and the release of cytosolic NF-κB dimers that are then free to migrate into the nucleus and regulate gene expression [39-41].

The entire NF-κB family is ubiquitously expressed and comprises five proteins: p65 (RelA), RelB, c-Rel, p105/p50 (NF-κB1) and p100/p52 (NF-κB2). The NF-κB transcription factors bind as dimers to their DNA binding sequences, which are called κB sites. This leads to positive as well as negative regulatory effects on target gene expression. Prior to stimulation, NF-κB proteins associate in the cytoplasm and form homo- and heterodimeric complexes in various compositions [42-44]. Specific functions and differently preferred consensus κB sites have been discovered for individual NF-κB subunits and thereby the different combinations of NF-κB proteins form an immense, complex variety of possible responses [45, 46]. The activity of those dimers is tightly controlled by inhibitory IκB proteins that sequester NF-κB dimers in the cytosol and need to be degraded for release.

2.4 The CARD11/CARMA1-BCL10-MALT1 signalosome

Antigen binding to the T cell receptor and concurrent co-receptor ligation initiates receptor clustering and reorganization of signaling components at the cell-cell contact site between an APC and a T lymphocyte, forming the immunological synapse [47]. In this context, the CARD11/CARMA1-BCL10-MALT1 signalosome forms an essential molecular link between the activation of TCR signaling and subsequent IKK/NF-κB activation. The complex consists of CARD11 (also known as CARMA1), BCL10 and MALT1 (Figure 2-2). Whereas BCL10 and MALT1 constitutively form heterodimers, recruitment to CARD11 and thus the immunological synapse is induced upon TCR stimulation. Thereby, proximal TCR signaling events are bridged by CBM assembly to distal NF-κB activation.

2.4.1 CARD11 – the linker protein

Caspase recruitment domain-containing protein 11 (CARD11) is also known as CARD-containing membrane-associated guanylate kinase protein 1 (CARMA1). It belongs to the family of MAGUK (membrane associated guanylate kinase) proteins together with CARD9, CARD10 and CARD14. They all display high homology in sequence and structure, but differ in their expression pattern [48]. CARD11 expression is largely restricted to lymphoid tissues [49, 50]. The protein is ~ 130 kDa in size and contains an N-terminal CARD domain followed by a coiled-coil (CC) and a linker region and encodes at the C-terminus MAGUK domain, which consists of a PDZ (PSD-95, Dlg and ZO-1), an SH3 (Src homology 3) and a catalytically inactive GUK (guanylate kinase) domain (Figure 2-2) [51].
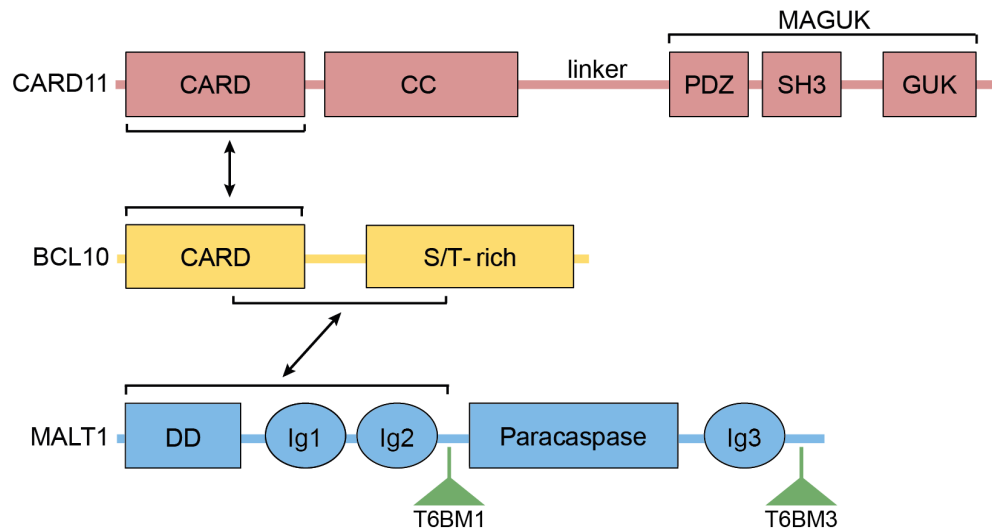
Figure 2-2: Scheme of CARD11, BCL10 and MALT1. Domains of the CBM proteins are depicted and interaction sites are highlighted. MALT1 contains two functional TRAF6 binding sites (T6BM), which are also highlighted.

CARD domains are important protein-protein interaction sites that are critical in the formation of signaling complexes in a variety of signaling pathways, including cell death and antigen stimulation [52]. Within the CBM complex, the CARD domain constitutes the recruitment site for the adapter protein BCL10 via heterotypic CARD-CARD interactions. The adjacent CC and linker regions are required for CARD11 oligomerization and activation [37, 38, 53]. In resting cells, the linker interacts with the CARD and the CC domain and represses CARD11 activation by maintaining it in a closed, inactive conformation [54]. Multiple phosphorylation sites are located in the CARD11 linker region, which are critical for the induction of conformational changes that convert it to an open form, which is able to oligomerize and recruit BCL10/MALT1 heterodimers [55]. The C-terminal MAGUK domain of CARD11 is essential for its membrane association, which is required for its interaction with PKCθ at the immunological synapse [56, 57]. In addition to the linker region, intra- and/or intermolecular interactions between the SH3 and the GUK domains also participate in maintaining CARD11 in its inactive conformation, as well as being necessary for CBM complex assembly and membrane localization [58].

2.4.2 BCL10 – the adaptor protein

Whereas CARD11 serves as a seed for CBM complex formation, BCL10 is an essential adaptor protein mediating the proximity of CARD11 and MALT1. This ~ 27 kDa protein consists of an N-terminal CARD domain and an adjacent serine/threonine (Ser/Thr)-rich region (Figure 2-2). While the CARD domains of BCL10 and CARD11 interact only upon stimulation, BCL10 constitutively binds to MALT1. This constitutive binding requires adjacent residues in addition to the CARD domain [40, 55, 59, 60]. The Ser/Thr-rich region of BCL10 is not essential for MALT1 association but appears to be important for stabilization [60, 61]. Thus, BCL10 is a critical bridging protein in the CBM complex.

Upon stimulation, CARD11 nucleates BCL10 CARD filament formation leading to subsequent NF-κB activation. The architecture of this assembly has been uncovered by cryo-electron microscopy, which shows helical filaments with a left-handed symmetry and three to four BCL10 subunits per helical turn [55, 62, 63]. The heterotypic CARD-CARD interaction between CARD11 and BCL10 could only be detected on the tip of these filaments, indicating the seed function of CARD11. The positively charged CARD11 surface is thought to recruit negatively charged BCL10 monomers. In turn, CARD11-bound BCL10 monomers expose their basic CARD surface and can again recruit other monomers via its negative surface. This leads to unidirectional elongation of BCL10 filaments, where the speed of extension appears to be unaffected by CARD11 [55, 62-64]. Furthermore, a star-shaped network of BCL10 filaments suggests that multiple filaments can be nucleated by one CARD11 molecule. In these assemblies, three types of homotypic CARD-CARD interactions (Types I, II, and III) were reported, and point mutations at these interfaces inhibit BCL10 filament formation [62, 63]. Type III interactions facilitate the charge-charge intra-strand contact between BCL10 CARD-CARD domains, whereas type I and II interfaces are essential for inter-strand contacts between proteins next to each other [62, 63]. MALT1 constitutively binds to the Ser/Thr-rich region of BCL10, decorating the BCL10 filaments and pointing towards the outside of the filaments.

2.4.3 MALT1 – the scaffold protein

MALT1 (mucosa associated lymphoid tissue lymphoma translocation protein 1) is the third main member of the CBM complex. The ~ 92 kDa MALT1 protein comprises an N-terminal death domain (DD), followed by two immunoglobulin-like (Ig) domains (Ig1 and Ig2) and a paracaspase (caspase-like) domain. At the very C-terminus, a third Ig (Ig3) domain is located (Figure 2-2). Binding of MALT1 to BCL10 was suggested to occur via the N-terminal Ig1 and Ig2, while the DD stabilizes the recruitment [59, 65]. Recently, the helical structure of the BCL10-MALT1 filament could be solved using cryo-electron microscopy (cryo-EM), adding new insights in the association of BCL10 to MALT1 [63]. This study could confirm reported architecture of BCL10 filaments (see 2.4.2), but also identified the direct interface between BCL10 and MALT1. Contrary to what was previous believed, MALT1 DD directly interacts with BCL10 at the rim of the CARD core filament in a 1:1 stoichiometry [63]. Thus, MALT1 decorates the reported BCL10 filaments and its C-terminus points toward the outside

of the filaments and thereby seems to be accessible for further mediator and post-translational modifications [62, 63].

MALT1 exists in two alternative spliced variants, known as isoform A (MALT1A) and isoform B (MALT1B) [66]. They differ in the inclusion of exon 7 (MALT1A), which encodes for 11 amino acids (aa) and contains a potential binding motif for the E3 ligase TRAF6 (tumor necrosis factor associated reporter-associated factor 6) (T6BM1). In addition to T6BM1, two further putative binding sites are located in the C-terminal region of MALT1 (T6BM2 and T6BM3) [39, 66, 67]. Mutational studies have revealed that T6BM1 and T6BM3 essentially contribute to TCR-triggered recruitment of TRAF6 and NF-κB activation [66].

Furthermore, MALT1 has proteolytic activity via its paracaspase domain that is activated upon antigen stimulation [68, 69]. MALT1 belongs to the family of vertebrate paracaspases (PCASP) and its protease domain dimerizes to form a catalytic dyad between cysteine 464 (C464) and histidine 415 (H415) in the active conformation, similar to classical caspases [70-73]. In contrast to caspases, MALT1 cleavage relies on an arginine (Arg) in its P1 site [74]. A two-step activation model was proposed involving conformational changes in the C-terminal Ig3 domain: First, MALT1 dimerizes, but is retained in an inactive state by Ig3-mediated auto-inhibition. Second, binding of substrates to MALT1 induces structural changes that hinder auto-inhibition and lead to full activation [72]. The mono-ubiquitination of MALT1B at lysine 633 (K633), which is located in the Ig3 domain, plays an essential role in induction of its catalytic activity [75]. In line, interference of conformational changes by using small molecule inhibitors, which bind at the interface between the paracaspase and the Ig3 domain, or blocking the dimerization of MALT1 by mutating glutamate 549 (E549), lead to the abrogation of catalytic activity [63, 76]. However, the exact mechanism and players for the regulation of Ig3 rearrangements and modifications are still unclear and need to be further investigated.

2.5 Regulation of the CBM by post-translational modifications

2.5.1 Induction of CBM assembly by CARD11 phosphorylation

The assembly and disassembly of the CBM complex is regulated by several post-translational modifications, such as phosphorylation or ubiquitination. The assembly of the CBM complex is mainly controlled by CARD11 phosphorylation. Several kinases have been identified, which phosphorylate CARD11 within the CARD-CC or linker region. The most prominent kinase is PKCθ, which is activated downstream of the TCR. In addition, activation of PDK1 by the co-receptor CD28 leads to phosphorylation and activation of PKCθ and further supports CARD11 phosphorylation by recruiting it to the membrane [77, 78]. The major phosphorylation sites of PKCθ at CARD11 are S552, S637 and S645 (Figure 2-3) [38]. Whereas phosphorylation at S552 and S645 impair the intra-molecular association of the linker region and the CARD-CC domain leading to CARD11 activation, phosphorylation of S637 is delayed and seems to contribute to a negative feedback mechanism that diminishes downstream signaling [79]. In this way, PKCθ phosphorylation can exert both positive and

negative effects on CARD11 activity (Figure 2-3). Identification of PP2A (protein phosphatase 2A), which antagonizes the phosphorylation at S645 and thereby counterbalances TCR activation, suggests that this site is important for IKK/NF-κB activation (Figure 2-3) [80]. In addition to PKCθ, the activity of the downstream kinase IKKβ is also required for full CARD11 activation [61, 81]. IKKβ phosphorylates CARD11 in the linker at S555 and induces conformational rearrangements (Figure 2-3) [81]. Furthermore, CaMKII (calmodulin-dependent protein kinase II) can phosphorylate CARD11 in the CARD domain at S109, suggesting that modifications within the linker as well as the CARD-CC region are required for full activation (Figure 2-3) [82]. A number of other kinases and phosphorylation sites are also reported to mediate CARD11 regulation.

For example, HPK1 (hematopoietic progenitor kinase 1) and AKT have been shown to phosphorylate CARD11 at several sites, which partially overlap with some previously described phosphorylation events [83, 84]. Additionally, CK1α (Casein kinase 1α) has been shown to exert a dual function on CARD11: first, by promoting and then terminating TCR-induced NF-κB activation [85]. It has been shown that direct CK1α binding to the CBM complex is required for activation of downstream signaling. Furthermore, an inhibitory phosphorylation of CARD11 at S608 was reported to impair the ability of CARD11 to activate NF-κB (Figure 2-3) [85].

2.5.2 Regulation of BCL10 by phosphorylation and ubiquitination

As well as CARD11, the adapter protein BCL10 is highly phosphorylated upon TCR stimulation, which was initially proposed to promote NF-κB signaling [86, 87]. CaMKII associates not only with CARD11 after stimulation but also with BCL10 and phosphorylates threonine 91 (T91) in its CARD domain (Figure 2-3) [88]. Despite the fact that phospho-defective or -mimetic mutations do not appear to interfere with CARD association, the role of this phosphorylation event still needs to be elucidated. In addition, glycogen synthase kinase 3β (GSK3β)-mediated phosphorylation of BCL10 has been shown to foster NF-κB signaling, but the exact phosphorylation sites still need to be mapped [89]. Several other papers have demonstrated that phosphorylation of BCL10 primarily induces negative feedback mechanisms to terminate T cell activation. Similar to CaMKII, IKKβ binds to CARD11 and BCL10. It can phosphorylate BCL10 at multiple serines (S134, S136, S138, S141 and S144) in the C-terminus that counteract NF-κB activation (Figure 2-3). Phospho-defective mutants lead to increased NF-κB DNA binding and enhanced IL-2 production [61]. Phosphorylation of S138, which in addition to IKKβ also can be mediated by CaMKII, primarily inhibits NF-κB activation (Figure 2-3) [90, 91]. These reported C-terminal phosphorylations are suggested to lead to structural changes of the C-terminus auf BCL10 and thereby impair its association to MALT1, which in turn terminates CBM assembly [61].
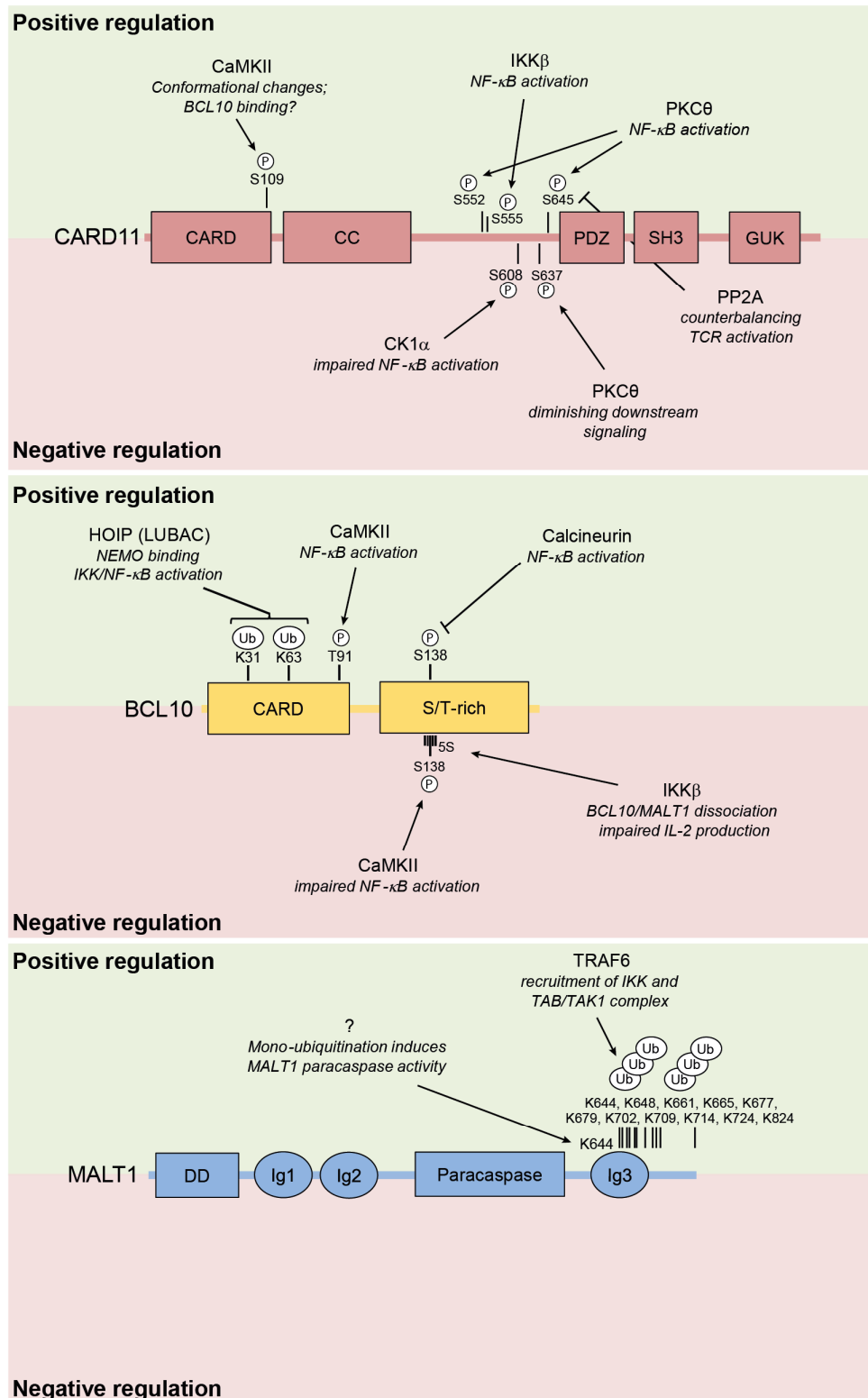
Figure 2-3: Summary of post-translational modifications, which participate in the regulation of CBM complex formation and termination. The modified sites are highlighted and corresponding kinases and phosphatases are named.

Furthermore, phosphorylation at S138 was reported to enhance BCL10 turnover by a proteasome-independent mechanism [92], although other studies did not confirm effects on BCL10 stability [93, 94]. Another indication, that BCL10 phosphorylation negatively regulates NF-κB activation, is suggested by the impact of the phosphatase Calcineurin [94, 95]. Knockdown of Calcineurin, or its inhibition by cyclosporine A, increases IKKβ- or CaMKII-mediated phosphorylation of Ser138 and leads to reduced IKK/NF-κB signaling, indicating a counterbalancing effect of BCL10 phosphorylation (Figure 2-3) [94, 95] .

Upon TCR stimulation, BCL10 undergoes K63-linked poly-ubiquitination promoting an efficient recruitment of the regulatory IKK subunit IKKγ/NEMO to BCL10 [41]. In addition, the formation of Met1-linked ubiquitination chains on K31 and K63 of BCL10, by the linear ubiquitin chain assembly complex (LUBAC), was suggested to support the mentioned IKKγ/NEMO association (Figure 2-3) [96]. However, K63-linked poly-ubiquitination of BCL10 also leads to p62/Sequestosome-1-dependent autophagy and subsequent BCL10 degradation [97, 98]. The HECT-type E3 ligases NEDD4 (neural precursor cell expressed developmentally down-regulated protein 4) and ITCH (Itchy homolog) could be shown to promote BCL10 ubiquitination and its degradation via endocytic vesicles rather than proteasomal degradation [98]. Thus, BCL10 ubiquitination is supporting IKK/NF-κB activation, but also results in BCL10 degradation, which is required for post-inductive termination of CBM complex signaling.

2.5.3 MALT1 has dual function in TCR-triggered NF-κB activation

MALT1 exerts a dual function in the CBM complex upon TCR stimulation. It promotes T cell activation via both its scaffold and protease functions.

As a scaffold, MALT1 contains several lysine residues that can function as acceptor sites for poly-ubiquitination in its C-terminus (Figure 2-3) [40]. Through TRAF6 binding sites in MALT1, TRAF6 is recruited to the CBM complex leading to the oligomerization and activation of TRAF6. Subsequently, TRAF6 mediates K63-linked poly-ubiquitination of MALT1, resulting in the recruitment of the IKK complex via the poly-ubiquitin binding motif of IKKγ/NEMO (Figure 2-4) [40, 41, 66]. IKKγ/NEMO itself is in turn also K63-linked poly-ubiquitnated by TRAF6 after recruitment to the CBM complex, supporting association of further signaling proteins [39, 99]. In parallel, TAK1 associates with BCL10, MALT1 and IKKγ/NEMO via the ubiquitin-binding domains of its adapter proteins TAB2 and TAB3 (Figure 2-4) [39, 40, 100]. As a consequence, TAK1 induces the phosphorylation of the catalytic subunit IKKβ on Ser177 and S181 resulting in its activation [101]. Activated IKKβ in turn phosphorylates IκBα on S32 and S36 and thereby induces the recruitment of the Cullin1/βTrCP1 complex. Thus, phosphorylated IκBα is K48-linked poly-ubiquitinated leading to its proteasomal degradation and the release of bound NF-κB dimers, which can then migrate into the nucleus and activate transcription of target genes (Figure 2-4) [43, 102, 103]. Upon TCR stimulation, the CBM complex also mediates the activation of JNK signaling. Besides IKK activation, TAK1 also serves as a kinase that activates the MAP

(mitogen-activated-protein) kinase pathway resulting in the activation of JNK (Figure 2-4) [104-106]. Collectively, these data show that the scaffolding function of MALT1 coordinate TRAF6 recruitment and activation as well as subsequently the binding and activation of the kinases TAK1 and IKK resulting in JNK and NF-κB activation.
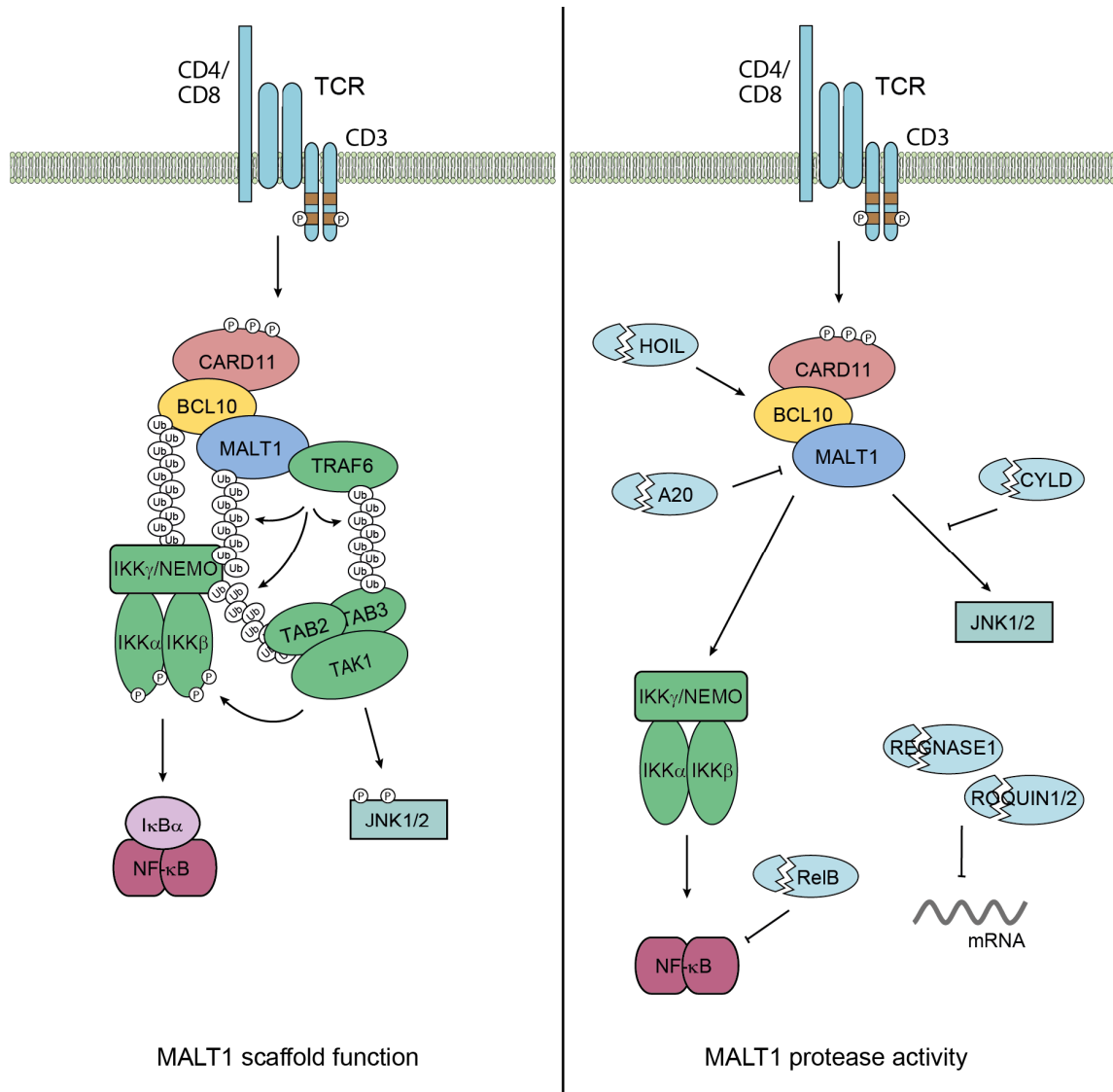
Figure 2-4: MALT1 exerts a dual function upon TCR signaling. MALT1 can act as a scaffold by recruiting TRAF6 to the CBM complex resulting in its K63-linked poly-ubiquitination. Thereby, the IKK and the TAB/TAK1 complex can associate with the CBM complex and lead to JNK and NF-κB activation. Furthermore, MALT1 has a protease activity, which is dispensable for IKK activation but can modulate NF-κB activation and T cell differentiation.

Besides its scaffolding activity, MALT1 also has protease activity. It has been demonstrated that the protease activity of MALT1 is dispensable for IKK activation, but modulates NF-κB activation by cleavage of negative regulators. Furthermore, MALT1 protease activity was shown to be required for T cell differentiation (Figure 2-4) [107-109]. MALT1 paracaspase

mutant (PM) mice show severe defects in T cell proliferation, IL-2 secretion and T_H17 differentiation, indicating the crucial role of MALT1 proteolytic activity [107-109]. Interestingly, these mice were protected from autoimmunity in a murine EAE and a T cell-induced colitis model, but developed spontaneous autoimmunity in multiple other organs, which was proposed to be caused by obvious defects in regulatory T (T_{reg}) cell differentiation and function. A defective T_{reg} compartment is not able to counterbalance immune activation by MALT1 scaffolding function [107-109]. Although development to thymic T_{reg} cells is totally impaired in MALT1 PM mice, there is still a small number of peripheral cells, but these T_{reg} cells are suggested to be disturbed in their counterbalancing function [107-109]. In line with published MALT1-deficient mice, MALT1 paracaspase mutant mice also exhibit compromised development of B1 and marginal zone (MZ) B cells. In addition, MALT1-deficient mice were shown to have a complete loss of T_{reg} cells in the thymus and in the periphery [110, 111].

Several MALT1 cleavage substrates that play a role in modulating NF-κB activation have been identified to date (Figure 2-4). The cleavage of mediators like A20, CYLD or RelB can augment activation. A20 and CYLD remove poly-ubiquitin chains from MALT1 or other mediator, which are required for efficient IKK complex recruitment [68, 112]. In addition, cleaved RelB is no longer able to compete with RelA or c-Rel for promotor binding and thereby exercises its inactivating function [113]. The discovery of Regnase-1 (also MCPIP1) as well as Roquin-1 and Roquin-2 as MALT1 cleavage substrates revealed an unexpected role for MALT1 in the regulation of post-transcriptional gene expression. All three proteins are involved in the processing of mRNAs and lead to the destabilization of a set of pro-inflammatory transcripts including IL-6, c-Rel, IRF4 or ICOS [114, 115]. The cleavage of HOIL1 by MALT1 was reported to represent a negative feedback mechanism that downregulates NF-κB activation at later stages of the T cell response. Cleaved HOIL1 can no longer catalyze the Met1-linked poly-ubiquitination of BCL10, which supports the recruitment of IKK/TAK1 to the CBM complex [116-118]. Thus, TCR-induced MALT1 protease activity plays an important role in modulating T cell activation and immune responses.

2.5.4 CK1α promotes CBM complex formation and NF-κB activation

Upon physiological conditions, CARD11 is strongly phosphorylated, inducing conformational changes to recruit BCL10/MALT1 heterodimers to CARD11 upon antigen receptor stimulation. Several kinases are reported to catalyze CARD11 phosphorylation (see 2.5.1) promoting its conformational rearrangements.

Among other kinases such as PKCθ, CK1α was shown to dynamically associate with the CBM complex upon TCR engagement [85]. It could be shown that CK1α directly binds to the coiled-coil and the linker region in CARD11 and catalyzes the phosphorylation on S608, which is supposed to inactivate CARD11 and thereby impair NF-κB activation [85]. However, knockdown experiments of CK1α in Jurkat T cells revealed strongly reduced IκBα phosphorylation/degradation and thus impaired NF-κB activation upon TCR stimulation [85].

Introducing CK1α CARD11-binding mutants (Y292A and D293A) to rescue CK1α knockdown, showed that CK1α strongly requires association to CARD11 and the CBM complex to exert its promoting effects [85]. Collectively, CK1α was suggested to have a dual function by first promoting IKK/NF-κB activation and in later phases terminate induction by inactivating phosphorylation of CARD11 on S608 (Figure 2-5). However, the impact level of CK1α inducing IKK/NF-κB could not be elucidated, yet.
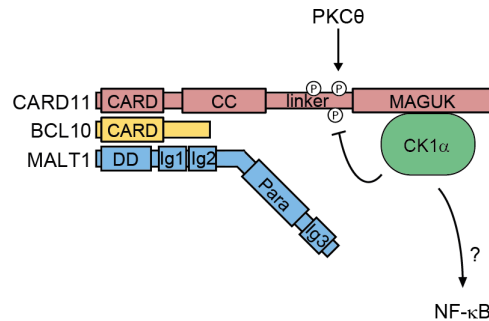
Figure 2-5: Model of the regulation of CBM signaling as suggested by Bidère et al., 2009 [85]. First, CK1α is suggested to promote NF-κB activation. In later phases, CK1α also terminates induction by inactivating phosphorylation of CARD11 on S608 [85].

In general, CK1α belongs to the casein kinase 1 (CK1) family, which encompasses the seven isoforms α, β, γ1, γ2, γ3, δ and ε in mammalian. Except for CK1β, all are expressed in humans showing high conservation within their kinase domain, but significant differences in regulatory non-catalytic C-terminal domains [119, 120]. CK1α represents the smallest isoform with a molecular weight of 32 kDa. Typical of a member of the superfamily of serine/threonine-specific kinases, CK1α has a bi-lobal structure including a small N-terminal lobe and a larger C-terminal lobe, which are connected by a hinge region forming the catalytic cleft for substrate and ATP binding [121-123]. CK1α is ubiquitously expressed and is constitutively active, indicating that recruitment is an important step for substrate phosphorylation. Protein kinase activity was suggested to be dependent on auto-phosphorylation of C-terminal residues [120, 124]. Furthermore, the C-terminal part contains specific phosphate moiety binding motifs that are required for substrate binding, but are also suggested to be involved in CK1α regulatory interactions [122, 123]. CK1α mainly recognizes substrates containing acidic or phosphorylated amino acid residues resulting in a canonical and a non-canonical consensus motif [121]. The canonical sequence is represented by pS/pT-x-x-S/T-x, whereas the site is primed by prior phosphorylation of a serine or a threonine. However, CK1α does not rely on a priming phosphorylation, but the phosphorylated serine/threonine can also be replaced by negatively charged acidic amino acids constituting the non-canonical motif (E/D-x-x-S/T-x) [121, 125, 126].

Best known and studied is the role of CK1α in the Wnt pathway. Wnt/β-catenin-mediated signaling plays an important role in cell proliferation and thus, mutations in the Wnt pathway have been found in several cancers [121]. In absence of Wnt ligand, CK1α associates with Axin and phosphorylates Axin, APC (adenomatous polyposis coli) and β-catenin. Notably,

CK1α phosphorylates APC on multiple residues only in a hierarchical manner following initial priming phosphorylation of APC by GSK3β. In turn, CK1α primes β-catenin for further phosphorylation by GSK3β and subsequent degradation exposing a closely regulated positive crosstalk between different post-translational modifications [121, 127, 128]. Binding of Wnt ligand to its receptor Frizzled leads to the inhibition of GSK3β and the disassembly of the destruction complex resulting in the prevention of β-catenin from phosphorylation and degradation. Thereby, accumulated β-catenin can translocate into the nucleus and activate the expression of TCF/LEF (T cell factor/lymphoid enhancing factor) [128-130].

2.6 Deregulation of CBM signaling is linked to B cell lymphoma

The CBM complex and the NF-κB pathway do not only function as a critical signaling pathway in lymphocyte activation, but can also participate in the development of lymphoid malignancies. Given the necessity of a functional BCR at many stages of pre- or mature B cell differentiation, it is not surprising that deregulation in the signaling components connecting proximal BCR events to downstream signaling pathways, especially NF-κB, contributes to the development of many lymphoid malignancies [131]. The effects of chronic BCR signaling were heavily investigated in diffuse large B cell lymphoma (DLBCL).

DLBCL represents the most common type of non-Hodgkin lymphoma, which can be divided into two major types based upon gene expression profiling: germinal center B cell-like (GCB) and activated B cell-like (ABC) DLBCL. While the GCB cell expression profile is similar to that of B cells in the germinal center and is associated with a more favorable prognosis, ABC cells resemble activated B cells, rely on the constant activation of the NF-κB pathway, and are associated with a much less favorable prognosis [132]. BCR-ligation through self-antigens, or the presence of an oncogenic mutation in the adaptor proteins CD79A/B, as well as gain-of-function mutations in CARD11, have been shown to cause addiction of ABC DLBCL cells to NF-κB signaling [133-135]. Pharmaceutical inhibition of upstream signaling by the Bruton's tyrosine kinase (BTK) inhibitor Ibrutinib resulted in complete abrogation of cell growth and apoptosis of ABC DLBCL cells that rely on proximal BCR signaling [135]. However, further downstream mutations have been shown to cause complete resistance of ABC DLBCL cells toward Ibrutinib treatment. Nevertheless, these cells are still sensitive to knockdown or knockout of essential members of this pathway (e.g. CARD11, MALT1 and IKK), resulting in cell apoptosis [136, 137]. In ABC DLBCL cells, the CBM complex is persistently assembled leading to constitutive poly-ubiquitination of MALT1 and subsequent IKK activation [55, 136]. Besides its scaffolding function within the CBM complex, MALT1 protease activity is also constitutively enhanced In ABC DLBCL cells and absolutely required for survival [138]. Inhibition of MALT1 protease activity by the small molecule inhibitor Mepazine enhances Ibrutinib's effects on BCR-dependent ABC DLBCLs and in addition, reduces survival of cells expressing oncogenic CARD11[139]. Collectively, the effects of oncogenic CARD11 are much more severe compared to the activation of NF-κB by expressing constitutively active IKKβ, suggesting that CARD11 may channel to other pathways besides NF-κB [131, 140, 141].

Under physiological conditions, CK1α was shown to associate with the CBM assembly and promote NF-κB activation upon TCR stimulation. In line, in ABC DLBCL cells, increased binding of CK1α to the CBM and especially heavily ubiquitinated MALT1 could be detected [85]. Conditional expression of oncogenic CARD11 L225LI in mice also resulted in constitutive association of CK1α with the CBM complex and subsequent B cell activation and proliferation [142]. Furthermore, knockdown experiments of CK1α in ABC DLBCL revealed that CK1α is essentially required for survival [85]. Recently, CK1α was also shown to bridge the association of β-catenin and its destruction complex to oncogenic CARD11 independently of BCL10/MALT1 recruitment in ABC DLBCLs, leading to the stabilization of β-catenin [143]. Upon stimulation, similar effects could be observed in CARD11 WT cells, indicating a common mechanism. Thus, association of CARD11 and CK1α is not only mono-directional to NF-κB activation, but feeds two distinct signaling pathways leading to cooperated induction of several target genes [143].

2.7 Aims of the study

Recognition of pathogens by antigen receptors expressed on T and B lymphocytes represents the initial step in mounting an adaptive immune response. The CBM complex serves as an essential step bridging TCR proximal signaling to MALT1 protease activation, canonical IKK/NF-κB signaling and JNK activation. Thus, the assembly and disassembly of this high molecular complex is tightly regulated by post-translational modifications such as phosphorylation and ubiquitination events.

Many studies have addressed the regulation of CARD11 and BCL10 by phosphorylation and ubiquitination, leading to the induction or termination of CBM complex assembly. Furthermore, the structural basis for the interactions of CARD11-BCL10 or BCL10-BCL10, which result in BCL10 filament formation, has been extensively elucidated. In this study, MALT1 phosphorylation, and how it participates in CBM regulation and signal transduction, was explored.

To date, MALT1 ubiquitination has been the focus of many studies, but phosphorylation has been mostly neglected. Several C-terminal acceptor sites for poly-ubiquitination could be identified in MALT1 regulating its scaffolding function by mediating recruitment of multiple downstream signaling members. However, the accumulation of several protein kinases to the CBM multiprotein complex strongly suggests that MALT1 is also prone to regulatory phosphorylation. The aims of this study were to identify potential stimulation-dependent MALT1 phosphorylation sites using mass spectrometry, and to investigate their functions in the regulation of MALT1 activity, CBM assembly and IKK/NF-κB signaling. Therefore, custom-made phospho-specific antibodies were generated against identified sites and used to monitor the kinetics of MALT1 phosphorylation in Jurkat T cells after stimulation. To obtain a better insight into the biological function of detected MALT1 phosphorylation, rescue experiments of MALT1-deficient Jurkat T cells and primary CD4 T cells with phospho-defective mutants were performed. Moreover, several studies could show that constant BCR signaling in ABC DLBCL cells leads to a strong ubiquitination and a constitutive activation of MALT1 and subsequent induction of IKK/NF-κB. Therefore, we further wanted to explore in this work to what extent the identified MALT1 phosphorylation emerged in these lymphoid malignancies. Furthermore, CK1α could be identified to phosphorylate MALT1 at least on one detected phosphorylation site. To gain further insight into the functions of CK1α in MALT1 phosphorylation and the IKK/NF-κB pathway, CK1α-deficient Jurkat T cells were generated and additionally, rescue experiments with several CK1α mutants were performed.

3 Results

MALT1 is heavily modified in the C-terminus upon T cell stimulation. So far, multiple potential ubiquitination sites have been identified that control MALT1 function. However, no other post-translational modifications, including phosphorylation, have been detected or functionally analyzed, to date. In an attempt to discover phosphorylation sites contributing to the regulation of MALT1 function, mass spectrometry experiments were performed.

3.1 MALT1 is essential for IKK/NF-κB activation

To generate a clean system that allows for analysis of the MALT1 functions in TCR-mediated IKK/NF-κB signaling, MALT1-deficient Jurkat T cell were generated. Utilizing the CRISPR/Cas9 system, two single-guide RNAs (sgRNAs) flanking both sites of MALT1 exon 2 were introduced into Jurkat T cells. This led to double strand breaks in intronic regions and thus a deletion of exon 2 using the NHEJ mechanism of the cells (Figure 3-1A) [66].
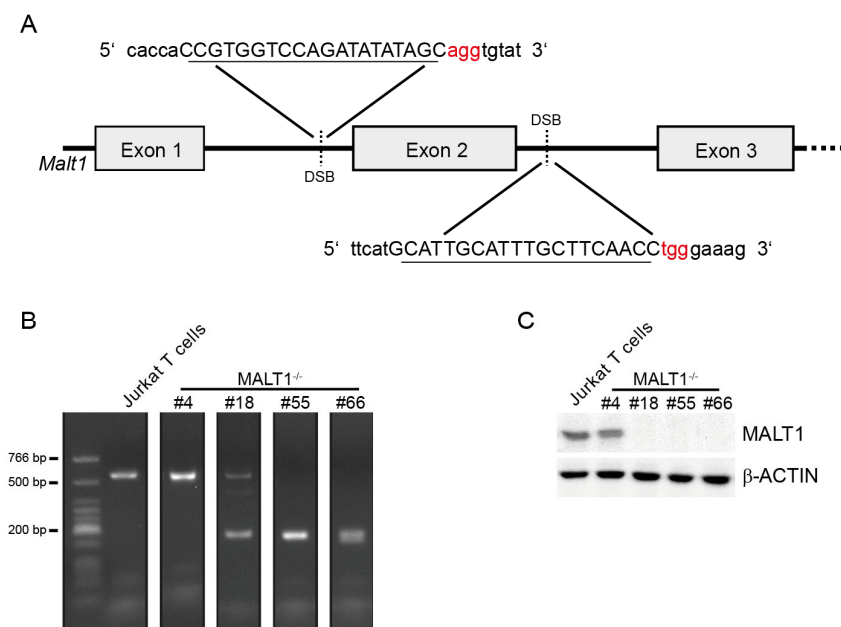
Figure 3-1: Generation of MALT1 KO Jurkat T cells. A) Schematic of the MALT1 genomic locus. Exon 2 of MALT1 was targeted using the CRISPR/Cas9 system with two sgRNAs flanking exon 2. Sequences are depicted and adjacent PAM sites are highlighted in red. B, C) Efficient knockout of MALT1 was verified by genomic PCR (B) and Western blotting (C).

The successful deletion of exon 2 was first monitored via PCR of genomic DNA showing a shorter fragment at the expected size of deletion (Figure 3-1B). Verifying these results by Western Blot analysis allowed the identification of several MALT1-deficient cell clones (Figure 3-1C). Interestingly, heterozygous genomic deletion of exon 3 in clone #18 also led to a loss of protein expression.
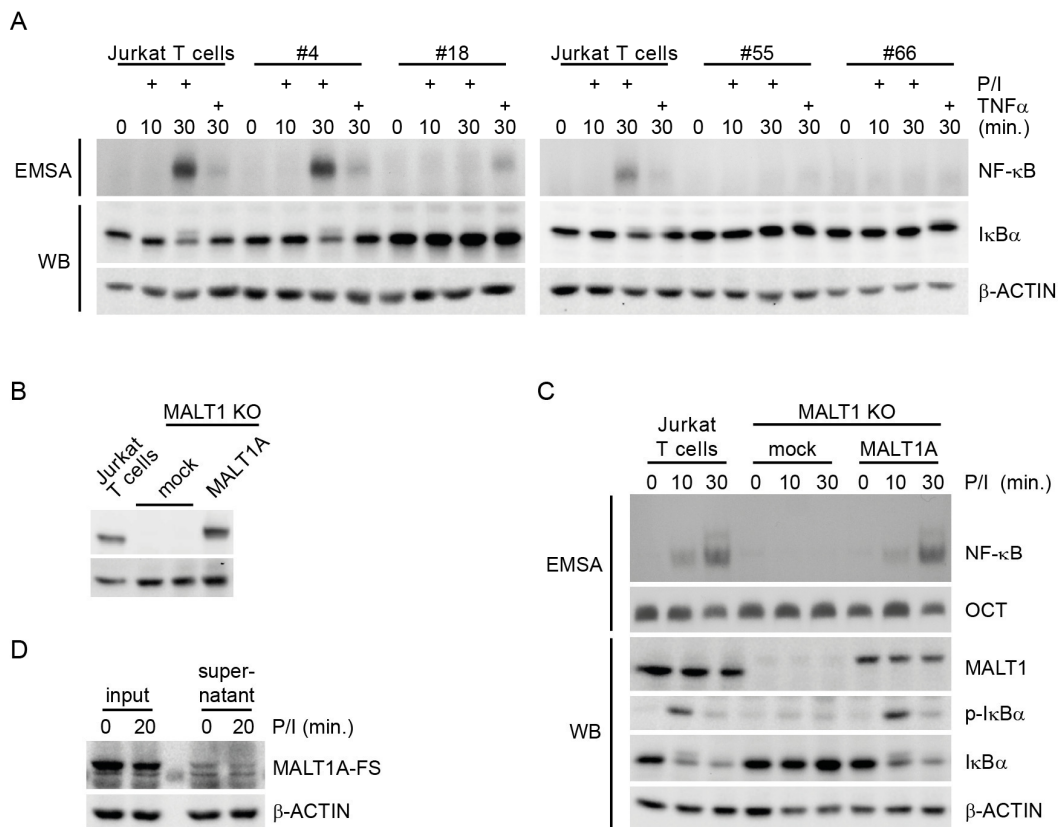
Figure 3-2: Validation of MALT1 KO Jurkat T cells. A) NF-κB signaling in MALT1-deficient Jurkat T cells in response to P/I stimulation was analyzed by EMSA and WB. B) MALT1-deficient Jurkat T cells were lentivirally reconstituted with MALT1A WT. Protein expression was analyzed by WB. C) NF-κB signaling was assessed in MALT1-deficient Jurkat T cells reconstituted with MALT1A WT and in parental Jurkat T cells. D) Efficient enrichment of MALT1 from extracts using ST-PD. Protein level of MALT1A-FS prior to (input) and following (supernatant) ST-PD is shown.

Several MALT1 KO clones were investigated for defects in NF-κB signaling (Figure 3-2). For this, Jurkat T cells were stimulated with PMA/Ionomycin (P/I) and TNFα to monitor the activation of the IKK/NF-κB pathway. P/I stimulation acts downstream of TCR/CD28 co-stimulation. PMA directly activates PKCθ and Ionomycin triggers Ca^{2+} release from the endoplasmatic reticulum into the cytosol, resulting in Calcineurin induction. Whereas P/I stimulation relies on MALT1 and efficient CBM complex assembly, TNFα stimulation activates the canonical NF-κB pathway at the level of IKK and is therefore independent of MALT1 (Figure 3-2A) [144]. MALT1-deficient clones display neither IκBα degradation by WB, nor NF-κB DNA binding activity by EMSA upon P/I stimulation, whereas TNFα stimulation resulted in weak NF-κB activation that was not altered in MALT1-deficient cells (Figure 3-2A) [66]. MALT1-deficient Jurkat T cells were lentivirally reconstituted with MALT1A WT tagged with a Flag-Strep-Strep-Tag (Flag-StrepII) epitope. MALT1A WT was expressed at endogenous levels, similar to that observed in parental Jurkat T cells (Figure 3-2B). P/I stimulation of reconstituted cells revealed that expression of MALT1A WT

could rescue the phenotype and resulted in similar IκBα phosphorylation/degradation and NF-κB activation, compared to the parental Jurkat T cells (Figure 3-2C). This indicates that reconstituted MALT1-deficient Jurkat T cells react like normal Jurkat T cells [66]. Expression of Flag-StrepII tagged MALT1 allowed efficient precipitation of MALT1 using a Strep-Tactin-pulldown (ST-PD), enabling the enrichment of MALT1 for mass spectrometry experiments.

3.2 Identification of MALT1 phosphorylation sites by LC-MS/MS

In an attempt to detect MALT1 phosphorylation sites, mass spectrometry experiments were executed after MALT1 enrichment using ST-PD. Cells were either unstimulated or treated for 20 min with P/I. After ST-PD, the enriched proteins digested by Lys-C and Trypsin. To enrich phosphorylated peptides, the digested peptides were incubated with titanium dioxide (TiO$_2$) beads and then measured in a mass spectrometer (LTQ Orbitrap XL). An LC-MS/MS run was performed (Figure 3-3) (further details are outlined in the material and methods).

P/I, 20 min.   StrepT-PD   Alkylation, Acidification and   TiO$_2$ enrichment   Mass spectrometry
                                         digestion (Lys-C and Trypsin)   analyser
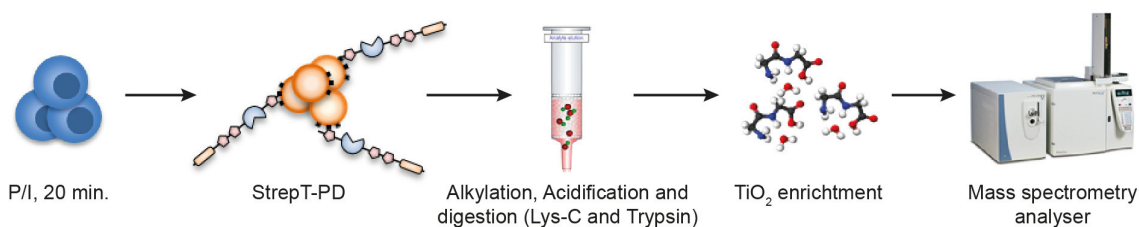
Figure 3-3: Identification of MALT1 phosphorylation sites by LC-MS/MS. Schematic depiction of the ST-PD, the sample preparation, and phospho-peptide enrichment leading up to measurement in a mass spectrometer.

Tandem mass spectrometry (MS/MS) was performed, in which two mass analyzers are coupled. The first mass analyzer detects peptides and the second analyzer is used to identify the amino acid sequence or modifications of the peptide. Therefore, the analyzers are connected via a collision cell, which is required for peptide fragmentation. Figure 3-4A shows an example of an MS1 and related MS2 spectrum. In the MS1 spectra, the measured mass-to-charge ratio (m/z) for every detected peptide is shown. Each peak with corresponding number represents a detected peptide. A mean of five MALT1 peptides were detected in several runs (Figure 3-4). MS/MS runs were carried out at the Core Facility Proteomics of the Helmholtz Center Munich in collaboration with Marco Rahm and Dr. Stefanie Hauck.

The MS2 spectrum shows the fragmentation of picked peptides. The fragment ions are indicated by 'b' if the charge is retained on the N-terminus and by 'y' if the charge is maintained on the C-terminus. These detected patterns allow identification of the peptide sequence and also putative phosphorylation sites. If phosphorylation occurs, the fragment shifts by a mass representing the size of the phospho-group (Figure 3-4).
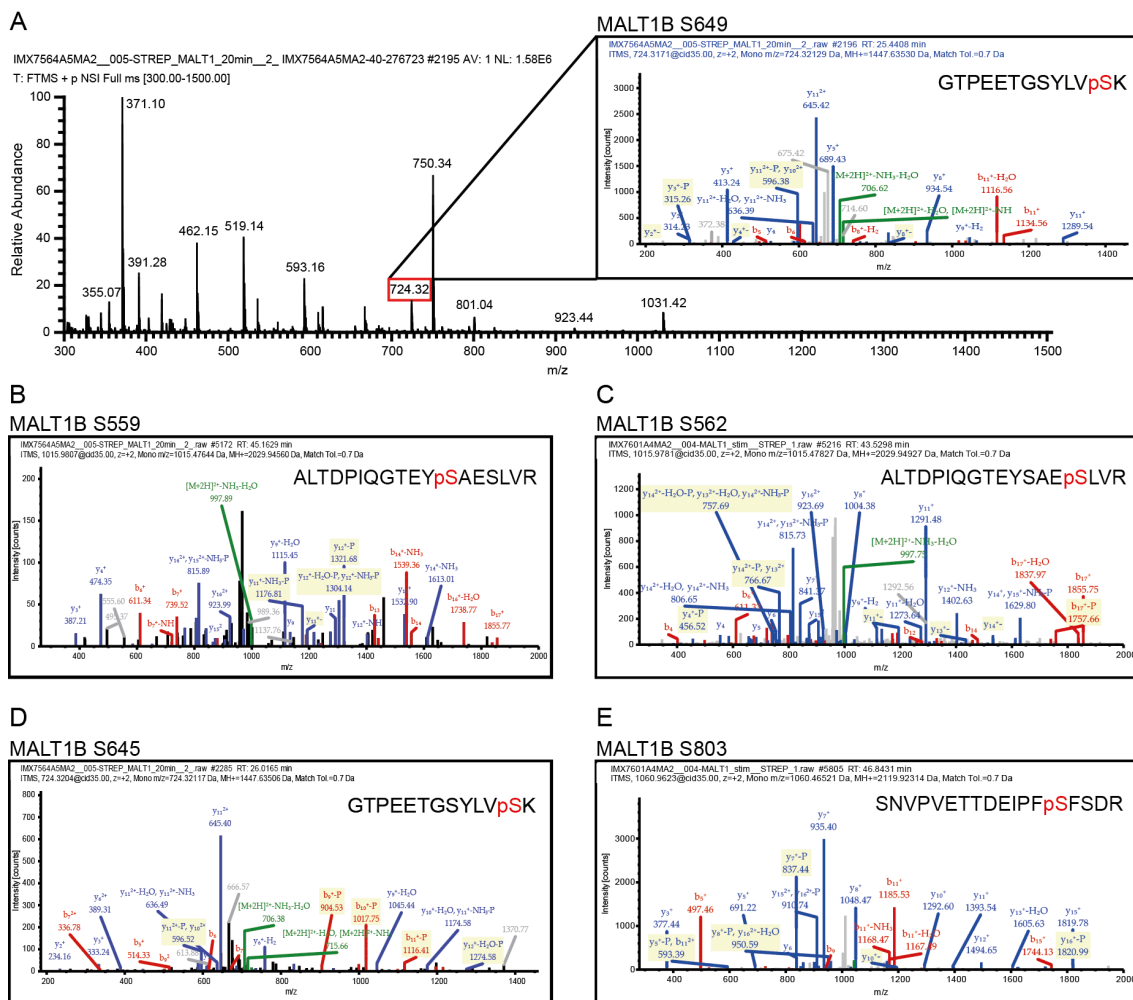
Figure 3-4: Mass spectrometry experiment to identify MALT1 phosphorylation sites. A) MS1 spectrum for MALT1 phosphorylation site S649 with the corresponding MS2 spectrum. In the MS1 spectrum, the MALT1 S649 peptide peak is highlighted in red. B - E) MS2 spectra of the other detected MALT1 phosphorylation sites. MS was carried out at the Core Facility Proteomics of the Helmholtz Center Munich by Marco Rahm and Dr. Stefanie Hauck.

In multiple mass spectrometry runs, three MALT1 phospho-peptides were identified following P/I treatment (Figure 3-5). In these, a total of five putative MALT1 phosphorylation sites corresponding to S570, S573, S656, S660 and S814 in MALT1A, or S559, S562, S645, S649 and S803 in MALT1B (Figure 3-5). In several cases, the peptides detected for S803 did not allow for clear differentiation between S803 and S805 phosphorylation. S805 is not listed in Figure 3-5 because of low probability, but could still be a putative phosphorylation site. Therefore, S805 is also highlighted in the sequence and both sites S803 and S805 are included in later experiments (Figure 3-5B). Although two potential modification sites could be identified in the same peptide, phosphorylation on both sites was not simultaneously detected. Furthermore, most phosphorylation site could be detected in multiple runs and phosphorylation events were only detected after stimulation, whereas unmodified peptides

have also been found in unstimulated conditions, indicating that all detected phosphorylation sites are dependent on T cell activation. Hereafter, I will only refer to the sites in MALT1B, as further experiments were performed using this isoform exclusively.

A

Phosphopeptide Sequence	Number of site-specific PSMs		Phosphosite MALT1A	Phosphosite MALT1B	PhosphoRS Site Probability	Ion Score
	unstim.	P/I				
ALTDPIQGTEYpSAESLVR	-	1	S570	S559	94 %	28
ALTDPIQGTEYSAEpSLVR	-	8	S573	S562	100 %	46
GTPEETGpSYLVSK	-	1	S656	S645	88 %	15
GTPEETGSYLVpSK	-	1	S660	S649	100 %	42
SNVPVETTDEIPFpSFSDR	-	3	S814	S803	99 %	87

B

MALT1 IsoB

```
  1 MSLLGDPLQA LPPSAAPTGP LLAPPAGATL NRLREPLLRR LSELLDQAPE GRGWRRLAEL AGSRGRLRLS
 71 CLDLEQCSLK VLEPEGSPSL CLLKLMGEKG CTVTELSDFL QAMEHTEVLQ LLSPPGIKIT VNPESKAVLA
141 GQFVKLCCRA TGHPFVQYQW FKMNKEIPNG NTSELIFNAV HVKDAGFYVC RVNNNFTFEF SQWSQLDVCD
211 IPESFQRSVD GVSESKLQIC VEPTSQKLMP GSTLVLQCVA VGSPIPHYQW FKNELPLTHE TKKLYMVPYV
281 DLEHQGTYWC HVYNDRDSQD SKKVEIIIDE LNNLGHPDNK EQTTDQPLAK DKVALLIGNM NYREHPKLKA
351 PLVDVYELTN LLRQLDFKVV SLLDLTEYEM RNAVDEFLLL LDKGVYGLLY YAGHGYENFG NSFMVPVDAP
421 NPYRSENCLC VQNILKLMQE KETGLNVFLL DMCRKRNDYD DTIPILDALK VTANIVFGYA TCQGAEAFEI
491 QHSGLANGIF MKFLKDRLLE DKKITVLLDE VAEDMGKCHL TKGKQALEIR SSLSEKRALT DPIQGTEYSA
561 ESLVRNLQWA KAHELPESMC LKFDCGVQIQ LGFAAEFSNV MIIYTSIVYK PPEIIMCDAY VTDFPLDLDI
631 DPKDANKGTP EETGSYLVSK DLPKHCLYTR LSSLQKLKEH LVFTVCLSYQ YSGLEDTVED KQEVNVGKPL
701 IAKLDMHRGL GRKTCFQTCL MSNGPYQSSA ATSGGAGHYH SLQDPFHGVY HSHPGNPSNV TPADSCHCSR
771 TPDAFISSFA HHASCHFSRS NVPVETTDEI PFSFSDRLRI SEK
```

Figure 3-5: Identified MALT1 phospho-peptides. A) Tabular overview of identified MALT1 phosphorylation peptides in mass spectrometry. PSM (peptide-spectrum-match) B) MALT1B protein sequence with identified phospho-peptides highlighted in red boxes.

All identified phosphorylation sites are within the C-terminal part of MALT1 containing the Ig3 domain and the third TRAF6 binding motif (T6BM3) (Figure 3-6A and B). It has previously been reported ubiquitination acceptor sites are also located in the C-terminus of MALT1, suggesting that this region is accessible and prone to post-translational modifications. The crystal structure of the MALT1 paracaspase domain together with the adjacent Ig3 domain shows the position of S559, S562, S645 and S649 (Figure 3-6B). S559 and S562 are located at the start of the linking α-helix that connects the paracaspase and the Ig3 domains. S645 and S649 are within a connecting loop in the Ig3 domain and near to K633 that is targeted by mono-ubiquitination [75]. All detected phosphorylation sites are highly conserved in mammals except for site S562, which does not exist in rodents (Figure 3-6C).
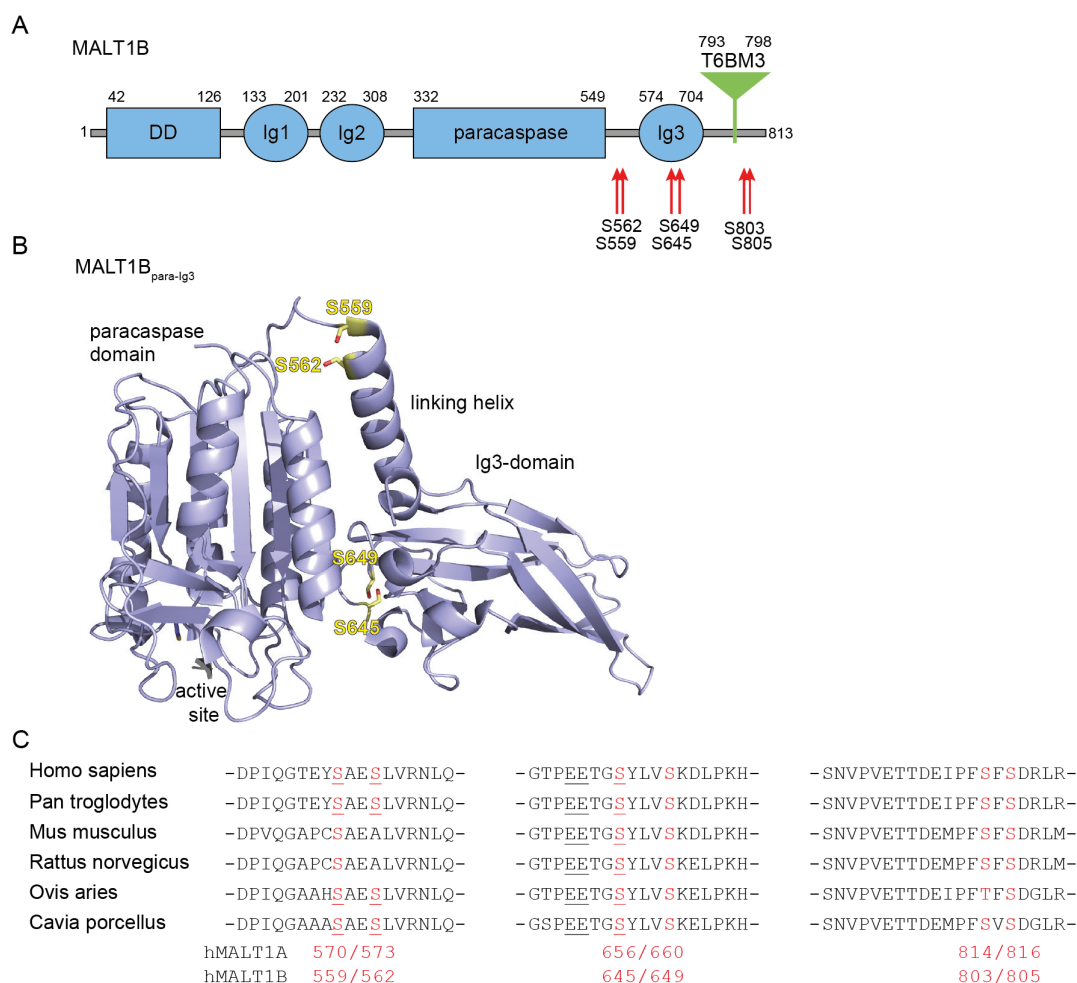
Figure 3-6: MALT1 phosphorylation sites. A) Domain organization of MALT1B protein with positions of phosphorylation sites indicated by red arrows. DD (Death domain), Ig (Immunoglobulin)-like domain. B) Crystal structure of ligand bound MALT1 paracaspase Ig3 domain (PDB code: 4I1P) with the positions of phosphorylated serine residues depicted. C) Evolutionary conservation of identified MALT1 phosphorylation sites.

3.3 Generation and validation of phospho-site specific antibodies

In order to validate the identified phosphorylation events, and to gain insights into the kinetics of the phosphorylation, site-specific antibodies were generated at the Monoclonal Antibody Core Facility of the Helmholtz Center Munich in cooperation with Andrew Flatley and Dr. Regina Feederle. Mice and rats were immunized by subcutaneous injection of synthesized peptides coupled to ovalbumin. Each peptide carried a phosphorylated serine residue for sites S562, S649 or S803 (Figure 3-7). Antibodies were generated only against phosphorylation sites with the highest probability.
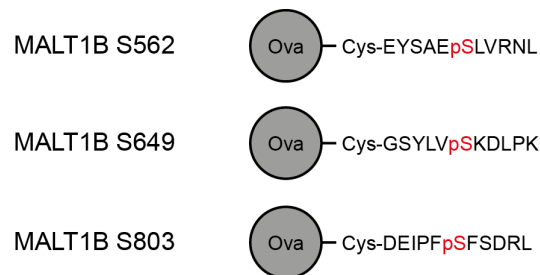
Figure 3-7: Scheme of synthetic peptides. Peptides were used to immunize mice and rats subcutaneously for the generation of phospho-specific antibodies. Antibodies were generated at the Monoclonal Antibody Core Facility of the Helmholtz Center Munich in cooperation with Andrew Flatley and Dr. Regina Feederle.

Overall, 70 primary hybridoma supernatants were generated for S562, 24 for S649 and 32 for S803. In a first screening, these supernatants were tested as Western Blot antibodies against MALT1 WT and a phospho-defective mutant containing a serine to alanine mutation at the respective site (S/A). Because of the stimulation-dependency of the detected phosphorylation, screening was also performed against lysates from unstimulated and stimulated Jurkat T cells (Figure 3-8).

The antibodies against S562 and S803 only showed a smear in the stimulated WT samples. The smear starts at the expected molecular size of MALT1 and appears to represent more highly modified forms, indicating that MALT1 is not only phosphorylated, but contains multiple modifications. The antibody against S649 shows a distinct band at the size of MALT1 and a similar higher molecular weight smear. However, at an approximated size of 130 kDa another distinct band appears. All tested antibodies did not react with the respective S/A mutant (Figure 3-8).
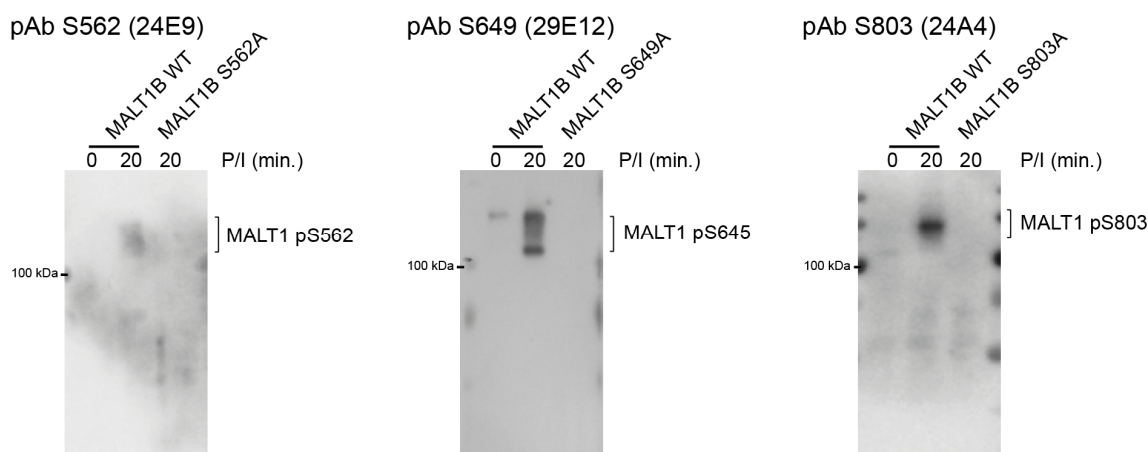
Figure 3-8: Primary screen of MALT1 phospho-site specific antibodies. Screen was performed using Western blotting. Several positive antibody clones could be identified for every phosphorylation site in a first screen. Only the further validated antibodies are shown here.

After primary identification, promising antibody clones were sub-cloned and expanded by the Monoclonal Antibody Core Facility. New hybridoma supernatants were then re-tested and

further validated (Figure 3-9). All three phospho-specific antibodies reacted strongly with the slower migrating, highly modified MALT1B WT only after T cell stimulation (Figure 3-9). Detection with anti-pS562-, anti-pS649- and anti-pS803-MALT1 antibodies was severely reduced when phospho-defective MALT1 mutants S562A, S649A and S803/805A were transduced, respectively. Phosphorylation at pS562 and pS649 was detected by Western blot after MALT1-IP and was completely abolished by phosphatase treatment, confirming the detection of phospho-MALT1 (Figure 3-9A and B). MALT1 pS803 was only efficiently recognized after anti-pS803-MALT1-IP followed by anti-MALT1 Western blot, indicating that the antibody reacts with pS803 in its native conformation (Figure 3-9C). Whereas the anti-pS562-MALT1 antibody exclusively detected hyper-modified and phosphorylated MALT1 (Figure 3-9A), anti-pS649- and anti-pS803-MALT1 antibodies still retained some activity against unphosphorylated MALT1 (Figure 3-9B and C). In the case of the anti-pS649-MALT1 antibody, detection was phosphatase insensitive, but was lost by S649A exchange, proving that the antibody also detects unmodified S649. In conclusion, three different antibodies were generated that allow monitoring of MALT1 phosphorylation status.
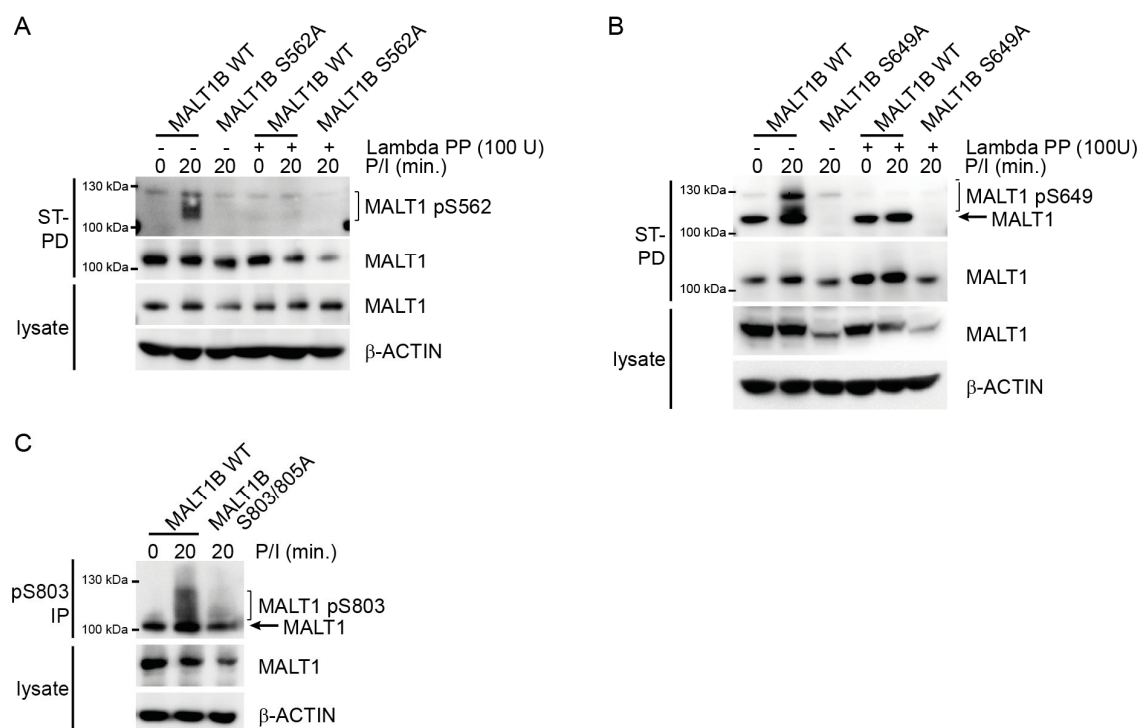
Figure 3-9: MALT1 phospho-antibodies. Generation and validation of antibodies against phosphorylated MALT1B S562 (A), S649 (B) and S803 (C). Site and phosphorylation specificity was determined using a phospho-defective serine to alanine (S/A) mutant and Lambda protein phosphatase (PP) treatment (A and B). Phosphorylated MALT1B S803 is detected by the antibody after anti-pS803-IP and MALT1 WB (C).

3.4 Analysis of MALT1 phosphorylation kinetics in Jurkat T cells

To investigate the role and the kinetics of the detected phosphorylation sites, their appearance in Jurkat T cells was analyzed after P/I and anti-CD3/CD28 stimulation

(Figure 3-10). Cross-linking of the TCR subunit CD3 and the co-receptor CD28 with specific antibodies led to the activation of TCR signaling, mimicking the interaction of a T cell with an APC. Therefore, anti-CD3/CD28 stimulation represents a more physiological stimulation than P/I. Stimulation series up to 8 hours were performed and correlated to early and late events in CBM complex assembly and disassembly as well as NF-κB regulation (Figure 3-10).

Since all three pMALT1 antibodies detected their respective phosphorylation sites in MALT1, we next utilized them to examine the T cell stimulation-dependent phosphorylation kinetics of endogenous MALT1 (Figure 3-10). Following stimulation of Jurkat T cells with anti-CD3/CD28 antibodies or P/I, we measured MALT1 phosphorylation as well as CARD11 activation, CBM complex assembly/disassembly, and NF-κB signaling over a time course up to eight hours (Figure 3-10 A and B).

Notably, whereas CARD11 phosphorylation on the activating S645 residue [38], and its ability to bind BCL10-MALT1 were already apparent after 2 min of P/I or CD3/CD28 stimulation, MALT1 phosphorylation at the three sites was delayed, beginning at 5-10 min and peaking by 20-30 min (Figure 3-10 A and B). Similarly, formation of the CBM complex occurred at approximately 2 min following stimulation, whereas MALT1 phosphorylation at S562 and S649 in complex with BCL10 was only visible after 10-30, demonstrating that CBM complex formation precedes MALT1 phosphorylation (Figure 3-10B). Furthermore, MALT1 phosphorylation appears to coincide with the onset of IκBα degradation and the induction of canonical NF-κB signaling (Figure 3-10A and B). No significant differences in the initial phosphorylation of the distinct sites were observed, but the duration of MALT1 S562 phosphorylation was sustained and still detectable after 1 – 8 h of stimulation. In contrast, S649 and S803 phosphorylation rapidly declined after only 30 – 60 min of stimulation (Figure 3-10A and B). Thus, MALT1 S562 phosphorylation was also present at later time points, after CBM complex disassembly resulting from BCL10 degradation (Figure 3-10A and B) [97, 98]. Thus, the data suggests that MALT1 phosphorylation may be involved in CBM downstream effects rather than initial CBM complex assembly.

Figure 3-10: A) Kinetics of MALT1 phosphorylation in Jurkat T cells after anti-CD3/CD28 stimulation. MALT1 phosphorylation was determined after MALT1 (S562 and S649) or pS803-IP and correlated to CARD11 phosphorylation on S645, CBM complex formation and IκBα phosphorylation/degradation. B) Kinetics of MALT1 phosphorylation in Jurkat T cells after P/I stimulation. MALT1 phosphorylation

was detected after MALT1- or BCL10-IP, alongside CBM complex formation, activating CARD11 S645 phosphorylation and IκBα phosphorylation/degradation.

To test if active MALT1 protease is phosphorylated, and to correlate MALT1 phosphorylation to MALT1 protease activity, we used a biotin-labelled MALT1 activity-based probe (ABP) which attaches covalently to active MALT1 after stimulation [145]. In extracts of Jurkat T cells, the MALT1 ABP precipitates a slower migrating MALT1 only after P/I stimulation, suggesting that active MALT1 is highly modified, which precisely correlates with the early appearance of mono- and poly-ubiquitinated MALT1 species after 5 min of stimulation (Figure 3-11). Indeed, active ABP-coupled MALT1 was also phosphorylated at S562 and S649, and again MALT1 phosphorylation on both residues was delayed and was first visible after 10 min of P/I treatment, a time point when MALT1 was already active. As noted earlier, whereas MALT1 S649 phosphorylation was transient, MALT1 S562 phosphorylation persisted during all time points of MALT1 protease activity (Figure 3-11). In parallel, MALT1 substrate cleavage was also monitored showing CYLD, HOIL1 and Regnase-1 cleavage from shortly after MALT1 activation and persisting throughout the stimulation time course (Figure 3-11). Thus, these data demonstrate that MALT1 protease activity and ubiquitination precedes MALT1 phosphorylation, suggesting that the latter may not be required for protease activation.
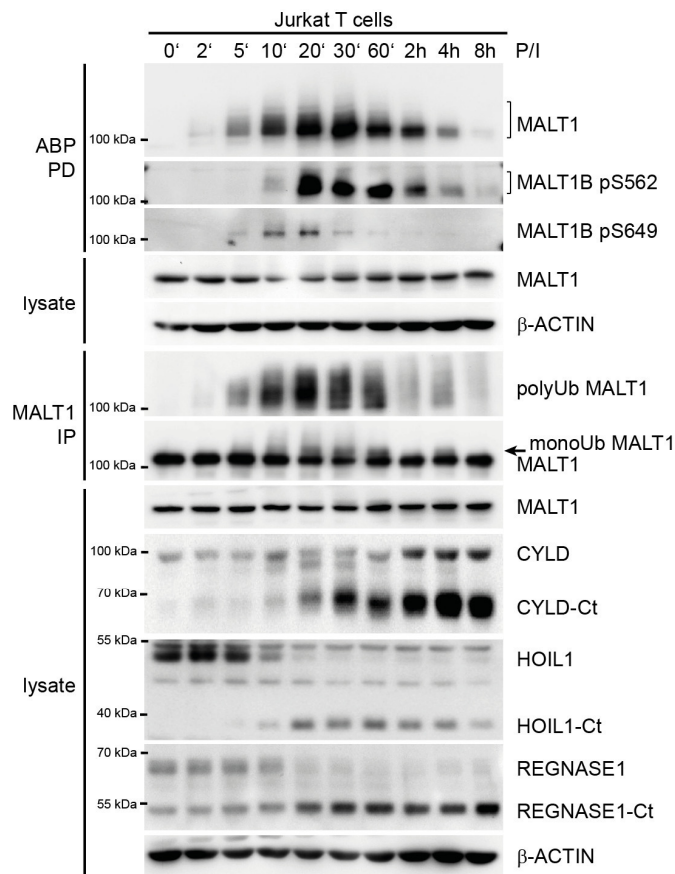
Figure 3-11: Active MALT1 is phosphorylated. MALT1 phosphorylation is monitored after biotin-PD using a specific MALT1 ABP in enriched active MALT1 fraction. Detection of slower migrating

modified MALT1 after MALT1-ABP PD was correlated to the appearance of mono- and poly-ubiquitinated MALT1 species and MALT1 substrate cleavage.

3.4.1 Detection of MALT1 phosphorylation in primary human CD4 T cells

To confirm that MALT1 is also phosphorylated in primary human T cells, CD4 T cells were isolated from donor blood and stimulated with P/I for 20 min (Figure 3-12).
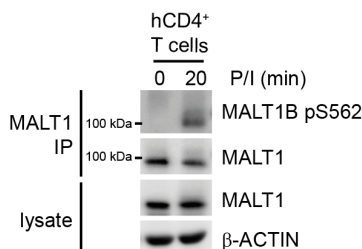
Figure 3-12: Phosphorylation of MALT1 in primary human CD4 T cells after P/I stimulation.

Using MALT1-IP, a strong band representing MALT1 phosphorylation on S562 could be detected after T cell stimulation, demonstrating that MALT1 is phosphorylated in primary T cells. MALT1 phosphorylation on S649 and S803 could not be detected in primary CD4 T cells, but whether this indicates the absence phosphorylation, or was instead due to flawed antibody detection, could not be determined. However, using LC-MS/MS and phospho-specific antibodies, T cell stimulation-dependent phosphorylation of numerous serine residues in the C-terminus of Malt1B could be identified.

3.4.2 MALT1 is hyper-phosphorylated in ABC DLBCL cell lines

As part of the CBM complex, MALT1 is essential for controlling NF-κB survival signaling in ABC DLBCL cells [136]. We therefore tested whether MALT1 is prone to chronic phosphorylation in ABC DLBCL cell lines by using anti-pMALT1 antibodies (Figure 3-13).

After MALT1 IP, phosphorylation of MALT1 on S562 (MALT1B) was detected in all four ABC DLBCL cell lines (HBL1, TMD8, OCI-Ly3, and U2932) even in the absence of stimulation (Figure 3-13A). No constitutive MALT1 phosphorylation on S562 was observed in the GCB DLBCL cell lines BJAB, SUDHL4, and SUDHL6, but phosphorylation in SUDHL4 and SUDHL6 was induced by P/I stimulation (Figure 3-13B). Due to lack of selectivity, the other phosphorylation sites could not be detected in ABC and GCB DLBCL cells. Since MALT1 phosphorylation was strongly detected in HBL1 and TMD8 cells carrying upstream mutations in the BCR adaptor CD79B, we treated these cells with BTK inhibitor Ibrutinib (Figure 3-13C). Phosphorylation of MALT1 was sensitive to BTK inhibitor treatment, revealing that it is dependent on chronic upstream BCR signaling. In contrast, MALT1 phosphorylation in OCI-Ly3 cells, carrying an oncogenic variant of CARD11, was more resistant to Ibrutinib treatment than the HBL1 and TMD8 cells. Furthermore, expression of oncogenic CARD11 L225LI in HBL1 cells, which reduces Ibrutinib toxicity [139], impaired the reduction in MALT1 S562 phosphorylation observed in response to BTK inhibition (Figure 3-13D). Thus,

constitutive CBM complex assembly, as a result of chronic BCR signaling or oncogenic CARD11 mutations, induces S562 phosphorylation of MALT1 in ABC DLBCL cells.
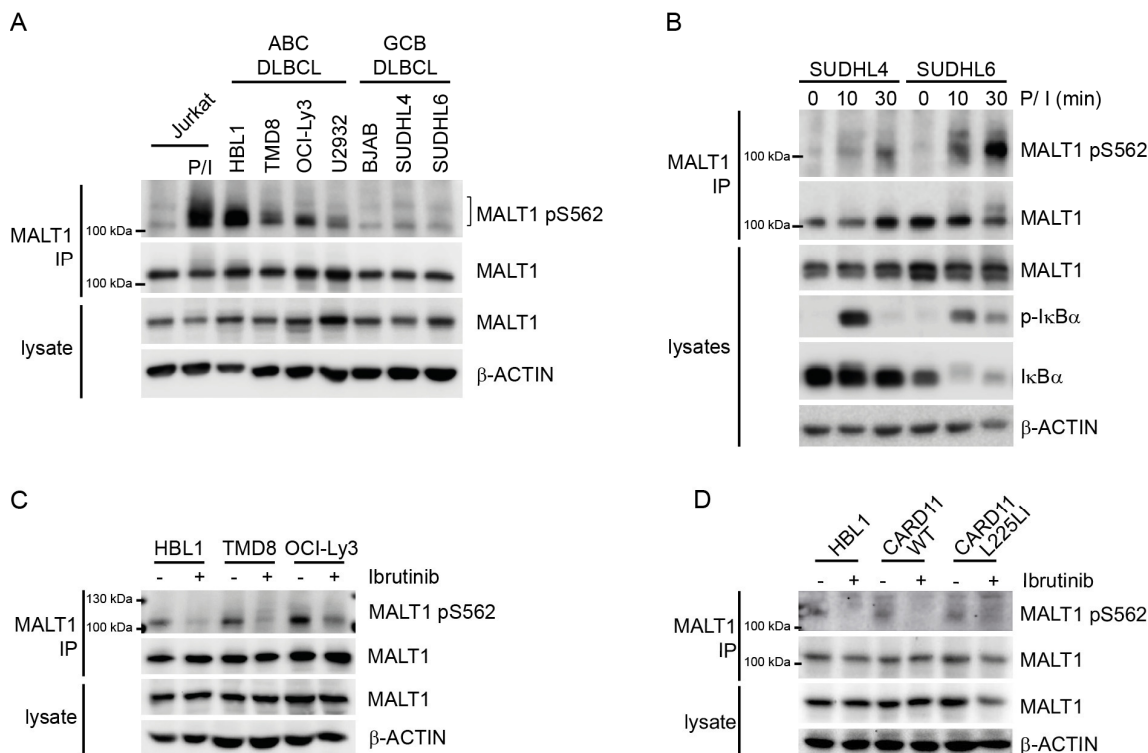
Figure 3-13: A) MALT1B S562 phosphorylation was assessed after MALT1-IP and WB in four ABC and three GCB DLBCL cell lines as depicted. B) MALT1B S562 phosphorylation was determined after MALT1-IP and WB following P/I stimulation in the GCB DLBCL cell lines SUDHL4 and SUDHL6. C) The ABC DLBCL cell lines HBL1, TMD8 and OCI-Ly3 were treated with the BTK inhibitor Ibrutinib (20 nM, 18 h) and MALT1B S562 phosphorylation was assessed after MALT1-IP and WB. D) The ABC DLBCL cell line HBL1 transduced with mock, CARD11 WT or CARD11 L225LI were treated with the BTK inhibitor Ibrutinib (20 nM, 18 h) and MALT1B S562 phosphorylation was assessed after MALT1-IP and WB.

3.5 Regulation of CBM complex and MALT1 by CK1α

3.5.1 Identifying CK1α as a putative kinase for MALT1 phosphorylation

In several studies, CK1α has been shown to associate with the CBM complex upon T cell activation and exert a dual function by first promoting IKK/NF-κB activation and, in later phases, terminate induction by inactivating phosphorylation of CARD11 on S608 (see 2.5.4 and Figure 2-5) [85, 143]. However, the exact mechanism of CK1α induction of IKK/NF-κB has not been elucidated to date. By using an online phosphorylation prediction tool named Scansite 4.0, CK1α was found to be a potential protein kinase acting upon MALT1 S562 and S645 (Figure 3-14).

Considering the consensus sites for CK1α, a primed and a non-primed site was described [126]. In the primed site, the serine or threonine, which is targeted by CK1α, is preceded by phosphorylated serine or threonine two amino acids towards the N-terminal part. A non-primed site for CK1α exists when the targeted serine or threonine has a negatively charged amino acid (aspartic acid (D) or glutamic acid (E)) two positions towards the N-terminus [121, 125, 126]. Thus, MALT1 S562 represent a putative primed site for CK1α and S645 a putative non-primed sequence (Figure 3-14).

A

Scansite 4.0

Score	Percentile	Motif	Motifgroup	Site	Sequence	Surface Accessibility
0,408	0,811%	Casein Kinase 1 (Casn_Kin1)	Acidophilic serine/threonine kinase group (Acid_ST_kin)	S562	GTPYSAESLVRNLQW	0,6442
0,548	9,114%	Casein Kinase 1 (Casn_Kin1)	Acidophilic serine/threonine kinase group (Acid_ST_kin)	S645	GTPEETGSYLVSKDL	0,4207

B

CK1α consensus

```
pT / pS   - x - x - S/T  - x    primed canonical
(E,D)n    - x - x - S/T  - x    non-primed canonical
```


Figure 3-14: CK1α consensus sites on MALT1. A) MALT1 phosphorylation sites S562 and S645 are predicted to be putative CK1α phosphorylation sites. Residues are highlighted in the domain organization of MALT1 (upper panel). Tabular overview of parameters used for prediction by Scansite 4.0 (lower panel). B) Consensus sequence for primed canonical and a non-primed canonical CK1α phospho-acceptor sites [126]. Below, sequences of the regions surrounding the identified MALT1 phosphorylation sites and potential primed and non-primed CK1α sites are indicated.

As mentioned before, CK1α associates with the CBM upon T cell stimulation, but the exact mechanism of CK1α induction of IKK/NF-κB has not yet been elucidated [85]. Since two identified phosphorylation sites correspond to putative CK1α binding sites, it is conceivable that MALT1 phosphorylation participates in mediating the positive effects of CK1α. Upon P/I stimulation, the CBM complex could be co-immunoprecipitated with CK1α confirming the reported association (Figure 3-15).

To clarify which CBM complex members were responsible for CK1α binding, its association was determined in CARD11 [146], BCL10 [63] and MALT1 KO Jurkat T cells generated by CRSPR/Cas9 technology [66] (Figure 3-15A).
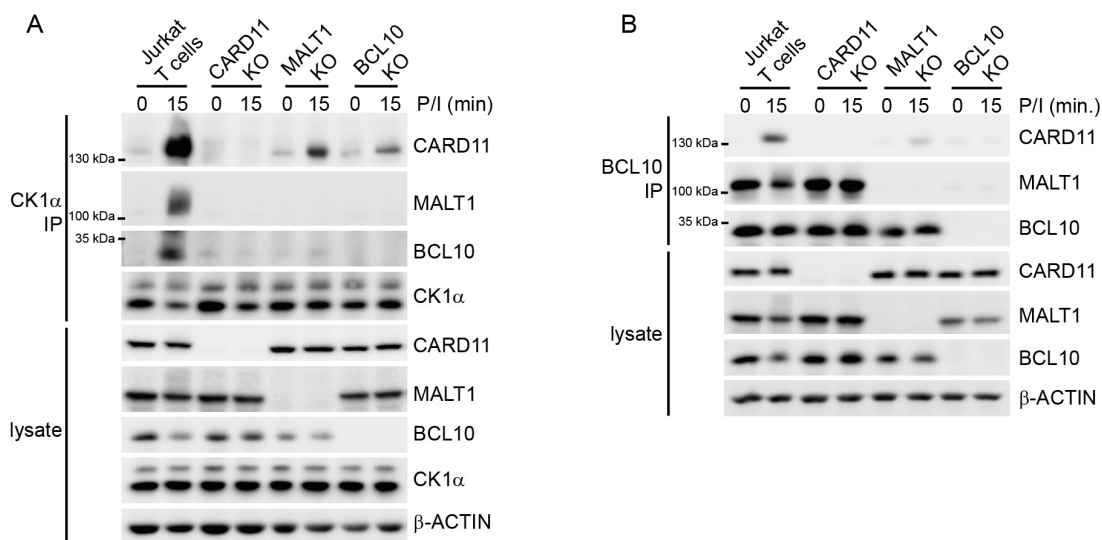
Figure 3-15: A) Binding of CK1α to CARD11, MALT1 and BCL10 in parental and respective KO Jurkat T cells following P/I stimulation, was determined after CK1α co-IP. B) CBM complex formation in parental Jurkat T cells and CARD11, MALT1 or BCL10 KO Jurkat T cells, was determined by BCL10-IP and WB following P/I stimulation [63, 146].

The absence of any one of these complex members abrogates CBM complex formation as observed following BCL10-IP (Figure 3-15B). In line with the proposed direct recruitment of CK1α to the coiled-coil and linker regions of CARD11 [85], the lack of CARD11 abolished CK1α binding to BCL10 and MALT1 (Figure 3-15A). A residual, but severely reduced, CK1α-CARD11 interaction was detectable in BCL10 or MALT1 KO cells, suggesting that both contribute directly or indirectly to efficient integration of CK1α into the CBM complex upon stimulation (Figure 3-15A).

To investigate the contribution of BCL10-MALT1 to the CK1α-CARD11 interaction in more detail, we expressed CK1α-FS and HA-CARD11 alone or together with Flag-MALT1 and Flag-BCL10 in HEK293 cells lacking endogenous CARD11 (Figure 3-16A). Binding of CARD11 to CK1α was augmented in the presence of BCL10 and MALT1, suggesting that the CBM holo-complex constitutes the optimal platform for CK1α recruitment (Figure 3-16A).

Moreover, we assessed association of CK1α-FS to HA-MALT1 (Figure 3-16B). Whereas MALT1 did not bind to CK1α in the absence of BCL10, CK1α associated with BCL10-MALT1 complexes in the absence of CARD11, and this interaction was not further augmented by CARD11 co-expression and CBM complex formation. Thus, the data show that BCL10-MALT1 confers an additional binding surface for the efficient recruitment of CK1α to the CBM complex.
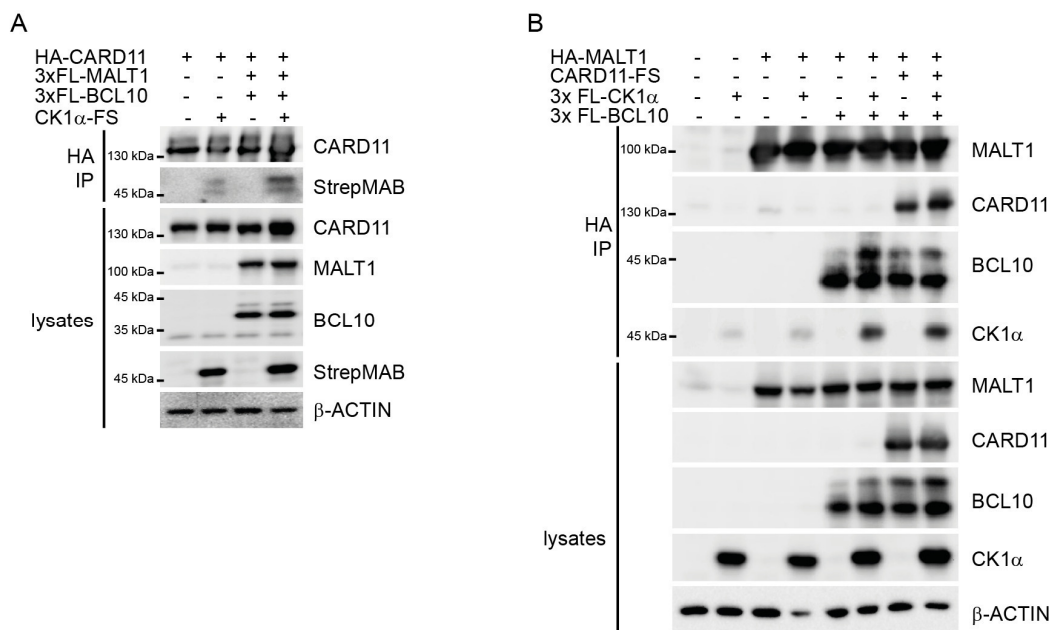
Figure 3-16: A) Binding of HA-CARD11 to CK1α-FS in the absence or presence of 3xFlag-BCL10 and 3xFlag-MALT1 in HEK293 cells. B) Association between HA-MALT1 and 3xFlag-CK1α either alone or in the presence of only 3xFlag-BCL10 or 3xFlag-BCL10 and CARD11-FS in HEK293 cells.

To determine whether CK1α could directly phosphorylate MALT1, *in vitro* kinase assays were performed (Figure 3-17). In a radioactive *in vitro* kinase assays, CK1α proved to be capable of phosphorylating MALT1 in general (Figure 3-17A). To examine the phosphorylation of MALT1 on S562 by CK1α, non-radioactive *in vitro* kinase assays were performed and analyzed by Western blotting using the anti-pS562 MALT1 antibody, which specifically only detects phosphorylated MALT1 (Figure 3-17B, see also Figure 3-9). Incubation of a shorter paracaspase-containing MALT1 fragment (aa 325 – 760) as well as a baculovirally-produced fragment of the complete C-terminal part (aa 334 – 824) of MALT1 with recombinant CK1α resulted in a strong phosphorylation of S562 (Figure 3-17B and C).

In each case, the phosphorylation of S649 and S803 could not be identified using the generated phospho-specific antibodies. Due to a lack of a site-specific antibody, the presence of phosphorylation of the non-primed CK1α site S645 could be neither confirmed nor excluded. Taken together, these results clearly show that CK1α binds to MALT1 and phosphorylates it on S562.
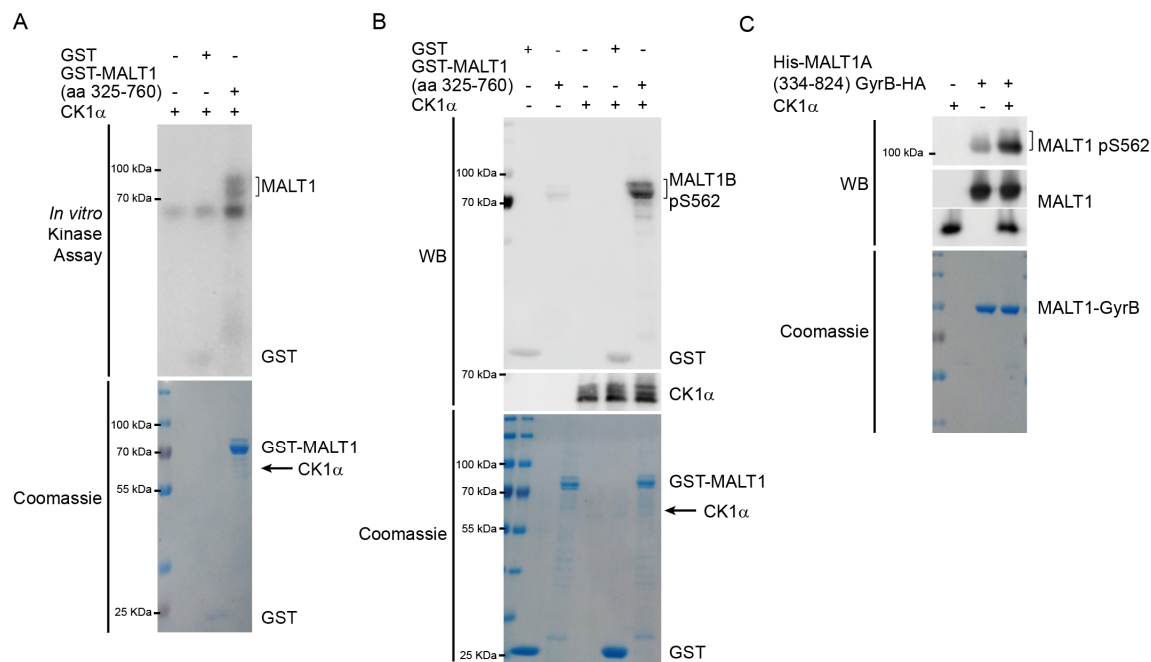
Figure 3-17: CK1α catalyzed MALT1 phosphorylation. A) Radioactive *in vitro* kinase assay, using bacterial GST-MALT1 (aa 325-760) as a substrate for CK1α, was performed and analyzed by radiography. B) Non-radioactive *in vitro* protein kinase assay as in A was analyzed by Western Blot using the phospho-specific antibody against MALT1B S562. C) Non-radioactive *in vitro* protein kinase assay using baculovirally-produced 6xHis-MALT1-GyrB-HA (aa 334-813) as a substrate for CK1α as in B.

3.5.2 CK1α is essential for CBM assembly and IKK/NF-κB activation

To gain precise insight into the roles and functions of CK1α in the regulation of CBM complex formation and NF-κB activation, CK1α-deficient Jurkat T cells were generated. Using the CRISPR/Cas9 system, exon 3 was targeted and a double strand break was induced into the genomic DNA. Its repair by non-homologous end-joining (NHEJ) resulted in a loss or a gain of several bases at the cleavage site leading to a frameshift and a premature stop codon (Figure 3-18A and B).

While in clone #6 a homozygous deletion of 27 bases can be observed, clone #1 shows a heterozygous alteration whereby each allele gained a variable number of bases (Figure 15B). Both clones resulted frameshifts in the mRNA of CK1α and therefore, a premature stop codon was generated that abolished the translation of CK1α as confirmed by Western blot analysis (Figure 3-18C). CK1α KO Jurkat T cells were viable and did not exhibit defects in cell growth under standard conditions.
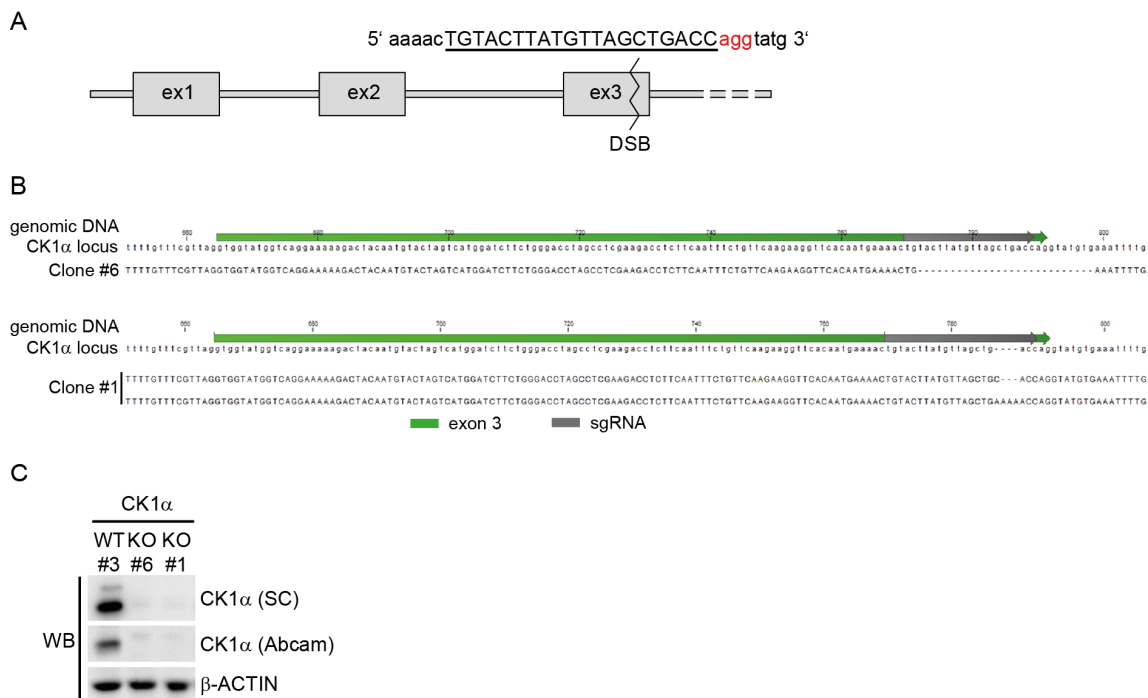
Figure 3-18: Generation of CK1α-deficient Jurkat T cells. A) Scheme of genomic locus of CK1α. Exon 3 is targeted using the CRISP/Cas9 system with depicted sgRNA. Adjacent PAM sequence is highlighted in red. B) Sequencing of genomic DNA of CK1α-deficient cell clones showed genomic alterations in exon 3. C) Efficient knockout of CK1α was confirmed by Western blot analysis.

To identify the effect of CK1α in CBM complex formation and downstream NF-κB activation, CK1α-deficient cells were stimulated, either with anti-CD3/CD28 antibodies or P/I (Figure 3-19A and B). Indeed, CK1α deficiency abolished NF-κB signaling. Loss of IκBα phosphorylation and degradation as well as NF-κB DNA binding could be observed in CK1α-deficient cells (Figure 3-19A and B). Furthermore, CK1α KO Jurkat T cells failed to induce MALT1 protease activity, as evident from the lack of P/I-dependent CYLD and HOIL1 cleavage. ERK phosphorylation and PKCθ-dependent phosphorylation of CARD11 on S645 in the linker region were normal in CK1α KO cells, indicating no effects on upstream signaling (Figure 3-19B). Moreover, loss of CK1α did not alter NF-κB signaling in response to TNFα stimulation (Figure 3-19C). Thus, CK1α KO in Jurkat T cells confirmed previous results demonstrating a critical role of CK1α for T cell stimulation. To gain better insights into the exact mechanism by which CK1α promotes T cell activation, CBM complex assembly in CK1α-deficient cells was examined (Figure 3-19D).
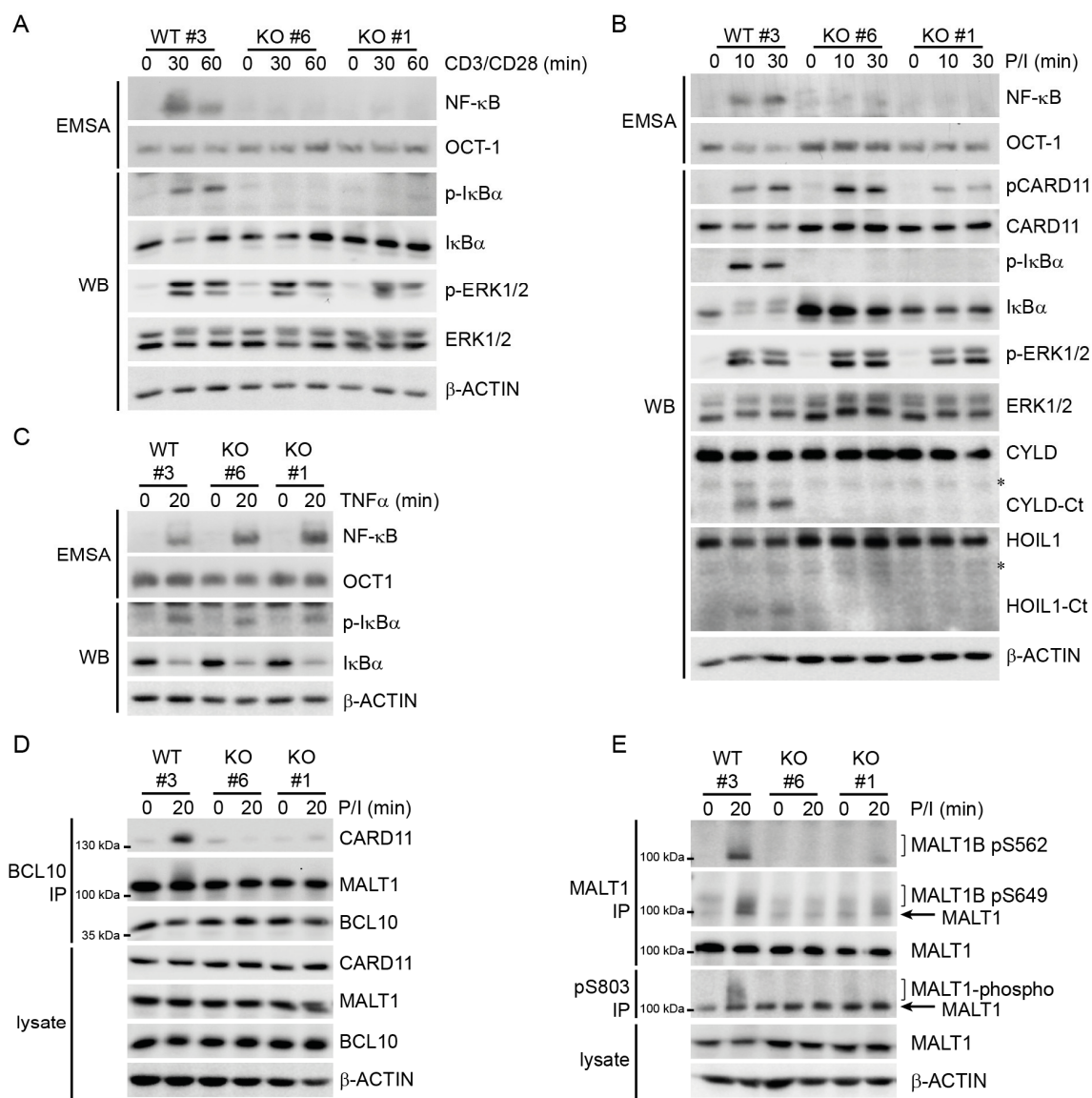
Figure 3-19: A) NF-κB signaling in CK1α-deficient Jurkat T cells, in response to anti-CD3/CD28 stimulation, was analyzed by EMSA and WB. B) NF-κB signaling and MALT1 substrate cleavage in CK1α-deficient Jurkat T cells in response to P/I stimulation was analyzed by EMSA and WB. C) Upon TNFα stimulation of CK1α-deficient Jurkat T cells, NF-κB signaling was analyzed by IκBα phosphorylation/degradation and NF-κB DNA binding in WB and EMSA, respectively. D) CBM complex assembly was determined in parental and CK1α-deficient Jurkat T cells after P/I stimulation using BCL10-IP and WB. E) MALT1 phosphorylation on S562, S649 and S803 was detected in parental CK1α-deficient Jurkat T cells after P/I stimulation and MALT1- or pS803-IP followed by WB.

Notably, the inducible CARD11-BCL10 interaction was completely lost in CK1α KO cells, whereas constitutive BCL10-MALT1 association was unaffected. Hence, CK1α is a crucial mediator for the stimulus-induced formation of the CBM complex. Using phospho-specific MALT1 antibodies, it could be shown that MALT1 phosphorylation on the three serine residues, 562, 649 and 803, was lost in the absence of CK1α (Figure 3-19E). Collectively,

the data demonstrate that CK1α triggers MALT1 phosphorylation, but considering its essential role for CBM complex formation, CK1α may directly and/or indirectly affect MALT1 phosphorylation.

To resolve the exact role of CK1α in CBM formation, MALT1 phosphorylation and NF-κB signaling, cells were lentivirally reconstituted with several C-terminally FS-tagged CK1α constructs.
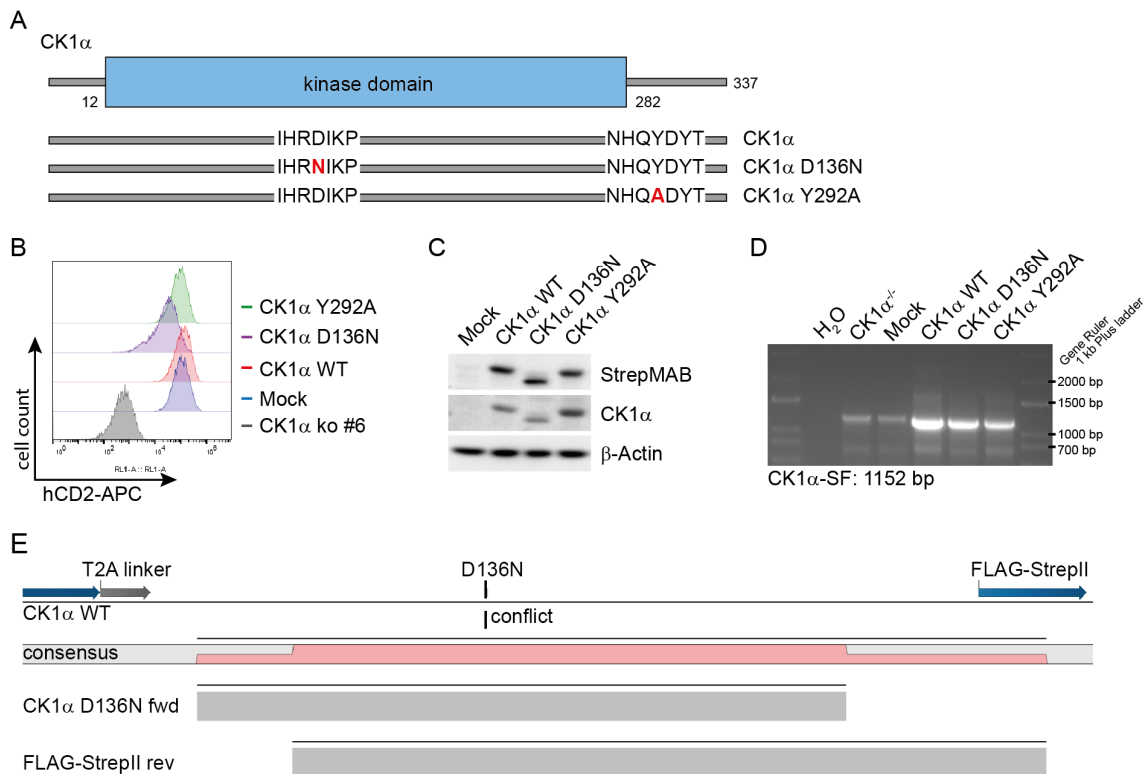
Figure 3-20: Lentiviral reconstitution of CK1α-deficient Jurkat T cells with different CK1α mutants. A) Schematic of CK1α and generated point mutants. B) CK1α-deficient Jurkat T cells were reconstituted with CK1α WT, a kinase-dead version (D136N), and a CARD11-binding mutant (Y292A). Levels of co-expressed surface marker hΔCD2 protein were determined by FACS. C) CK1α WT, D136N and Y292A protein expression was analyzed by WB. D, E) mRNA of CK1α variants was isolated from infected cells and correct size of mRNA was analyzed by amplifying the cDNAs using specific ST-tag PCR primer (D). By sequencing expression of the correct full length CK1α mRNA and the presence of respective mutations was verified (E).

In addition to CK1α wildtype, a catalytically inactive variant (D136N) and a CARD11-binding-mutant (Y292A) were introduced into cells to determine whether kinetic activity or CK1α recruitment is responsible for the observed effects in CBM assembly and MALT1 phosphorylation [85] (Figure 3-20A). The plasmid used for lentiviral transduction bears a truncated version of the gene for the surface marker hΔCD2, which is linked by a thoseaasigna virus sequence (T2A) to the CK1α cDNA. Mutants were equally expressed as determined by staining of the surface marker hΔCD2 in FACS and Western blotting

(Figure 3-20B and C). Notably, CK1α D136N migrated slightly faster in SDS-PAGE compared to WT or Y292A. To exclude a deletion in D136N, mRNA of the lentivirally reconstituted mutants were isolated and transcribed into cDNA. PCR analyses, and subsequent sequencing of transduced constructs, revealed that D136N mRNA was intact and contained the missense mutation (Figure 3-20D and E). Unspecific amplification of the endogenous mRNA was excluded by using a reverse primer binding in the FS epitope. Thus, different migration seems to result due to an altered conformation, inhibition of auto-phosphorylation of CK1α, or other unknown factors.
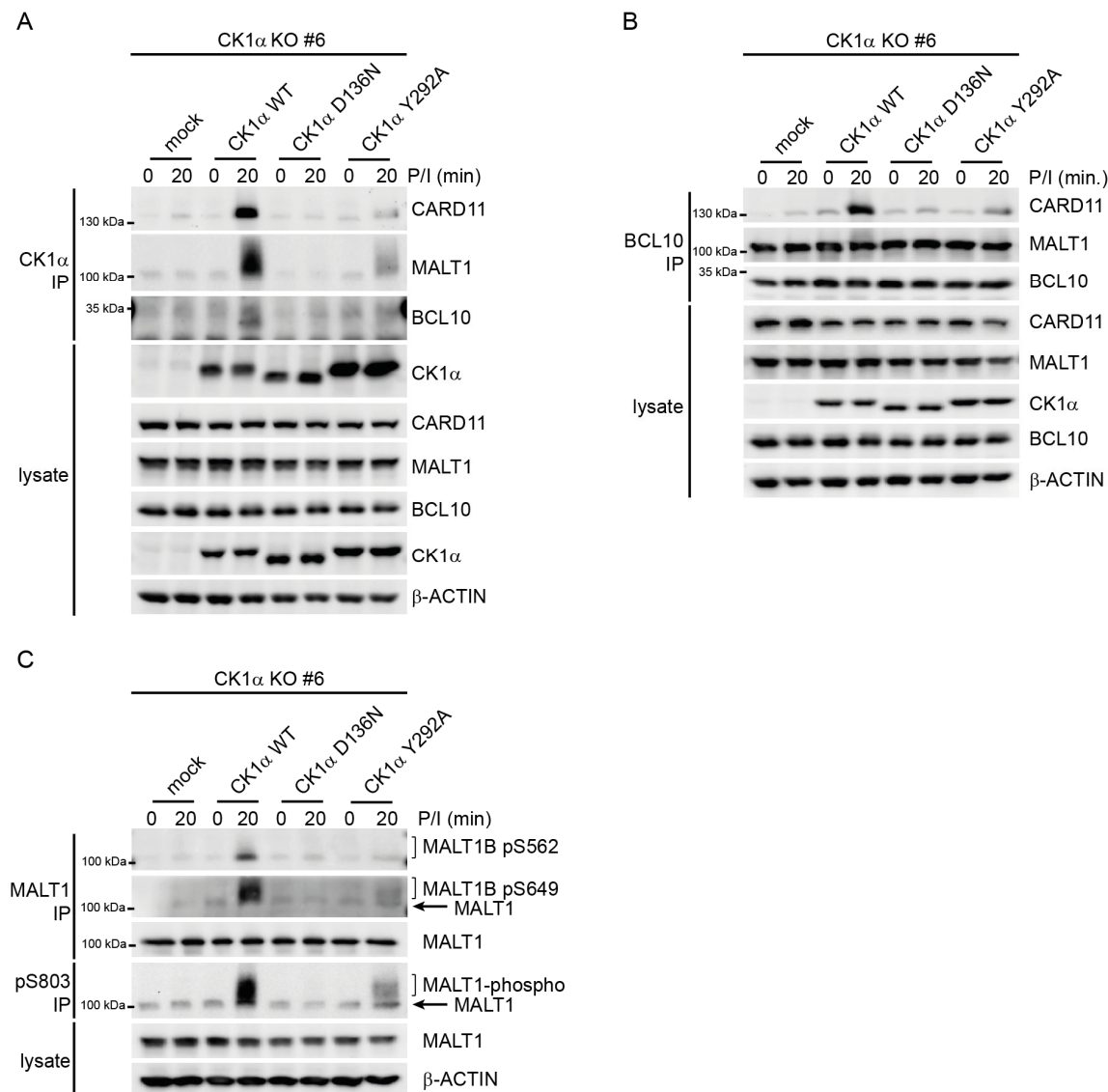
Figure 3-21: Kinase activity of CK1α is essential for CBM assembly and MALT1 phosphorylation. A) CK1α recruitment to CARD11, BCL10 and MALT1 was determined by anti-CK1α–IP and WB in CK1α-deficient Jurkat T cells reconstituted with CK1α WT, kinase-dead D136N mutant or CARD11-binding Y292A mutant. B) Requirement of CK1α kinase activity and CARD11 binding for CBM complex formation was monitored by BCL10-IP and WB in Jurkat T cells expressing CK1α WT, D136N or Y292A. C) Analyses of MALT1 phosphorylation on S562, S649 and S803 in Jurkat T cells expressing CK1α WT, D136N or Y292A.

Introducing CK1α WT into these deficient cells could restore the complete functionality of CBM complex formation. Upon P/I stimulation, CK1α WT binds to CARD11, MALT1 and BCL10 (Figure 3-21A). In contrast, both kinase-dead (D136N) and CARD11-binding (Y292A) mutants displayed severely reduced association with the CBM complex (Figure 3-21A). Indeed, CK1α catalytic activity and binding to CARD11 were not only required for its recruitment to CARD11, BCL10 and MALT1, but were also essential for the formation of the entire CBM complex, as evident after BCL10-IP (Figure 3-21B). In line, the loss of C-terminal MALT1 phosphorylation could also not be rescued by introduction of the mutants (Figure 3-21C). Whereas expression of the CK1α CARD11-binding defective (Y292A) variant resulted in strongly reduced CBM assembly and MALT1 phosphorylation, the catalytically inactive (D136N) mutant completely impaired CBM signaling, indicating that catalytic activity of CK1α is essential and was the main reason for failed assembly.

Coinciding with impaired CBM assembly and MALT1 phosphorylation, NF-κB and JNK signaling, as well as MALT1 protease activation, were severely impaired in the absence of CK1α catalytic activity or impaired CARD11 recruitment (Figure 3-22). While preventing CK1α-CARD11 interaction by the expression of CARD11 Y292A mutant led to strongly decreased IκBα phosphorylation and degradation after CD3/CD28 and P/I stimulation (Figure 3-22A), introduction of the kinase-dead (D136N) CK1α resulted in complete loss of IKK/NF-κB signaling (Figure 3-22B). Furthermore, MALT1 paracaspase activity was reduced or diminished respectively in CK1α mutants, indicating the essential role of CK1α not only in CBM complex formation, but also in promoting activation of MALT1 and downstream signaling (Figure 3-22). Collectively, these results clearly show that CK1α does not only have a potential bridging function, but that its catalytic activity is also essential in T cell activation.
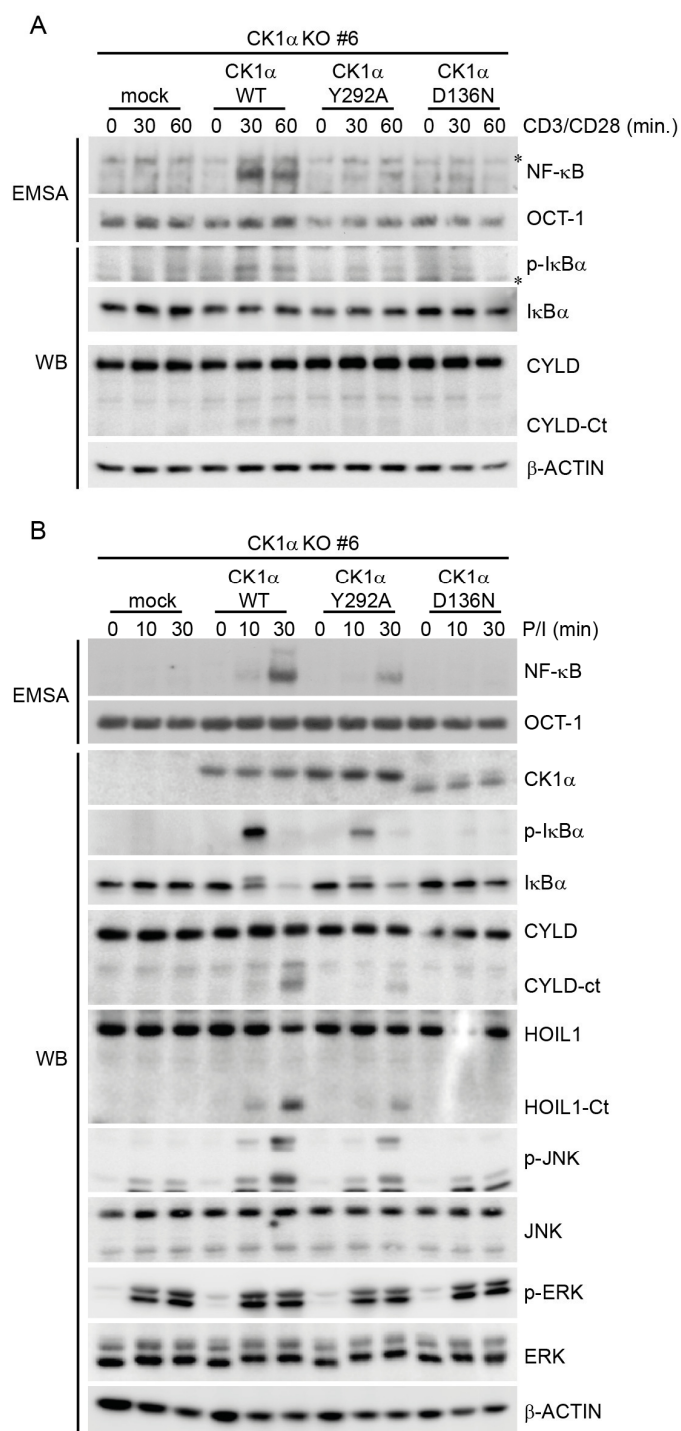
Figure 3-22: CK1α is required for full NF-κB activation. A, B) Effects of CK1α kinase-dead and CARD11-binding mutant on NF-κB signaling, and MALT1 substrate cleavage after CD3/CD28 (A) or P/I (B) stimulation were assessed by EMSA and WB. MAPK pathway activation was analyzed by Western blotting (B).

It has been demonstrated that CK1α directly associates with CARD11 and is able to catalyze inactivating phosphorylation on S608 [85]. To address whether CK1α kinase activity also regulates signaling downstream of CARD11, the oncogenic CARD11 L225LI variant was used, which bypasses the upstream processes by promoting constitutive CBM assembly and NF-κB activation [134]. In line, CK1-α was shown to constitutively associate with oncogenic CARD11 L225LI [142, 143]. Here, either CARD11 WT or oncogenic CARD11 L225LI mutant was introduced into CK1α reconstituted Jurkat T cells by electroporation. An NF-κB reporter plasmid was simultaneously transfected und used to assess NF-κB pathway activity (Figure 3-23).
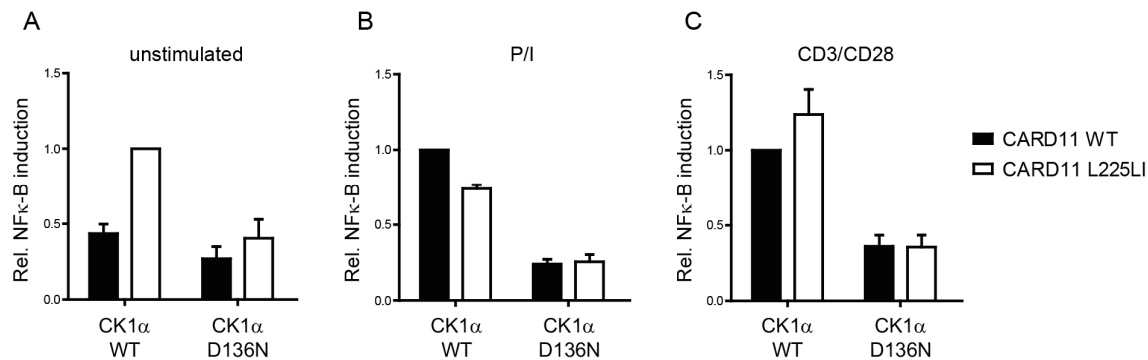
Figure 3-23: NF-κB reporter assay following transfection of CARD11 WT or L225LI mutant in CK1α-deficient Jurkat T cells reconstituted with CK1α WT or kinase-dead (D136N) mutant. NF-κB activation was determined in unstimulated cells (A) as well as after P/I (B) and anti-CD3/CD28 stimulation.

Transient expression of oncogenic CARD11 L225LI variant in CK1α WT reconstituted Jurkat T cells resulted in a more potent induction of the NF-κB reporter gene, compared to CARD11 WT. However, constitutive NF-κB activation in CARD11 L225LI-expressing cells was lost in Jurkat T cells expressing kinase-dead CK1α D136N, demonstrating that oncogenic CARD11 signaling is also mediated by CK1α kinase activity (Figure 3-23A). As expected, NF-κB activation after P/I or anti-CD3/CD28 stimulation was severely reduced in CARD11 WT- and oncogenic CARD11 L225LI-expressing cells in absence of catalytic activity of CK1α (Figure 3-23B and C). Thus, NF-κB activation by a constitutive CBM complex still relies upon CK1α activity, strongly arguing for an additional and kinase-dependent downstream function of CK1α.

3.6 NF-κB activation relies of MALT1 phosphorylation

3.6.1 Reconstitution of MALT1 KO Jurkat T cells with phospho-mutants

To investigate the contribution of MALT1 phosphorylation to CBM assembly, MALT1 protease activity and IKK/NF-κB activation, MALT1-deficient Jurkat T cells were rescued with lentiviral phospho-defective serine to alanine (S/A) mutant constructs. Because of the

close proximity to the phosphorylation sites, double mutants were generated (S559/562A, S645/649A and S803/805A) (Figure3-24).
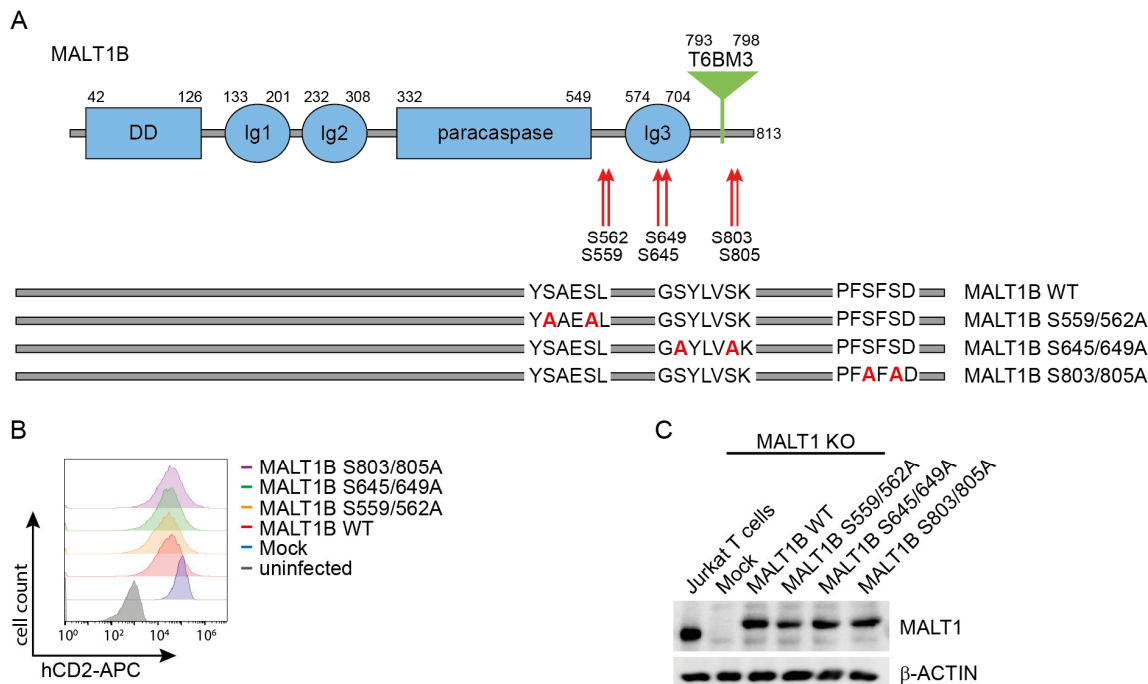
Figure 3-24: A) Structural organization of MALT1 with highlighted positions of generated mutants and amino acidic changes in the protein sequence. B) Expression of the surface marker hΔCD2 was determined by FACS. C) Protein expression levels of MALT1 S/A mutants were determined by WB.

Efficient reconstitution of MALT1 KO Jurkat T cells with lentiviral MALT1B WT and phospho-defective S/A variants was determined by expression of the co-infected surface marker hΔCD2 by FACS (Figure 3-24B) and MALT1 protein by WB (Figure 3-24C). All MALT1 constructs were expressed at similar levels as endogenous MALT1.

3.6.2 MALT1 phospho-defective mutants show reduced NF-κB activity

To determine effects on canonical NF-κB signaling, IκBα phosphorylation/degradation and NF-κB DNA binding were monitored at different time points after stimulation with P/I or CD3/CD28 in the reconstituted cells (Figure 3-25 and 3-26).

The strongest phosphorylation of IκBα could be detected after 10 min of P/I stimulation, resulting in complete IκBα degradation by 20 min in MALT1B WT reconstituted cells. Phospho-defective MALT1 S/A variants showed initial IκBα phosphorylation with similar kinetics, but IκBα degradation was impaired (Figure 3-25A). Upon CD3/CD28 stimulation, similar results were obtained, but to a lesser extent and with slightly delayed loss of IκBα protein by 30 min (Figure 3-25B).
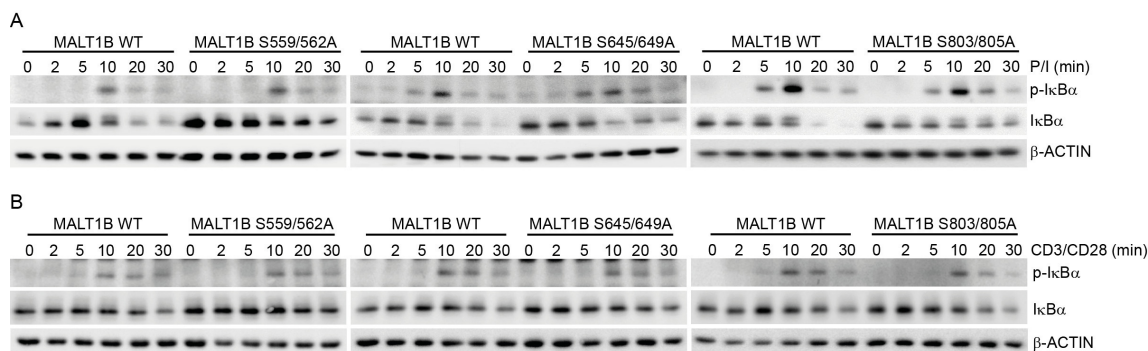
Figure 3-25: Analysis of NF-κB signaling in MALT1 S559/562A, S645/649A and S803/805A after P/I stimulation (A) and anti-CD3/CD28 stimulation (B) compared to MALT1B WT.

In line with this, NF-κB activation was also strongly reduced in cells expressing phospho-defective MALT1 S/A variants (Figure 3-26). Reduced NF-κB binding activity in MALT1 S/A mutants was not only detected in the initial phase of signaling, but also persisted up to 8h following P/I or CD3/CD28 stimulation (Figure 3-26).
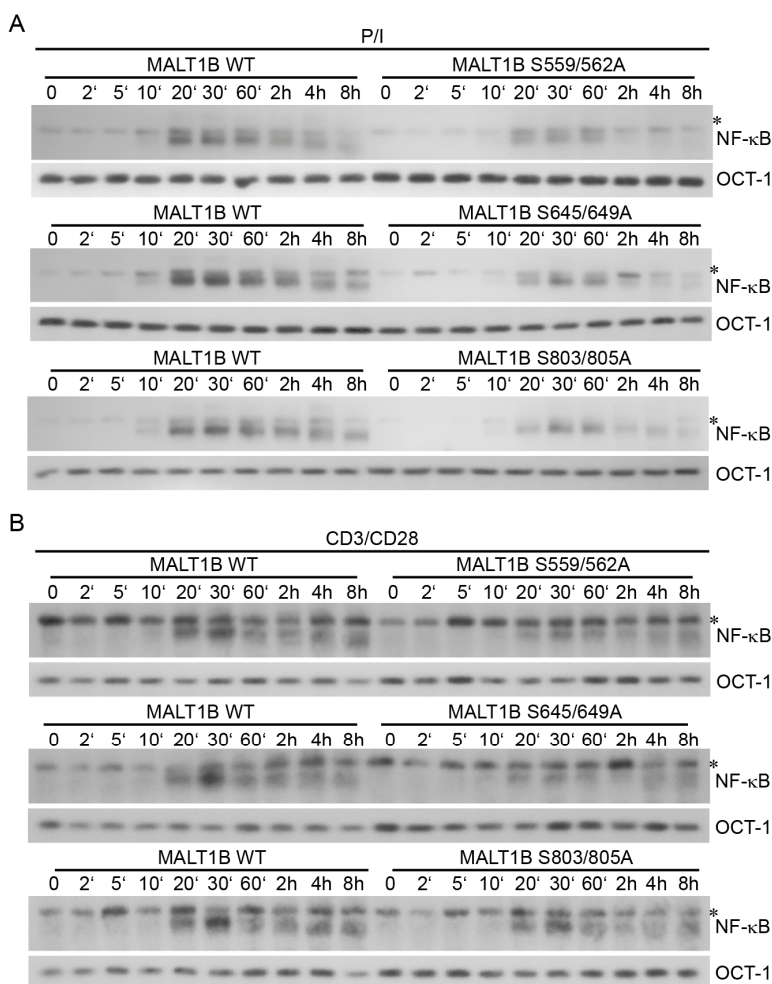
Figure 3-26: Effects of MALT1B S/A mutants on NF-κB activation after P/I (A) or CD3/CD28 (B) stimulation were investigated by EMSA. Unspecific bands are marked with asterisk.

Consistent with these results, IκBα protein expression levels in MALT1 S/A mutants were less reduced compared to MALT1B WT in longer P/I and CD3/CD28 stimulation time points (data not shown). Collectively, these data show that IκBα is stabilized in Jurkat T cells expressing phospho-defective MALT1 S/A variants.

To determine the influence of the phosphorylation sites on MALT1 paracaspase activity, MALT1 cleavage of several substrates was analyzed (Figure 3-27).
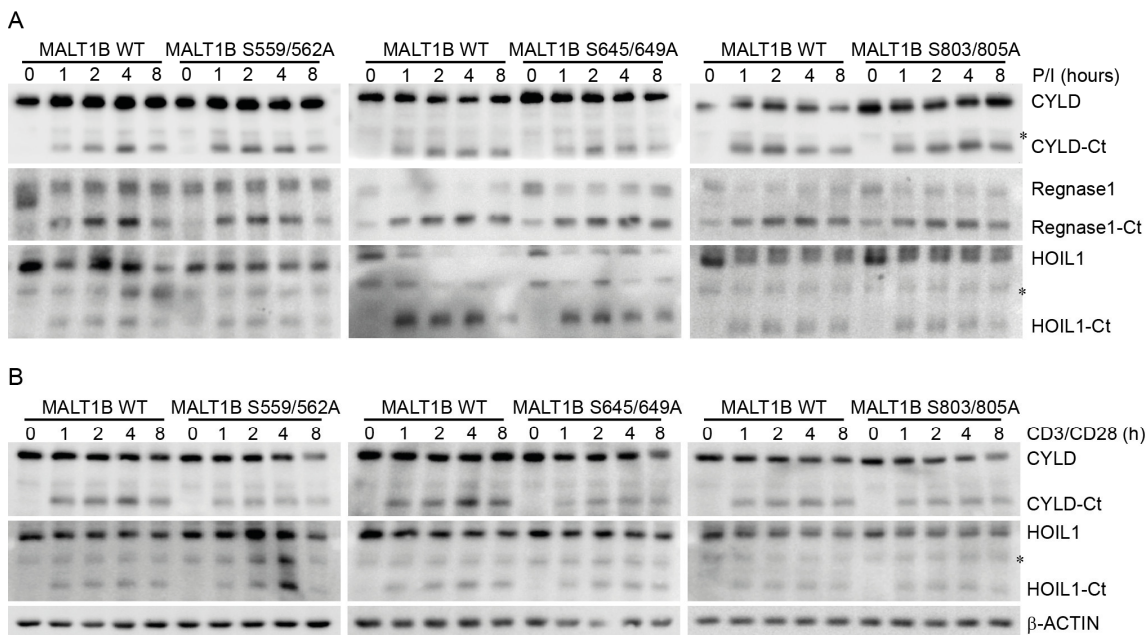
Figure 3-27: Effects of MALT1B S/A mutants on MALT1 substrate cleavage (CYLD, HOIL1 and Regnase1) after P/I (A) or CD3/CD28 (B) stimulation were investigated by Western blotting. Regnase1 cleavage could not be determined after CD3/CD28 stimulation. Unspecific bands are marked with an asterisk.

MALT1 protease activity was not altered by the phospho-defective mutations, as determined by cleavage of CLYD, HOIL1 and Regnase1 after P/I and CD3/CD28 stimulation (Figure 3-27). After 1 h stimulation, the cleavage fragments of all three substrates could be sufficiently detected by Western blotting. The amounts of the fragments were not altered compared to MALT1B WT, indicating that the identified MALT1 phosphorylation sites do not participate in the regulation of MALT1 paracaspase activity.

Furthermore, the influence of the MALT1 S/A variants in regulating MALT1-independent activation of the MAP kinase ERK, as well as MALT1-dependent p38 and JNK phosphorylation, were investigated upon P/I stimulation and analyzed by Western blotting (Figure 3-28). The activation of p38, ERK as well as JNK was unchanged in MALT1 S/A mutants compared to MALT1B WT. Thus, detected MALT1 phosphorylation sites appear to have no influence in the regulation of MAP kinase pathways, regardless of whether their activation is MALT1-dependent or independent.
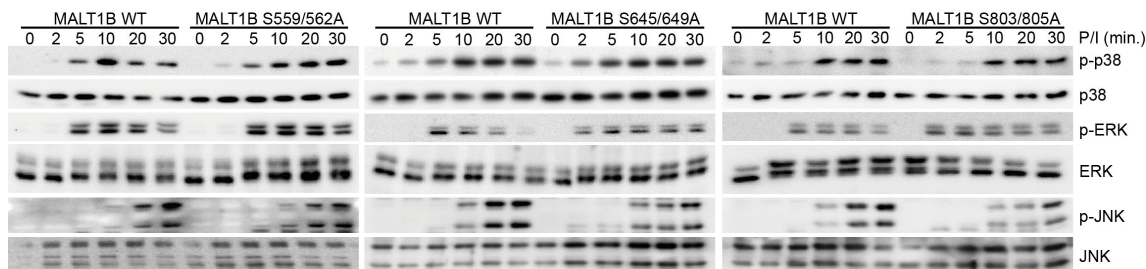
Figure 3-28: Effects of MALT1B S/A mutants on activation of MAP kinases p38, ERK and JNK after P/I stimulation were investigated by Western blotting.

To validate these results with another read-out and furthermore, to analyze whether defective MALT1 phosphorylation has an effect T cell activation, the expression of IL-2 was determined (Figure 3-29).
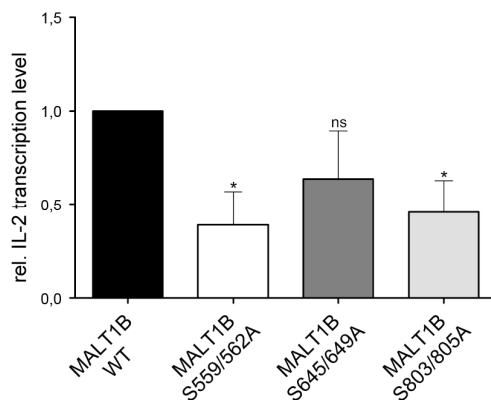
Figure 3-29: Effects of MALT1 S/A variants on IL-2 expression in reconstituted MALT1-deficient Jurkat T cells upon P/I stimulation. Levels in MALT1B WT normalized to 1.

After P/I stimulation, IL-2 expression was determined by RT-PCR. The expression in MALT1B WT was normalized to 1 and the ratios of relative levels in MALT1 S/A mutants are shown (Figure 3-29). Consistent with IκBα degradation and NF-κB activation, phospho-defective MALT1 mutants showed reduced IL-2 expression. Thus, the reduced activation of NF-κB is reflected by reduced target gene expression.

3.6.3 CBM assembly and NEMO recruitment are not altered by MALT1 S/A mutations

Previous experiments clearly showed reduced NF-κB activation in phospho-deficient MALT1 variants. It could be shown that the degradation of IκBα was changed by the MALT1 S/A mutations, indicating a role for MALT1 phosphorylation on the level of CBM complex formation or recruitment of further pathway members, for example IKKγ/NEMO. To elucidate the ongoing mechanism, MALT1 ST-PD and NEMO-IP were performed (Figure 3-30).
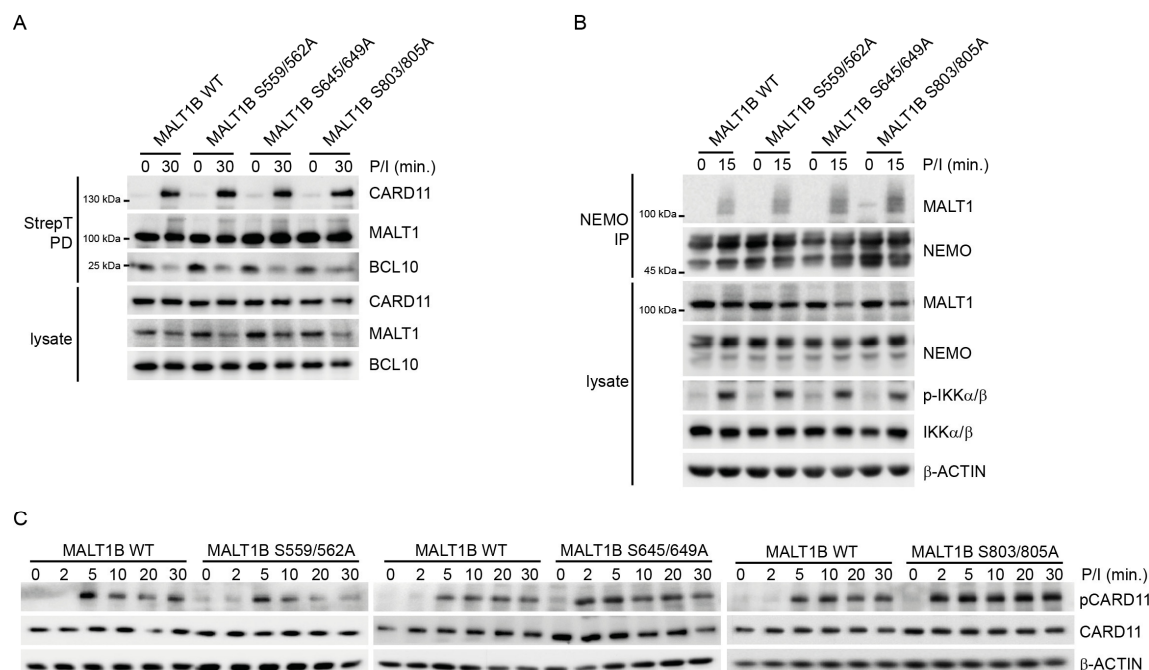
Figure 3-30: A) Determination of CBM complex formation in S/A mutants by ST-PD after P/I stimulation. B) NEMO/IKKγ recruitment to S/A mutants and IKKα/β activation after P/I stimulation.

CBM complex formation was not altered by S/A mutations compared to MALT1B WT (Figure 3-30A). In addition, the initial activation of CARD11 by phosphorylation on S645 was also not changed in cells expressing phospho-defective MALT1 S/A variants (Figure 3-30C). Furthermore, general post-translational modifications of MALT1 such as mono- or poly-ubiquitination also seemed to be not changed by introducing the S/A mutants, indicated by similar higher molecular smears following P/I stimulation (Figure 3-30A). To investigate the recruitment of IKKγ/NEMO to the CBM complex, a NEMO-IP was performed and stained for associated MALT1 variants (Figure 3-30B). MALT1 S/A mutants did not show different recruitment potential of IKKγ/NEMO and additionally, the activation of IKKα/β upon P/I stimulation was not altered by expression of phospho-defective MALT1 variants compared to MALT1B WT (Figure 3-30B).

Collectively, these data show that MALT1 phosphorylation does not participate in the regulation of CBM assembly and disassembly or affect the recruitment of the downstream mediator IKKγ/NEMO. However, IκBα degradation is strongly reduced in cells expressing MALT1 S/A mutants, indicating that MALT1 phosphorylation does not affect all MALT1 functions, but is selectively required to channel CBM signaling to IκBα degradation and the canonical NF-κB pathway.

3.7 MALT1 phosphorylation promotes NF-κB signaling in primary CD4 T cells

3.7.1 Generation of a MALT1 KO mouse

To corroborate that MALT1 phosphorylation is critical for IκBα degradation and activation of primary T cells, a retroviral transduction system was used to rescue CD4 T cells from MALT1-deficient mice with human MALT1B constructs [40, 66].

Therefore, MALT1 KO mice were established using murine embryonal stem (ES) cells targeting exon 3 of MALT1 (Malt1$^{tm1a(EUCOMM)Hmgu}$) generated by the European Conditional Mouse Mutagenesis Program (EUCOMM). In cooperation with Dr. Florian Giesert from the Institute of Developmental Genetics from the Helmholtz Center Munich, ES cells were injected into blastocysts from C57/BL6N mice.

Two loxP sites for the recombinase Cre were introduced into the genome of the ES cells flanking MALT1 exon 3. Furthermore, a lacZ promotor and a neomycin cassette flanked by FRT sites for the recombinase Flp were integrated into the genomic DNA to enable the identification of positive ES cell clones (Figure 3-31).

Malt1$^{tm1a(EUCOMM)Hmgu}$

Figure 3-31: Schematic organization of the genomic MALT1 locus with integrated lacZ and neomycin cassettes flanked by FRT sites and loxP sites. Exon 3 is also flanked by loxP sites, allowing the deletion of this exon by appropriate breeding.

Born chimera mice were bread with R26-Flp-deleter mice leading to a deletion of the lacZ reporter and the neomycin cassette. Afterwards, the offspring was bred to R26-Cre-deleter mice resulting in a heterozygous loss of MALT1 exon 3. Mating of heterozygous mice with one another yielded a ratio of homozygous, heterozygous and WT mice in accordance with Mendel's rules.

3.7.2 MALT1 deficiency impairs differentiation into B1 and MZ B cells as well as into Treg cells

First, the phenotype of newly generated MALT1 Ex3 KO mice was compared to already established MALT1 KO mice with regard to the immune system [110, 111].

The development of T cells in the thymus was not changed in heterozygous and homozygous MALT1-deficient mice compared to WT littermates. A normal distribution of double negative, double positive and single positive T cells, respectively, was observed (Figure 3-32A and B). Furthermore, maturation of T cells into single positive T cells could be

determined at comparable levels to WT littermates in the spleen and lymph nodes (LN) (Figure 3-32A and B).
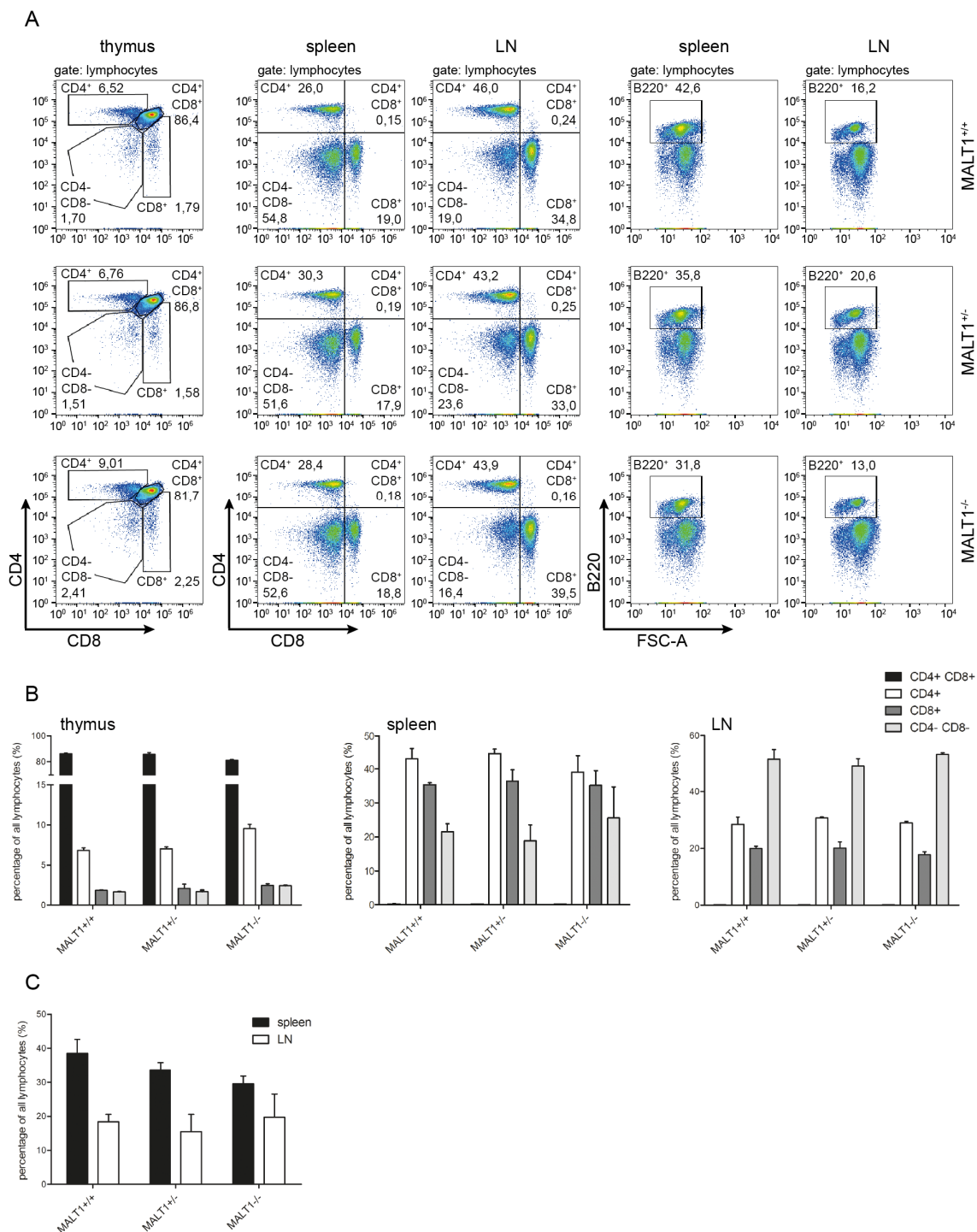
Figure 3-32: Differentiation into T and B lymphocytes. A) Evaluation of differentiation and maturation of T cells in the thymus, spleen and lymph nodes (LN) as well as of B cells in the spleen and LN of heterozygous and homozygous MALT1 KO mice compared to WT littermates. B) Frequency of distinct T cell populations in thymus, spleen and LN are shown. C) Analysis of B cell population in spleen and LN.

In addition, the amount of B cells in the spleen and LN was also not altered in heterozygous or homozygous MALT1 KO mice compared to WT littermates (Figure 3-32A and C). Collectively, these data fit to published MALT1 KO phenotypes [110, 111], indicating that MALT1 deficiency has no influence in T and B cell development and maturation.

The MALT1 knockout mice published by Ruland et al. and also Ruefli-Brasse et al. showed that MALT1 deficiency led to the loss of FoxP3$^+$ T$_{reg}$ cells in the spleen, LN and thymus, as well as loss of B1 B cells in the peritoneal cavity. Furthermore, a strong reduction in marginal zone (MZ) B cells in the spleen was observed in these mice [110, 111]. So, the composition of these cell types was investigated in the newly generated MALT1 Ex3 KO mouse (Figure 3-33).
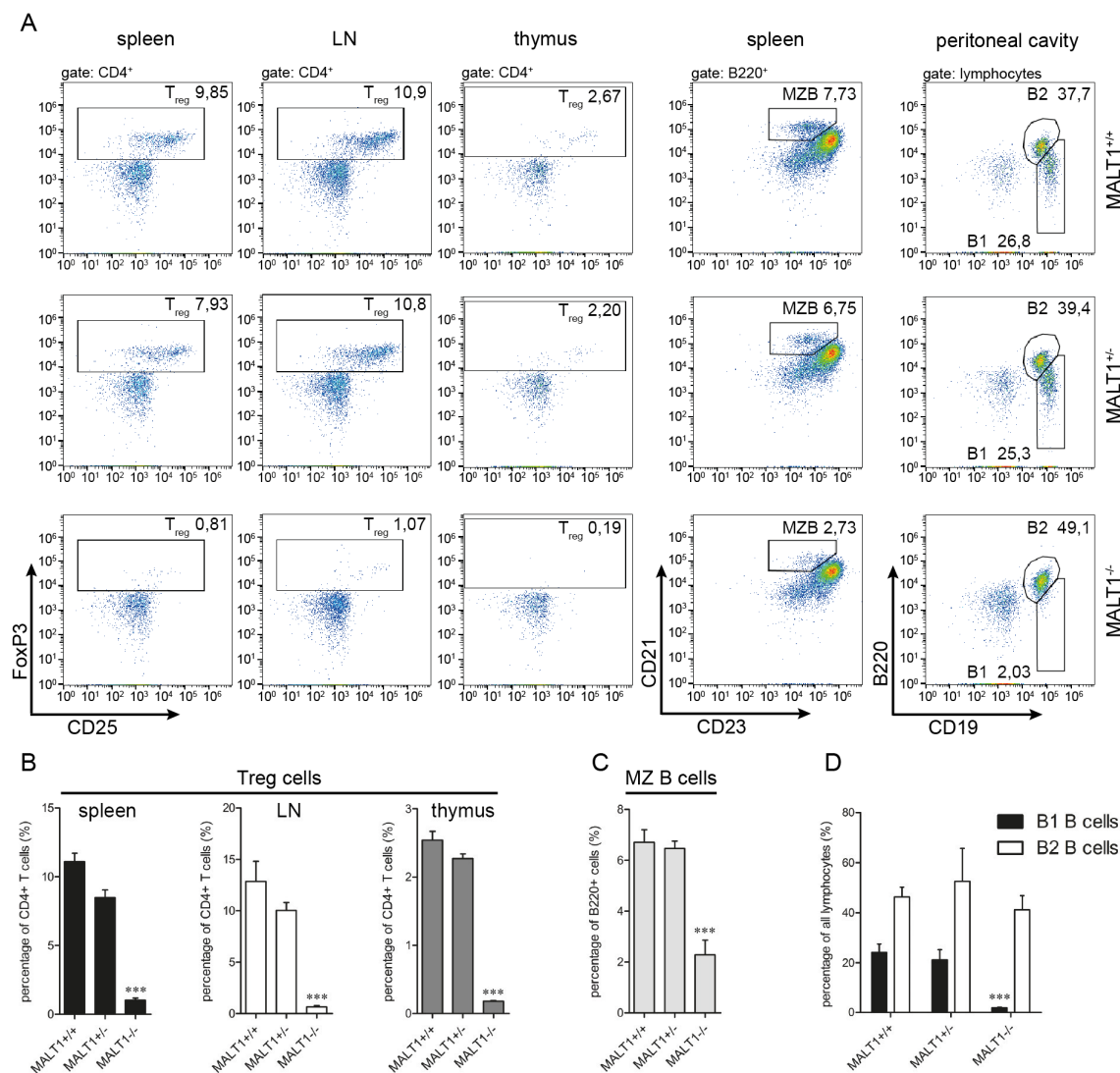
Figure 3-33: A) T$_{reg}$ formation in the spleen, lymph nodes and thymus was determined by FACS. Furthermore, the fraction of marginal zone (MZ) B cells in the spleen and B1 B cell levels in peritoneal cavity were determined. B) Percentage of T$_{regs}$ in the spleen, LN and thymus are indicated. A mean ± SD of four biological replicates is shown (*** $p < 0.0005$). C) Frequency of MZ B cell levels in the spleen. A mean ± SD of four biological replicates is shown (*** $p < 0.0005$). D) Comparison of the

amounts of B1 and B2 B cells in the peritoneal cavity. A mean ± SD of four biological replicates is shown (*** $p < 0.0005$).

Whereas heterozygous deficiency of MALT1 did not affect cell differentiation into regulatory T cells, MZ or B1 B cells, homozygous MALT1 KO mice exhibited a strong reduction in all three cell populations compared to WT littermates (Figure 3-33). Statistical analyses showed a severe reduction in Treg formation in the spleen, LN and thymus as well as B1 B cells in peritoneal cavity (Figure 3-33B and D). Furthermore, there was a significant decrease in MZ B cells in MALT1 KO mice compared to WT littermates (Figure 3-33C). In contrast, B2 B cells were not affected by MALT1 deficiency (Figure 3-33A and D).

Taken together, the validation of the generated MALT1 KO mice clearly indicates the essential role of MALT1 in T cell differentiation and thus in the formation of Tregs, MZ and B1 B cells. The detected phenotype of the newly generated MALT1 Ex3 KO mice is similar to the published phenotypes and allows the use of these mice for further experiments.

3.7.3 MALT1 deficiency impairs T cell activation

CD4 T cells were isolated from spleen and stimulated with P/I for the indicated times. MALT1 protein expression was determined and simultaneously NF-κB activation was checked, as evidenced by IκBα phosphorylation and degradation. Efficient loss of MALT1 protein could be observed in CD4 T cells isolated from MALT1 KO mice (Figure 3-34). In contrast, heterozygous genomic knockout of MALT1 did not result in a reduction in MALT1 protein levels. Whereas CD4 T cells isolated from heterozygous mice as well as WT littermates still reacted to P/I stimulation and clearly showed IκBα degradation, T cells isolated from homozygous MALT1 KO mice did not respond to stimulation and did not show phosphorylation or degradation of IκBα (Figure 3-34). Therefore, it could be shown that MALT1 is essential for T cell activation.
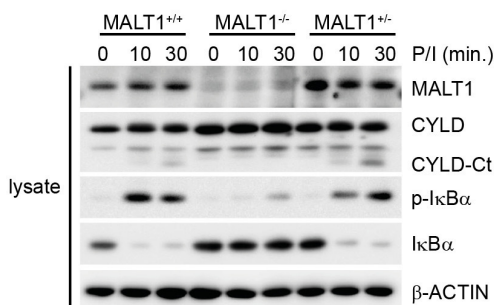
Figure 3-34: MALT1 expression was determined in CD4 T cells isolated from heterozygous and homozygous MALT1 KO mice as well as WT littermates by WB. Furthermore, no IκBα phosphorylation and degradation could be observed in MALT1 KO CD4 T cells after P/I stimulation.

3.7.4 BCL10-MALT1 association is essential for NF-κB signaling

Recently, Dr. Florian Schlauderer and Dr. Katja Lammens of the Gene Center Munich at the LMU could resolve the structure of the BCL10-MALT1 filament using cryo-electron

microscopy at a resolution of 4.9 Å, adding new insights into the association of BCL10 to MALT1 [63]. In this study, the direct interface between BCL10 and MALT1 with V81 and L82 as central interacting residues of MALT1 could be identified. In a cooperation with our group, structure-guided mutations were introduced to show that point mutations of these interaction sites disrupted the BCL10-MALT1 interaction and thereby, completely impaired CBM complex assembly, MALT1 activation and subsequent IKK/NF-κB induction in Jurkat T cells [63].

To strengthen the data obtained in Jurkat T cells, primary CD4 T cells were reconstituted with MALT1B WT and respective variants. Retroviral MALT1 construct are directly linked to a Thy1.1 surface marker by an internal ribosomal entry site (IRES) sequence, which allows selection of positively infected cells in FACS analyses. Whereas reconstitution of MALT1B rescued stimulus-dependent IκBα loss and IL-2 expression upon stimulation, no IκBα degradation or IL-2 expression could be observed in cells reconstituted with an empty mock control (Figure 3-35). In addition, Thy1.1-negative CD4 T cells failed to respond to stimulation (Figure 3-35). Therefore, it could be assumed that detected effects result from introduced MALT1 variants and thereby allow monitoring of effects of mutations in a near to physiological setting.
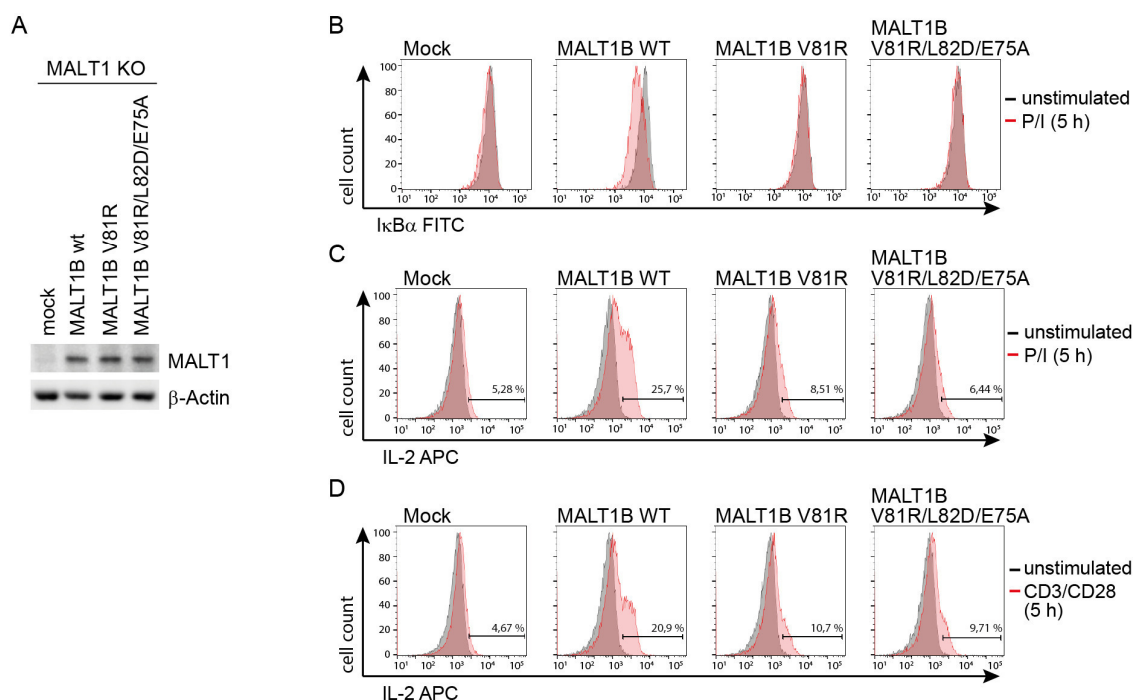
Figure 3-35: Comparison of single cell analyses of IκBα degradation and IL-2 expression in Thy1.1-negative and -positive CD4 T cells reconstituted with either empty mock control or MALT1B WT. FACS analyses were performed after P/I stimulation. To determine IκBα degradation, cells were stimulated for 20 min with P/I. IL-2 expression was detected after 5h P/I stimulation.

Subsequently, primary CD4 T cells were equally reconstituted with MALT1B WT, MALT1B V81R and V81R/L82D/E75A mutants, which disrupted the BCL10-MALT1 interface [63] (Figure 3-36).
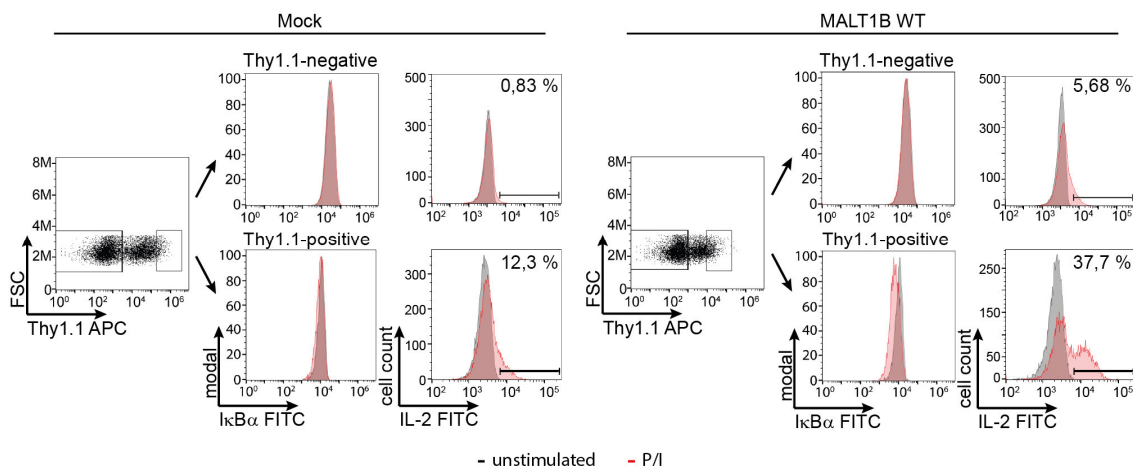
Figure 3-36: A) MALT1 protein expression of MALT1B WT and BCL10-MALT1 interface mutants was determined in WB. All variants are expressed at similar levels. B) Single cell analyses of IκBα protein levels, prior to and following P/I stimulation, was analyzed in CD4 T cells reconstituted with MALT1B WT and interface mutants by intracellular staining and FACS. C) Single cell analyses of IL-2 production, prior to and following, P/I stimulation, was analyzed in MALT1B WT and interface mutant reconstituted CD4 T cells by intracellular staining and FACS. D) Single cell analyses of IL-2 production, prior to and following CD3/CD28 stimulation, was analyzed in MALT1B WT and interface mutant reconstituted CD4 T cells by intracellular staining and FACS.

Whereas reconstitution of MALT1B rescued stimulus-dependent IκBα loss upon stimulation, no IκBα degradation could be observed in cells reconstituted with MALT1B V81R and MALT1B V81R/L82D/E75A. In line, IL-2 expression was strongly decreased in mutants upon P/I and CD3/CD28 stimulation, indicating impaired IKK/NF-κB signaling (Figure 3-36) [63]. Thus, data obtained in primary CD4 T cells supported the results observed in Jurkat T cells revealing that constitutive BCL10-MALT1 association is essential for CBM assembly and NF-κB activation [63]. Collectively, these experiments were also used to verify the retroviral transduction system, and to prove that detected effects are caused by introduced MALT1 before MALT1 phospho-defective MALT1 S/A variants were investigated.

3.7.5 MALT1 phosphorylation promotes IκBα degradation and NF-κB signaling

To investigate the impact of MALT1 phosphorylation in IκBα degradation and activation of primary CD4 T cells, MALT1B WT and phospho-defective mutants were retrovirally introduced into MALT1 KO CD4 T cells [40, 66]. In addition to MALT1B S559/562A, S645/649A and S803/805A used in previous experiment, a retroviral MALT1B phospho-defective mutant that lacks all six potential phospho-acceptor serine (MALT1B 6xS/A) was included in the analyses (Figure 3-37). Analysis of the expression of the surface marker

Thy1.1 was used to monitor the infection efficiency of CD4 T cells with MALT1B variants (Figure 3-37). In addition, Thy1.1 was used for selection to analyze single cells in FACS experiments.
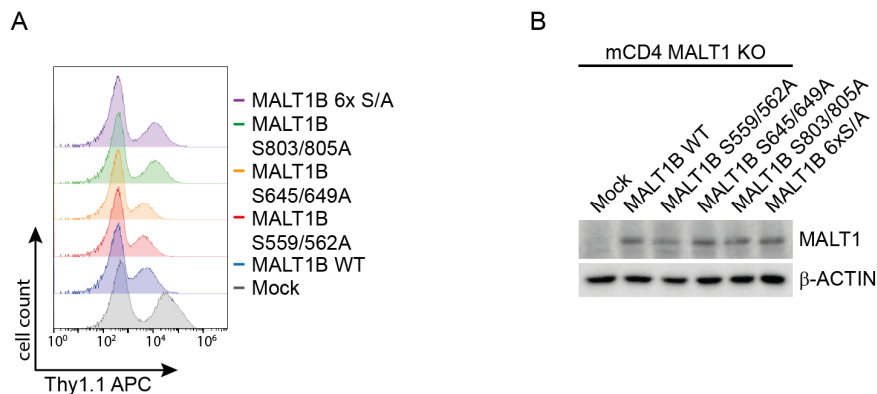
Figure 3-37: A) FACS analysis of Thy1.1 surface marker to determine the infection efficiencies. B) After enrichment of high Thy1.1-positive cells by MACS sorting, Western blotting revealed that MALT1 variants are expressed at similar MALT1 protein levels.

Infection efficiencies of 30 – 50% were achieved for the different constructs (mock, WT and S/A mutants) (Figure 3-37A). Enrichment of high Thy1.1-positive cells using magnetic cell sorting system (MACS, Miltenyi) and subsequent Western blotting revealed that MALT1 constructs are expressed at similar levels (Figure 3-37B).

Impact of MALT1B phospho-defective mutants in NF-κB signaling in CD4 T cells were determined by IκBα expression in single cells prior to and upon 20 min P/I stimulation (Figure 3-38A and B). Whereas reconstitution with MALT1B WT rescued stimulus-dependent IκBα loss, empty mock control did not respond to stimulation as also previously described (Figure 3-36 and 3-38A and B). IκBα degradation was still detectable in the MALT1B-phospho-defective mutants S559/562A, S645/649A and S803/805A, but significantly less pronounced when compared to MALT1B WT (Figure 3-38A and B). Strongest effects were detected using MALT1B S803/805A. In addition, MALT1B 6xS/A was included in this analysis and displayed even further enhanced stabilization of IκBα after P/I stimulation of CD4 T cells (Figure 3-38A and B).
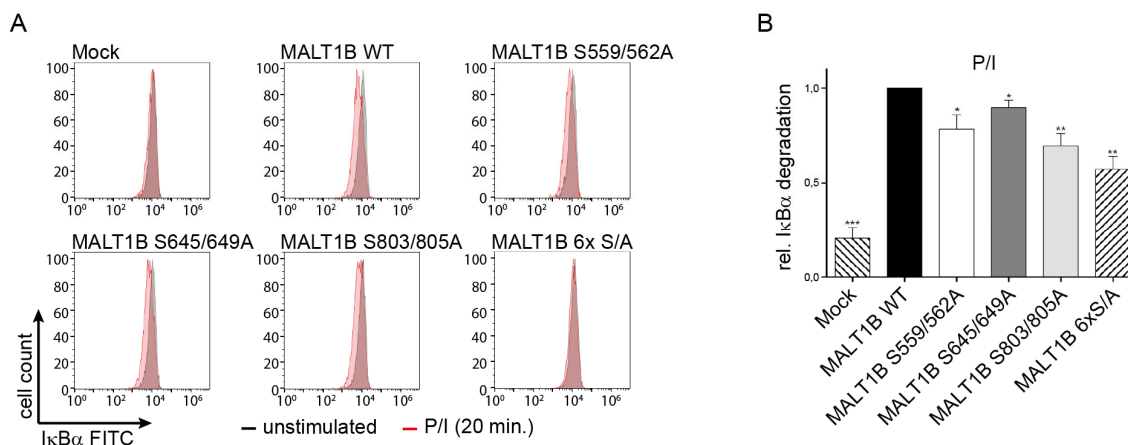
Figure 3-38: A, B) Single cell analyses of IκBα protein levels prior to and after P/I stimulation was analyzed in MALT1B WT and S/A mutant reconstituted CD4 T cells by intracellular staining and FACS (A). Median fluorescence intensity of IκBα-FITC was quantified and induction of IκBα degradation was determined by comparing the ratio of unstimulated to stimulated cells. Relative IκBα degradation between MALT1B WT and S/A mutant cells was compared and statistically analyzed (B). The data represent the mean ± SD of 6 independent experiments (* $p < 0.05$, ** $p < 0.005$, *** $p < 0.0005$).

To analyze whether defective MALT1 phosphorylation affects T cell activation, intracellular IL-2 expression was measured by FACS in reconstituted CD4 T cells after CD3/CD28 or P/I stimulation (Figure 3-39). Whereas expression of MALT1B WT rescued induction of IL-2 in MALT1 KO CD4 T cells, upregulation of IL-2 was significantly impaired in the double phospho-defective mutants and even more severely reduced in MALT1B 6xS/A mutant (Figure 3-39). The impact of MALT1B S559/562, S645/649 or S803/805A did not differ compared to each other, but combinatory MALT1B 6xS/A mutant resulted in strongly reduced IL-2 expression, indicating additive effects of identified C-terminal MALT1 phosphorylations in triggering optimal NF-κB activation and IL-2 production (Figure 3-38 and 3-39).
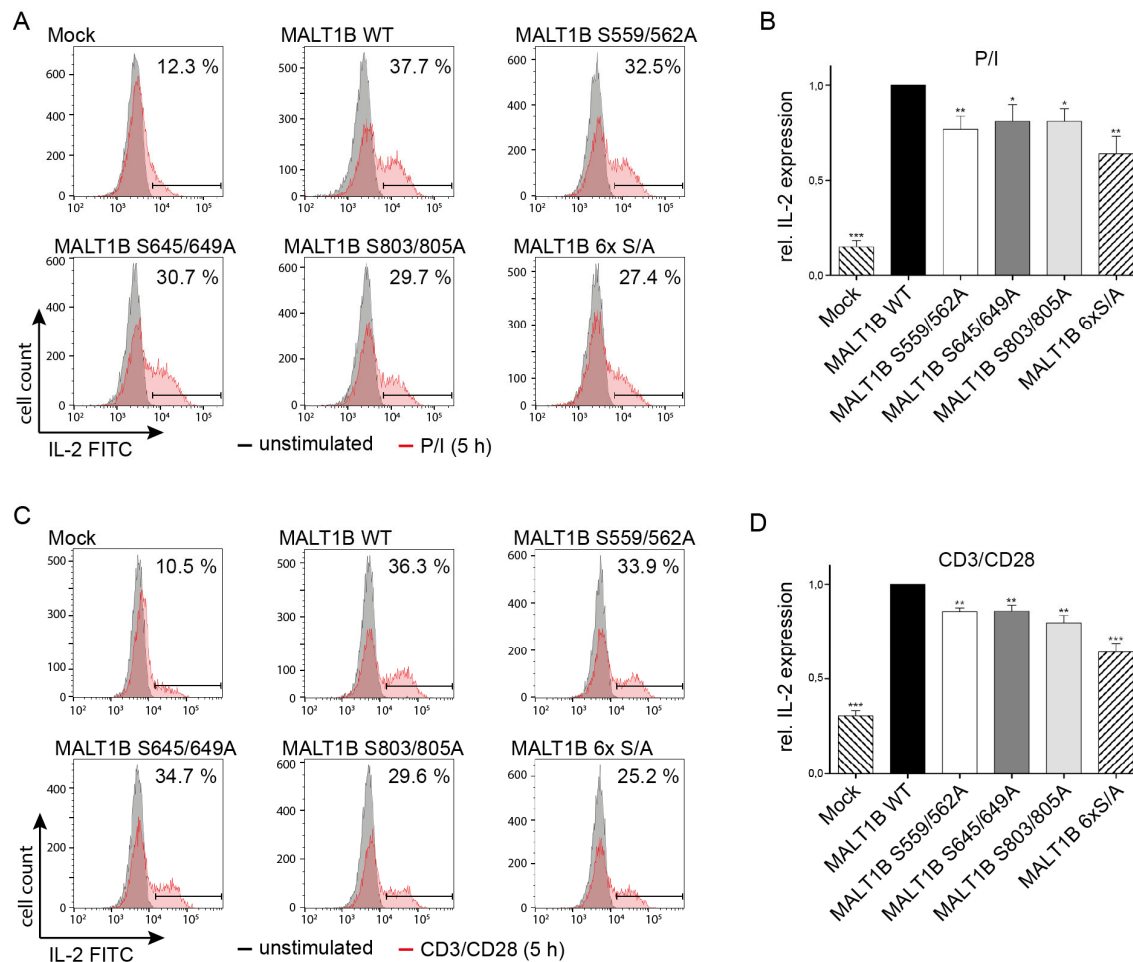
Figure 3-39: A, B) Single cell analyses of IL-2 production prior to and after P/I stimulation was analyzed in MALT1B WT and S/A mutant CD4 T cells by intracellular staining and FACS (A). Median fluorescence intensity of IL-2-FITC was quantified and IL-2 induction was determined by the percentage of IL-2 expressing cells in unstimulated and stimulated cells. Relative IL-2 induction between MALT1B WT and S/A mutant cells was compared and statistically analyzed (B). The data represent the mean ± SD of 6 independent experiments (* $p < 0.05$, ** $p < 0.005$, *** $p < 0.0005$). C, D) Single cell analyses of IL-2 production prior to and after CD3/CD28 stimulation was analyzed in MALT1B WT and S/A mutant reconstituted CD4 T cells by intracellular staining and FACS (C). Median fluorescence intensity of IL-2-FITC was quantified and IL-2 induction was determined by the percentage of IL-2 expressing cells in unstimulated and stimulated cells. Relative IL-2 induction between MALT1B WT and S/A mutant cells was compared and statistically analyzed (D). The data represent the mean ± SD of 6 independent experiments (** $p < 0.005$, *** $p < 0.0005$).

4   Discussion

Antigen stimulation of T cells through TCR engagement induces the activation of several signaling pathways that act in concert to eventually result in cytokine production, differentiation, proliferation and survival of T lymphocytes. One of the main players in T cell activation is the NF-κB pathway, in which the CARD11-BCL10-MALT1 (CBM) complex serves as an essential step bridging proximal TCR signaling to downstream IKK/NF-κB activation. As part of the CBM complex, MALT1 is a crucial regulator in this pathway, exerting a dual role operating as a scaffold and exhibiting proteolytic activity.

In this study, several lines of evidence were provided that support a model in which the regulation of MALT1 scaffolding function is controlled by phosphorylation, in addition to poly-ubiquitination. First, several novel MALT1 phosphorylation sites could be identified in a mass spectrometry approach. Second, it was shown, using phospho-specific antibodies, that MALT1 is hyper-phosphorylated at multiple sites upon T cell activation. In addition, kinetic analyses suggested that the peak of phosphorylation coincides with the activation of CBM-mediated NF-κB signaling. Third, CBM-associated CK1α was identified as a potential MALT1 protein kinase, whose catalytic activity is essential for CBM complex formation as well as triggering downstream signaling. Fourth, MALT1 phospho-defective S/A variants were severely impaired in rescuing NF-κB signaling and T cell activation in MALT1-deficient Jurkat T cells or murine CD4 T cells. Finally, it was shown that MALT1 is chronically phosphorylated is ABC DLBCL cells that are addicted to constitutive BCR signaling, indicating that MALT1 phosphorylation is not exclusive to TCR stimulation.

4.1   MALT1 is hyper-phosphorylated upon T cell activation

Upon TCR engagement, MALT1 is prone to multiple covalent modifications as evident by severely retarded migration of MALT1 in denaturing gels [40, 85]. To date, MALT1 modifications have been assigned to regulatory K63-linked poly-ubiquitination on multiple C-terminal lysines and mono-ubiquitination on K633 regulating NF-κB and MALT1 protease activation, respectively [40, 75, 147]. In this study, C-terminal MALT1 phosphorylation could be shown to participate in the regulation of MALT1 functions.

4.1.1 Detection of MALT1 phosphorylation sites

Using TiO$_2$-bead enrichment, five novel MALT1 phosphorylation sites could be identified corresponding to MALT1B S559, S562, S645, S649 and S803 in an unbiased, qualitative mass spectrometry approach. Sites were detected on three separate phosphorylated peptides. While unmodified peptides could also be detected in unstimulated cell samples, phosphorylation sites could only be mapped upon T cell stimulation, revealing a clear stimulation-dependency of detected sites.

Numerous studies have demonstrated that all three members of the CBM complex, CARD11, BCL10 and MALT1, are heavily modified and carefully regulated by post-

translation modifications. Thereby, C-terminal MALT1 was shown to be modified at multiple sites by K63-linked poly- and mono-ubiquitination upon stimulation [40, 75, 147]. However, mass spectrometry was never performed to detect ubiquitination in any of these studies. To date, acceptor sites have only been identified in mutational analysis, and corresponding variants were further examined. Thus, this study provides the first approach that resulted in determination of stimulation-dependent MALT1 modifications using targeted mass spectrometry and subsequent analysis. Prior to this work, only a few MALT1 phosphorylation sites had been identified, and these were only detected in global proteomic approaches without further investigation into their regulation or functions [148-150]. Further, the majority of these proteomic approaches were not performed in lymphocytes, but instead in whole human liver tissues [148], human breast cancer cells [149] or HeLa cells [150] without any stimulation. These studies reported N-terminal MALT1 phosphorylation at S42, S70 and S123. However, considering the structure of BCL10/MALT1 heterodimers and the integration of MALT1 into BCL10-filaments, these sites, if any, seem to affect only the MALT1 that is not included in CBM assembly, but are negligible for CBM-integrated MALT1 (Figure 4-1).

The only study of MALT1 phosphorylation in lymphocytes was performed in a murine A20 B lymphocyte cell line after BCR stimulation in a quantitative SILAC mass spectrometry approach. In this work, the sites S645 and S803 were identified at the same time as mass spectrometry analyses in Jurkat T cells were performed for this work [151]. However, no further analyses of the function of MALT1 phosphorylation in regulation of BCR signaling were pursued, but nevertheless these data confirmed two of the sites also detected by us. Interestingly, it is difficult to obtain a decent coverage of MALT1 peptides by mass spectrometry in general. Using MALT1-IP to enrich for the protein and subsequent LC-MS/MS analysis resulted in a protein coverage of only 31 % after trypsin digestion. Combination with other digestive enzymes such as chymotrypsin or Lys-C increased coverage up to 50 to 60 %, but still peptides from the C-terminus of MALT1 were underrepresented (data not shown). MALT1 peptides, which were generated from digestion of immunoprecipitated MALT1, had an average length of 16 to 18 amino acids and tended to be alkaline, potentially resulting in poor flight behavior in mass spectrometry. Furthermore, the C-terminal part of MALT1 has been previously shown to be heavily modified by mono- and/or poly-ubiquitination, leading to multiple modified peptides, which may complicate the detection of peptides. In addition, ubiquitin-coupled lysines are not recognized by trypsin and therefore typical cutting sites may be lost, resulting in even larger peptides. Collectively, these facts demonstrate that MALT1 is difficult to detect in mass spectrometry revealing reasons why no MALT1 post-translational modifications have been identified by MS to date.

In line, the MALT1 peptide detected for S803 did not allow for a clear differentiation between S803 and S805 phosphorylation in several runs. Whereas S803 could be clearly identified with high confidence, the phosphorylation of S805 could not be detected with high probability, but also not excluded (Figure 3-4 and 3-5). It is conceivable that there is a chronology in S803 and S805 phosphorylation resulting in a peptide that is modified at multiple sites, thereby leading to inaccurate detection. Overall, this work clearly proves that MALT1 is not only ubiquitinated, but also hyper-phosphorylated at multiple sites upon T cell stimulation.

Interestingly, the detected MALT1 phosphorylation events were restricted to the region C-terminal of the paracaspase domain, consisting of the Ig3 and a small remaining part comprising T6BM3 [66]. As observed in the structure resolved by cryo-electron microscopy, BCL10 filaments are built in a strictly regulated architecture, where they form helical filaments with a left-handed symmetry and three to four BCL10 subunits per turn. MALT1 binds to the CARD domain of BCL10 via its N-terminal DD in a 1:1 stoichiometry decorating

Figure 4-1: Structural organization of MALT1 domains in the context of the BCL10-MALT1 filament. A) MALT1 associates with BCL10 via its DD and the C-terminus emanates from the inner core forming a flexible outer surface. B) BCL10 and MALT1 interaction site I (BM-I) shown as ribbon model in blue (BCL10) and orange (MALT1), respectively. The interacting residues are shown in stick representation. C) BCL10-MALT1 form a 'paddle-wheel-structure' as revealed by cryo-EM with a density filtered to 25 Å. Protruding MALT1 C-terminus is heavily modified and represents a platform for the recruitment of further mediator. Adapted from Schlauderer et al., 2018 [63].

the outside of the filaments [62, 63]. Thereby, the MALT1 C-terminus protrudes out from the inner core of the filaments and forms a 'paddle-wheel-structure' representing a flexible platform for the recruitment of further mediators (Figure 4-1A and C). Thus, it is reasonable that reported MALT1 modifications (mono- and poly-ubiquitination) are restricted to the MALT1 C-terminus [40, 75, 147] and also identified MALT1 phosphorylation sites S559,

S562, S645, S649 and S803 are located in this part connecting the CBM complex to other signaling members as well as protease substrates (Figure 4-1C). Interestingly, MALT1 phosphorylation events detected in the other mentioned studies (S42, S70 and S123) are located in the DD and are therefore protected in reported filament structures from association with protein kinases (Figure 4-1A) [148-150]. In these studies, cells were not stimulated and therefore, MALT1 is most likely phosphorylated at these sites in a basal manner and prior to BCL10 filament formation, but the biological relevance of these N-terminal sites has not been investigated to date.

In the binding interface of BCL10 and MALT1, V81 and L82 were identified as central interacting residues of MALT1 and L104 as an essential site of BCL10 (Figure 4-1B) [63]. Point mutations of these interaction sites disrupted the BCL10-MALT1 interaction and thereby impaired CBM complex assembly, MALT1 activation and subsequent IKK/NF-κB induction in Jurkat T cells [63]. In line, IκBα degradation and IL-2 expression were impaired in primary MALT1 KO CD4 T cells reconstituted with respective MALT1 mutants as shown in this study (Figure 3-36). Collectively, these data show that constitutive association of BCL10 and MALT1 is a prerequisite for CBM assembly and for intact NF-κB signaling.

4.1.2 Regulation of MALT1 phosphorylation

In order to analyze the phosphorylation sites identified by mass spectrometry in more detail and determine their biological functions, phospho-specific antibodies against MALT1B S562, S649 and S803 were generated, allowing for the detection of the kinetics of MALT1 phosphorylation in Jurkat T cells upon stimulation by Western Blot analysis.

The assembly and disassembly of the CBM complex is tightly regulated by several post-translational modifications such as ubiquitination and phosphorylation. Initiation of CBM complex formation involves hyper-phosphorylation of CARD11 in the linker region, resulting in conformational changes to an open form, which allows the recruitment of BCL10/MALT1 heterodimers via heterotypic CARD-CARD interactions (Figure 4-2 and 3-10). Several kinases, such as PKCθ and IKKβ, have been identified that phosphorylate CARD11 [38, 61, 81]. In particular, phosphorylation of S645 by PKCθ appears to be required for CARD11 activation, but it seems that multiple phosphorylation events are required to pass the threshold for full activity [81]. In line, time course analyses of P/I and CD3/CD28 stimulation in Jurkat T cells showed rapid phosphorylation and activation of CARD11 after 2 to 5 min and subsequently formation of the CBM complex (Figure 3-10).

MALT1 scaffold recruits TRAF6 via its binding domains to the CBM complex, allowing the TRAF6-mediated K63-linked poly-ubiquitination of BCL10 and MALT1. The C-terminal part of MALT1 contains several lysine residues that can function as acceptor sites for ubiquitination (Figure 4-2 and 3-11) [40, 62, 66]. In line, MALT1 mono- and poly-ubiquitination could be detected in time course analysis following 10 to 60 min P/I stimulation (Figure 3-11).
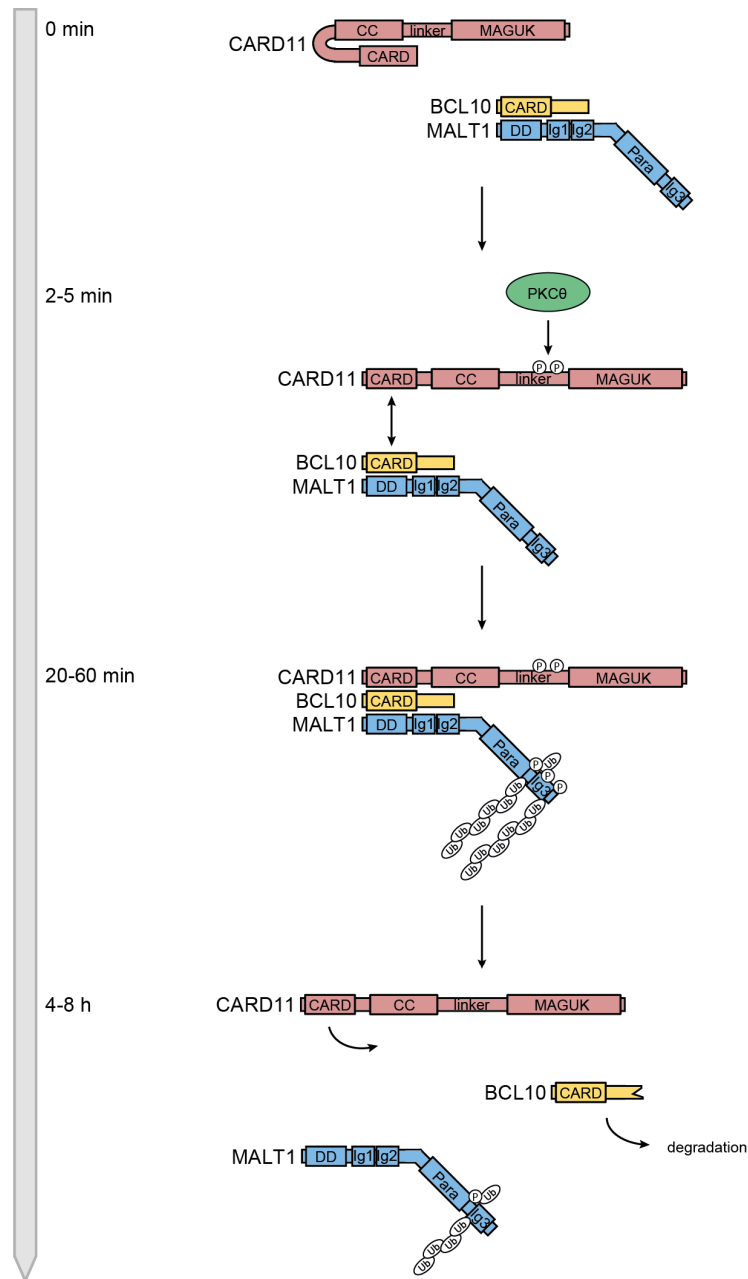
Figure 4-2: Schematic order of events after T cell activation. While CARD11 is in its closed conformation and BCL10 constitutively binds to MALT1 in unstimulated cells, T cell stimulation rapidly leads to CARD11 phosphorylation and activation, resulting in its conformational rearrangement and CBM complex formation. Subsequently, MALT1 scaffold recruits further mediators resulting in its mono- and poly-ubiquitination as well as phosphorylation. In addition, MALT1 protease is activated leading to the cleavage of BCL10 supporting the termination of the CBM assembly and thus terminating T cell stimulation.

All three identified MALT1 phosphorylation sites (S562, S649 and S803) showed similar kinetics and their peak coincided with activation of the CBM complex (Figure 4-2 and 3-10). Whereas CARD11 activation and CBM complex formation was already present after 2 min P/I or CD3/CD28 stimulation, MALT1 phosphorylation was delayed and was first detectable after 5 to 10 min with a peak by 20 to 30 min (Figure 3-10), revealing that CBM complex formation precedes MALT1 phosphorylation. Furthermore, MALT1 ubiquitination was already detected before phosphorylation, indicating that MALT1 phosphorylation does not affect its ubiquitination. In line, MALT1 S/A mutants did not show a difference in slower migrating variants in denaturing gels, which are mainly attributed to K63-linked poly-ubiquitination and mono-ubiquitination on K633 (Figure 3-30) [40, 75, 147]. However, MALT1 phosphorylation and poly-ubiquitination exhibit a similar kinetic, suggesting a potential cooperating role of phosphorylation and ubiquitination in regulating the recruitment of downstream signaling proteins.

Although the initial phosphorylation of the distinct sites did not differ, MALT1B S562 phosphorylation was persistent and still detectable after 1 to 8 h of stimulation (Figure 4-2 and 3-10). Whereas S649 and S803 phosphorylation rapidly declined after only 30 to 60 min of stimulation, MALT1 S562 phosphorylation was still present at later time points, after CBM complex disassembly resulting from BCL10 degradation (Figure 4-2 and 3-10) [97, 98, 152]. Thus, the data suggested that MALT1 phosphorylation is not relevant for CBM complex disassembly. In line, MALT1 S/A mutants were not impaired in their binding to BCL10 (Figure 3-30), indicating a different role of MALT1 phosphorylation compared to BCL10 phosphorylation, which is suggested to induce conformational changes and thereby impair its association with MALT1 [61, 90]. However, it could not be excluded that other, unidentified MALT1 phosphorylation sites may have an influence on the regulation of the association of BCL10 to MALT1. Notably, the different kinetics of MALT1 phosphorylation also suggest a putative cooperation of different phosphatases. Whereas MALT1 S649 and S803 are rapidly dephosphorylated after peaking, MALT1 S562 is prolonged modified, indicating the involvement of several phosphatases. Thus, it is conceivable that recruitment of different phosphatases is also participating in the regulation of the MALT1 phosphorylation and thus NF-κB activation.

Collectively, MALT1 is hyper-phosphorylated within the CBM complex upon T cell activation. The detected kinetics suggests that MALT1 phosphorylation is not involved in the regulation of CBM assembly, but participates in CBM downstream effects.

4.1.3 Function of MALT1 phosphorylation

MALT1 exerts a dual function in the CBM complex upon TCR stimulation. It promotes NF-κB activation via both its scaffold and protease functions. The protease activity of MALT1 is required for modulating NF-κB activity and balancing optimal T cell activation by cleavage of several substrates such as A20, BCL10, CYLD, HOIL1, RelB, Regnase-1 and Roquin1/2 [68, 69, 112, 114, 115, 118, 153, 154]. The activation is mainly controlled by mono-ubiquitination on K633 [75]. Western blot analysis of active MALT1 following enrichment

using an active-based probe [145], demonstrates that active MALT1 is phosphorylated on S562 and S649, in addition to the reported ubiquitination (Figure 3-11). In contrast to when the mono-ubiquitin acceptor site K633 is mutated, phospho-defective MALT1 S/A mutants did not show effects in substrate cleavage, revealing that these phosphorylation events do not play a role in regulating protease activity (Figure 3-27). However, it cannot be excluded that other phosphorylation sites may participate in the regulation of MALT1 paracaspase activity.

As a scaffold, MALT1 C-terminus contains several lysine residues that can function as acceptor sites for poly-ubiquitination. Via its TRAF6 binding sites, MALT1 recruits TRAF6 to the CBM complex resulting in TRAF6 mediates K63-linked poly-ubiquitination of BCL10 and MALT1 (see 4.1.2 and Figure 4-2) [40, 62, 66]. Poly-ubiquitination of the BCL10 and MALT1 C-terminus leads to the recruitment of the IKK and the TAB/TAK1 complex, resulting in the phosphorylation and proteasomal degradation of $I\kappa B\alpha$ [39, 40, 100].

MALT1 poly-ubiquitination and phosphorylation on S562, S649 and S803 exhibited a similar kinetic, suggesting a potential role for MALT1 phosphorylation in the recruitment of further downstream interactors (Figure 4-2 and 3-10). Interestingly, phospho-defective MALT1 S/A mutants were neither impaired in the recruitment of $IKK\gamma$/NEMO to the CBM complex, nor in activation of $IKK\alpha/\beta$ (Figure 3-30). In line, the activation of TAK1 through recruitment to the CBM complex does not only result in the degradation of $IKK\gamma$/NEMO and the subsequent activation of $IKK\alpha/\beta$, but also initiates the JNK signaling pathway [104, 105]. However, activation of JNK was not altered in phospho-defective MALT1 S/A mutants compared to WT (Figure 3-28), suggesting that TAB/TAK1 recruitment is not affected by inserted mutations and thus not regulated by detected C-terminal phosphorylation. Nevertheless, MALT1 phospho-defective S/A mutants showed severely impaired $I\kappa B\alpha$ degradation upon P/I and anti-CD3/CD28 stimulation, demonstrating clear effects of MALT1 phosphorylation in CBM downstream signaling. In line, MALT1 phosphorylation coincides with the onset of $I\kappa B\alpha$ degradation and the induction of canonical NF-κB signaling in time course analyses in Jurkat T cells (Figure 3-10). Notably, MALT1 is phosphorylated on S562, S649 and S803 with similar kinetics upon TCR stimulation, suggesting a concerted role in the regulation of NF-κB activation. Furthermore, combinatory mutation of all six detected phosphorylation sites (S559, S562, S645, S649, S803 and S805) increased the effects of pairwise mutations in NF-κB activation, indicating an additive effect of these phosphorylation events. The MALT1 6xS/A mutant showed the strongest impairment in $I\kappa B\alpha$ degradation and IL-2 expression compared to the WT and pairwise mutations in primary murine CD4 T cells (Figure 3-38 and 3-39). Thus, multiple modifications on MALT1 cooperate in driving optimal NF-κB activation, which may allow for an 'all-or-nothing' activation above a certain signal threshold similar to that reported for CARD11 [155].

Interestingly, Carvalho et al could show that BCL10, MALT1 and IKK inducibly associate with $I\kappa B\alpha$ in a complex that is physically distinct from the CBM signalosome, but probably matures from it [156]. Whereas the IKK and TAB/TAK1 complex are recruited via K63-linked poly-ubiquitin chains attached to BCL10 and MALT1, the regulation of $I\kappa B\alpha$ association has

4 Discussion

not yet been investigated. Since IκBα degradation, but not IKK complex recruitment and activation, is impaired in phospho-defective MALT1 S/A mutants (Figure 3-25 and 3-30), MALT1 phosphorylation may be involved in regulation of the association of IκBα to the CBM complex mediating the formation of a 'supercomplex' consisting of the CBM and IKK, TAK1 as well as IκBα [157]. However, it was not possible to detect a potentially very transient CBM supercomplex that contains NEMO/IKKγ as well as IκBα/NF-κB with the available tools, but future experiments elucidating the regulation of CBM downstream signaling in the context of the BCL10-MALT1 filaments will certainly help to unravel how these modifications cooperate in the regulation of CBM downstream signaling.

4.1.4 MALT1 is constitutively phosphorylated in ABC DLBCL cells

NF-κB is a regulator of genes that control cell proliferation and cell survival. Hence, dysregulation of the NF-κB pathway can result in the development of cancer or inflammatory diseases. One example of a malignancy associated with deregulated NF-κB signaling is diffuse large B cell lymphoma (DLBCL), which is the most common type of non-Hodgkin lymphoma. DLBCL can be divided in germinal center B cell-like (GCB) and activated B cell-like (ABC) DLBCL. ABC DLBCL cells rely on constitutive activation of NF-κB and are forced into cell apoptosis by inhibition of this pathway [158].

By working with several DLBCL cell lines, it could be shown that MALT1 is constitutively phosphorylated in ABC DLBCL cells, which are addicted to chronic BCR signaling and thus rely on the permanent activation of NF-κB signaling (Figure 3-13). Several oncogenic mutations of upstream signaling proteins, such as the co-receptor CD79A/B, constitutively drive CBM assembly, IκBα degradation and NF-κB activation [133-135]. Treating these cells with the BTK inhibitor Ibrutinib impairs the activation of NF-κB through constant upstream signaling and leads these addressed cells into apoptosis. Furthermore, Ibrutinib treatment also reduced MALT1 S562 phosphorylation, indicating that upstream signaling drives MALT1 phosphorylation also in these cell types (Figure 3-13). Notably, ABC DLBCL cells that also have oncogenically mutated CARD11, such as OCI-Ly3, do not respond to Ibrutinib treatment as strongly as cells without [135]. In line, OCI-Ly3 cells show residual MALT1 S562 phosphorylation even after Ibrutinib treatment, indicating the potential of mutated CARD11 to promote CBM assembly and recruitment of further mediators even in the absence of upstream signaling. In addition, overexpression experiments of CARD11 WT or oncogenic L225LI mutant in HBL1 cells results in similar effects after Ibrutinib treatment [139]. Oncogenic CARD11 L225LI could still induce MALT1 S562 phosphorylation and cell activation whereas overexpression of CARD11 WT failed to rescue the effects (Figure 3-13). Taken together, these results indicate that MALT1 phosphorylation is not solely restricted to T cells but could also be detected in B lymphocytes.

ABC DLBCL cells depend on the constitutive activation of the NF-κB pathway. Knockdown or knockout of essential members of the canonical NF-κB pathway, such as MALT1, force ABC DLBCL cells to undergo apoptosis [136, 157]. Interestingly, lymphoma cell viability also

seems to rely on MALT1 phosphorylation. Rescue experiments with phospho-defective MALT1 S/A mutants with simultaneous knockdown of endogenous MALT1 were performed by Tabea Erdmann and Georg Lenz at the University of Münster (data not shown). The experiments showed that ABC DLBCL cell viability is influenced by C-terminal MALT1 phosphorylation. While pairwise mutation of S559/562 and S645/649 did not show effects on survival, mutation of S803/805 as well as mutation of all six phosphorylation sites lead to reduced viability, indicating that especially the very C-terminal serines S803 and S805 are required to mediate survival in certain ABC DLBCL cells lines such as HBL1 and OCI-Ly10. Notably, the region surrounding S803 and S805 is predicted to be a PDK1 binding site (Scansite 4.0). PDK1 association to its binding site requires initial phosphorylation of included serines. It could be shown that in B lymphocytes, the PI3K-PDK1 pathway is activated after antigenic engagement of the BCR and that deficiency or inhibition leads to impaired NF-κB activation. Furthermore, inhibition of PDK1 strongly affected the viability of ABC DLBCL cells, suggesting a crucial role in maintaining viability [159]. Strikingly, MALT1 protease activity is required for cell growth and survival in ABC DLBCL cells, but not in T cells [137]. Because of resembled effects through inhibition of PDK1 or MALT1 paracaspase activity, it was proposed that MALT1 activity could be mediated by PDK1 in ABC DLBCL cells [159]. It is tempting to speculate that C-terminal MALT1 phosphorylation at S803 and S805 participate in mediating PDK-1 association. However, MALT1 paracaspase activity was not affected in MALT1-deficient Jurkat T cells reconstituted with MALT1 S803/805A. Hence, it would be interesting to verify the binding of PDK1 to the C-terminal part of MALT1 and confirm a potential dependency of PDK1 toward MALT1 phosphorylation at S803 and S805. In addition, PDK1 was shown to be essential for TCR stimulation [77]. Activation of PDK1 is supposed to result in association and activation of PKCθ as well as the recruitment of CARD11 into lipid rafts leading to the induction of the IKK complex. So far, direct interaction of PDK1 to CARD11 could be shown, but not to BCL10 [77]. However, association with MALT1 was not investigated in this work. Hence, it is conceivable that interference between PDK1 and MALT1 may support recruitment of the CBM complex into lipid rafts and that MALT1 phosphorylation on S803/805 participates in forming a functional interface. Therefore, reduced survival of ABC DLBCL cells reconstituted with MALT1B S803/805A could also depend on whether efficient signal transduction from the BCR to the CBM complex is still functional.

Collectively, the strong effects of MALT1 phosphorylation in ABC DLBCL cell survival open up new potential strategies for lymphoma treatment. However, the exact mechanisms of MALT1 phosphorylation in ABC DLBCL cells and their effects in regulation of survival still require further investigation.

4.2 CK1α activity triggers CBM complex assembly and affects downstream signaling

CK1α has been shown to associate with the CBM complex and exert both positive and negative regulatory effects on the CBM complex and NF-κB signaling [85]. CK1α knockdown experiments showed impaired CBM complex formation and reduced activation of the downstream NF-κB pathway in Jurkat T cells [85]. In addition, in several ABC DLBCL cell lines it could be shown that CK1α constitutively associates with CARD11 and MALT1 and inhibition or knockdown of CK1α resulted in cell death, whereas GCB DLBCL cell lines did not show these results, indicating a special role in more aggressive ABC lymphoma [85, 143]. However, CK1α also mediates inhibitory phosphorylation of CARD11 on S608, which impairs the ability of CARD11 to activate NF-κB. It has also been demonstrated that knockdown of endogenous CK1α, and simultaneous expression of a catalytically inactive murine CK1α D136N mutant, led to stronger NF-κB activation compared to WT, suggesting that the kinetic activity of CK1α is responsible for the negative regulation [85]. Thereby CK1α can exert a dual function on CARD11, and thus the NF-κB pathway in general, by first promoting and then terminating TCR-induced NF-κB signaling [85], implying that it is a critical regulatory component in orchestrating lymphocyte activation.

Since an association between CK1α and the CBM complex could be confirmed (Figure 3-15), and since the phosphorylation site S562 and S645 of MALT1 are CK1α consensus sites (Figure 3-14), it was hypothesized that CK1α might bind to, phosphorylate and regulate MALT1, in addition to CARD11. Interesting, a residual but severely reduced CK1α-CARD11 interaction was detectable in BCL10 or MALT1 KO Jurkat T cells, suggesting that both contribute directly or indirectly to efficient integration of CK1α into the CBM complex upon stimulation (Figure 3-15). In line, the association of CK1α to CARD11 was enhanced in overexpression experiments of all three CBM components in HEK293 cell, indicating that the CBM complex constitutes the optimal platform for CK1α recruitment (Figure 3-16). Furthermore, CK1α associated with BCL10-MALT1 complexes in the absence of CARD11 in overexpression experiments in HEK293 cells, revealing an additional binding surface in BCL10-MALT1 for the efficient recruitment of CK1α to the CBM complex.

To gain better insight into the role of CK1α in CBM assembly and/or disassembly, CK1α-deficient Jurkat T cells were generated. It could be shown that CK1α deficiency led to the inhibition of CBM assembly and complete impairment in NF-κB activation (Figure 3-19), revealing that CK1α is an essential regulator in CBM-mediated NF-κB induction. The impact of CK1α deficiency resembles the effects reported for PKCθ knockout [160], indicating an essential role of CK1α in the CBM assembly. Reconstitution of CK1α KO Jurkat T cells with catalytically inactive CK1α clearly demonstrated that the main role of CK1α kinase activity is to foster CBM formation and thus to promote T cell activation (Figure 3-21 and 3-22), whereas CK1α was previously reported to negatively regulate CARD11 by phosphorylation on S608 [85]. Although these effects could be confirmed (data not shown), rescue experiments clearly underscore the fact that the dominant function of CK1α catalytic activity

is to drive CBM complex formation and subsequent NF-κB activation. In line, oncogenic CARD11 L225LI mutations, which result in constitutive CBM assembly and thus NF-κB activation [134], also relied on the catalytic activity of CK1α (Figure 3-23), indicating that CK1α catalytic activity also participates in the regulation of signaling events downstream of CARD11. However, bypassing the CBM complex by using TNFα stimulation showed no interference with IκBα phosphorylation/degradation and subsequent NF-κB activation in CK1α-deficient Jurkat T cells (Figure 3-19C). Thus, the data clearly reveal that CK1α functions on the level of the CBM complex.

Interestingly, initial CARD11 phosphorylation on S645 catalyzed by PKCθ is unchanged in the absence of CK1α, indicating that CK1α is not involved in upstream events [38, 81]. Notably, in the WNT signaling pathway CK1α phosphorylates the APC protein (adenomatous-polyposis-coli) on multiple residues in a hierarchical manner following initial priming phosphorylation of APC by GSK3β. CK1α itself can also function as a priming kinase that initiates the hierarchical phosphorylation of β-catenin by GSK3β [127, 161]. In line, GSK3β was also shown to associate with the CBM complex and to promote NF-κB signaling [89, 143]. Thus, it is tempting to speculate that after the initial phosphorylation of CARD11 by PKCθ or other potential initiator kinases, CK1α contributes to CARD11 hyper-phosphorylation besides known S608 site and thereby induces the conformational changes that provide accessibility of the CARD-domain for BCL10-MALT recruitment. Such crosstalk between CK1α and other protein kinases could support the reported switch-like mechanism for IKK/NF-κB activation by the CBM signaling complex [155]. Nevertheless, potential sites still remain to be identified and further work is needed to fully understand the effects of CK1α in CBM assembly. CK1α-dependent phosphorylation of CARD11 was already investigated in initial mass spectrometry experiments during this work. Therefore, CARD11 was immunoprecipitated from CK1α-deficient Jurkat T cells reconstituted with CK1α WT or the catalytically inactive D136N variant and subsequently analyzed in mass spectrometry-based proteomic approaches in cooperation with Özge Karayel and Prof. Matthias Mann at the Max-Planck Institute of biochemistry. Although initial experiments revealed new stimulation-dependent CARD11 phosphorylation sites, these sites were CK1α-independent. Importantly, the tools are now available and therefore new CK1α-dependet CARD11 phosphorylation sites may be discovered in the near future, helping us to gain better insights in the impact of CK1α in CBM assembly and NF-κB activation.

Furthermore, CK1α can catalyze MALT1 phosphorylation (Figure 3-17). Despite the fact that CK1α can phosphorylate MALT1 on S562 *in vitro*, it is unlikely that it directly catalyze phosphorylation of all sites in the MALT1 C-terminus. Nevertheless, as with CARD11 hyper-phosphorylation, it is possible that CK1α is either primed by initial phosphorylation or alternatively, primes phosphorylation by other protein kinases to induce switch-like activation. As mentioned before, expression of oncogenic CARD11 L225LI also relied on CK1α catalytic activity for efficient NF-κB activation. Thus, it is tempting to speculate that MALT1 phosphorylation constitutes the missing link between CBM assembly and NF-κB activation.

Due to the importance of CK1α within the NF-κB pathway and the previously described effects of the detected MALT1 phosphorylation sites, a new model for the signal transduction in the NF-κB pathway following TCR stimulation is proposed (Figure 4-3).
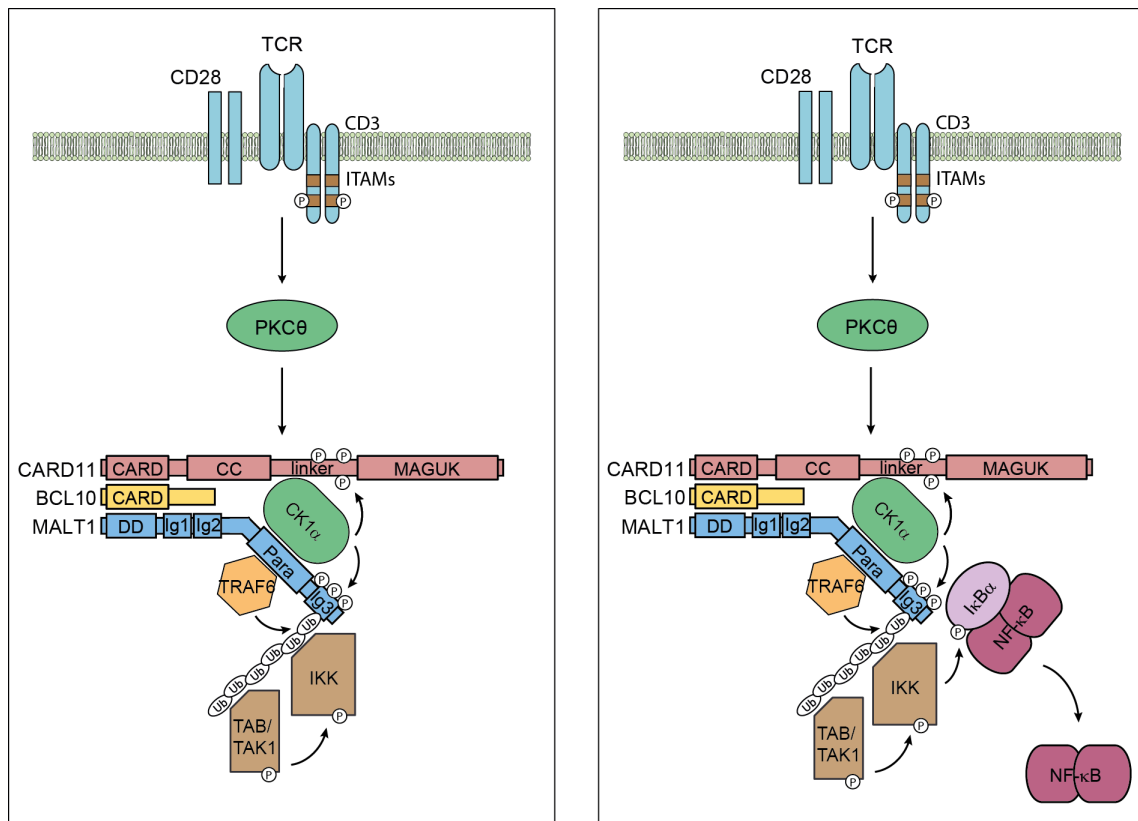
Figure 4-3: Model of the role of CK1α and the influence of MALT1 phosphorylation within the NF-κB pathway. After TCR stimulation, CARD11 is mainly activated through phosphorylation by CK1α and PKCθ. This leads to the formation of the CBM assembly and the subsequent recruitment of the IKK and the TAB/TAK1 complex. In parallel, CK1α is hypothesized to phosphorylate the C-terminus of MALT1 supporting the association of IκBα to the holo-complex and the formation of a second distinct supercomplex consisting of BCL10, MALT1, IKK and IκBα. IKKα/β in turn phosphorylates IκBα and thereby induces its proteasomal degradation, resulting in free NF-κB dimers, which can translocate into the nucleus and lead to target gene expression.

After TCR engagement and following activation of downstream kinases, CARD11 is first phosphorylated by PKCθ and subsequently supposedly by CK1α in a hierarchical manner to overcome a certain threshold leading to full CARD11 activation [155]. Thereby CARD11 converts into an open, active form, leading to the association of constitutively bound BCL10/MALT1 heterodimers via CARD-CARD interactions. By specific binding motifs in MALT1, the E3 ubiquitin ligase TRAF6 is recruited and then catalyzes the K63-linked poly-ubiquitination of BCL10 and MALT1 [40, 66]. Thus, the IKK complex is recruited to the CBM complex and IKKγ/NEMO is also poly-ubiquitinated by TRAF6 [41]. This leads to the binding of the TAB/TAK1 complex to the holo-complex and TAK1 in turn phosphorylates and

subsequently activates IKKα/β [39, 101]. In parallel, CK1α phosphorylates the C-terminus of MALT1 and one can now hypothesize that this induces a conformational rearrangement that supports the association of IκBα to MALT1 and the formation of the distinct BCL10-MALT1-IKK-IκBα complex [156]. Thereby, IκBα is phosphorylated by IKKα/β, which leads to its proteasomal degradation. As a consequence, NF-κB dimers are free and translocate into the nucleus, where they induce transcription of several target genes such as IL-2 [43, 102, 103].

4.3 Conclusion and perspectives

Activation of the NF-κB transcription factor family plays a central role in the adaptive immune response. Upon stimulation of either the T or B cell receptor, NF-κB is activated and regulates the transcription of a range of genes, involved in inflammation, cell proliferation, differentiation and survival. The formation of the multi-protein CARD11-BCL10-MALT1 complex serves as an essential step connecting proximal antigen-receptor signaling to downstream IKK/NF-κB signaling. The CBM assembly and disassembly as well as downstream signal transduction is highly regulated by post-translational modifications including ubiquitination and phosphorylation. In this study, MALT1 phosphorylation sites could be identified by mass spectrometry for the first time. In time course analyses, first insights in the order of events in CBM assembly and downstream NF-κB activation could be obtained, revealing the hierarchical processes of CARD11 phosphorylation, MALT1 ubiquitination and phosphorylation as well as BCL10 degradation. However, it would be interesting to further dissect the kinetics by integrating already known positive and negative regulatory events into reported data. Thus, time points when CK1α associates to the CBM or when BCL10 gets phosphorylated upon TCR stimulation would provide new insights into the precise order of events. In this context, detection of new regulating modifications via global mass spectrometry approaches would help to further unravel the exact mechanism of the regulation of the CBM machinery.

Recently, the helical structure of BCL10-MALT1 filaments could be resoved using cryo-EM, revealing the direct interface between BCL10 and MALT1. It could be shown that MALT1 binds via its DD to the rim of the BCL10 CARD domain and MALT1 V81 and L82 could be determined as central interacting residues in this interface [63]. Mutation of these sites impaired constitutive BCL10-MALT1 association and thereby led to loss of CBM assembly [63]. In turn, this caused severe inhibition of IκBα degradation and IL-2 expression in primary MALT1 KO CD4 T cells reconstituted with respective MALT1 variants as shown in this work. Furthermore, the resolved structure of BCL10-MALT1 filaments revealed that the MALT1 C-terminus protrudes from the inner core, forming a flexible outer surface that allows recruitment of further mediators [62, 63]. In line, the MALT1 phosphorylation sites identified in this study, as well as previously described acceptor sites for ubiquitination, are located in the C-terminus. In this regard, the integration of identified post-translational modification into

structural data would be interesting to elucidate the precise regulation of the CBM signalosome.

ABC DLBCL cells are addicted to chronic BCR signaling resulting in constitutive CBM assembly and subsequent NF-κB activation [133-135]. MALT1 as a scaffold in the CBM complex could be shown to be strongly ubiquitinated in these cells even without stimulation. In this work, MALT1 was also shown to be hyper-phosphorylated in basal conditions supporting ABC DLBCL cell survival. CK1α as well as PDK1 deficiency could already be shown to lead to strongly reduced viability in these cells. In this context, future experiments are needed to unravel deregulated pathways in ABC DLBCL cells that lead to maintained MALT1 modifications and NF-κB activation. Identification of potential driving enzymes may provide potential novel targets for therapeutic treatments.

Although the exact mechanism(s) of MALT1 phosphorylation after TCR signaling and in chronic activation still needs to be further elucidated, the identification of MALT1 phosphorylation events in this study has revealed a new level in the regulation of the CBM-mediated NF-κB pathway.

5 Materials

5.1 Instruments and equipment

Agarose gel chambers	NeoLab, Heidelberg
Attune Acoustic Focusing Cytometer	Life Technologies, Carlsbad, USA
Autoradiography MP films	GE Healthcare, Freiburg
Bacterial culture flasks	BD, Heidelberg
Cell-counting chamber Neubauer	NeoLab, Heidelberg
Cell culture flasks	BD, Heidelberg
Cell culture plates	BD, Heidelberg; Nunc, Rochester, USA
Cell strainer (100 μM)	NeoLab, Heidelberg
Centrifuge Avanti J-26 XP	Beckmann Coulter, Krefeld
Cell culture centrifuge, 5804	Eppendorf, Hamburg
Cooling cell culture centrifuge, 5810R	Eppendorf, Hamburg
Cooling table centrifuge, 5417R	Eppendorf, Hamburg
Table centrifuge, 5471C	Eppendorf, Hamburg
Chemiluminescence ECL films	GE Healthcare, Freiburg
CO_2 incubators	Binder, Tuttlingen
Cryo tubes	Greiner Bio-One, Frickenhausen
Developer Optimax	Protec, Dorfwiesen
Electroporation cuvettes, Gene Pulser	Bio-Rad, München
Electroporator, Gene Pulser Xcell System	Bio-Rad, München
EMSA gel chamber, X952.1	Roth, Karlsruhe
Film Cassettes	Roth, Karlsruhe
Freezers	Liebherr, Ochsenhausen
Geldocumentation System	Intas, Göttingen
Gel dryer 583	Bio-Rad, München
Heatblock	Techne, Staffordshire, UK
Incubators	Sartorius, Göttingen; Heraeus, Hanau
Incubator Shaker I26	New Brunswick Scientific, Hamburg
LightCycler480	Roche, Mannheim
LightCycler plates 96 well	4titude, Berlin

MACS columns	Miltenyi Biotec, Bergisch Gladbach
MACS rack	Miltenyi Biotec, Bergisch Gladbach
Magnetic stirrer	IKA Labortechnik, Staufen
Microscopes	Leica, Wetzlar
Microtiter plate (U- or V-shape), 96-well	Greiner Bio-One, Frickenhausen
Microwave	SHARP, Hamburg
Nanodrop 2000	Thermo Fisher Scientific, Waltham, USA
Petri dishes	Greiner Bio-One, Frickenhausen
pH-Meter	Sartorius, Göttingen
Pipettes	Eppendorf, Hamburg
Plastic cuvettes	Brand, Wertheim
Plastic filter tips TipOne (RNase free)	StarLab, Hamburg
Plastic pipettes	Greiner Bio-One, Frickenhausen
Plastic tips	Eppendorf, Hamburg
Power supplies	Consort, Turnhout, Belgium
Precision scales	Kern, Balingen
PVDF membrane	Merck Millipore, Darmstadt
Rotator	NeoLab, Heidelberg
SDS-PAGE chamber	Roth, Karlsruhe
Semi-dry blotter	PHASE, Lübeck; Peqlab, Erlangen
Thermocycler	Eppendorf, Hamburg
Thermomix comfort	Eppendorf, Hamburg
Tissue Culture Hoods Safeflow 1.2	Nunc, Wiesbaden
Tubes	Eppendorf, Hamburg
ViCell-XR cell viability analyzer	Beckman Coulter, Krefeld
Vortexer	Scientific Industries, Bohemia, USA
Whatman paper	Roth, Karlsruhe
Water Bath	Thermo HAAKE, Karlsruhe

5.2 Chemicals

5.2.1 General chemicals

Adenosine triphosphate (ATP)	Sigma-Aldrich, Taufkirchen
Acrylamide/Bisacrylamide	Roth, Karlsruhe
Agar	Roth, Karlsruhe
Agarose	Biozym, Hessisch Oldendorf
Ammonium persulfate (APS)	Bio-Rad, München
Ampicillin	Roth, Karlsruhe
Autoradiography developing solution	Sigma-Aldrich, Taufkirchen
Autoradiography fixing solution	Sigma-Aldrich, Taufkirchen
Boric acid	Roth, Karlsruhe
Bovine serum albumin (BSA)	GE Healthcare, Freiburg
Brefeldin-A	Sigma-Aldrich, Taufkirchen
Calcium chloride	Roth, Karlsruhe
Disodium hydrogen phosphate	Roth, Freiburg
Dimethyl sulfoxide (DMSO)	Sigma-Aldrich, Taufkirchen
DNA 1kb plus ladder	Invitrogen, Carlsbad, USA
dNTP-Mix	Thermo Fisher Scientific, Waltham, USA
Dithiothreitol (DTT)	Sigma-Aldrich, Taufkirchen
Ethylenediaminetetraacetic acid (EDTA)	Roth, Freiburg
Ethyleneglycol-bis(2-aminoethylether) N,N,N′,N′-tetraacetic acid (EGTA)	Sigma-Aldrich, Taufkirchen
Ethanol (p. a.)	Merck, Darmstadt
Ethidiumbromide	Roth, Freiburg
Ethidium monoazide bromide	Sigma-Aldrich, Taufkirchen
Glycerol	Roth, Freiburg
Glycine	Roth, Freiburg
Heparine	Sigma-Aldrich, Taufkirchen
HEPES	Roth, Freiburg
Isopropyl alcohol (p.a.)	Merck, Darmstadt
LB	Roth, Freiburg

Lumi-Glo ECL reagent	NEB, Frankfurt
Lymphoprep	Stemcell Technologies, Köln
Magnesium chloride	Roth, Freiburg
Methanol (p.a.)	Merck, Darmstadt
Nonidet P40 substitude (NP-40)	Sigma-Aldrich, Taufkirchen
PageRuler Prestained Protein Ladder	Thermo Fisher Scientific, Waltham, USA
Paraformaldehyde (PFA)	Sigma-Aldrich, Taufkirchen
Polybrene	Sigma-Aldrich, Taufkirchen
Poly dI-dC	Roche, Mannheim
Potassium chloride	Roth, Freiburg
Potassium hydrogen phosphate	Roth, Freiburg
Protease inhibitor mix (Roche complete)	Roche, Mannheim
Protein-G-Sepharose	Invitrogen, Carlsbad, USA
Protein loading buffer (Rotiload)	Roth, Freiburg
Saponine	Roth, Freiburg
Sodium acetate	Roth, Freiburg
Sodium azide	Roth, Freiburg
Sodium chloride	Roth, Freiburg
Sodium dodecyl sulfate (SDS)	Roth, Freiburg
Sodium fluoride	Sigma-Aldrich, Taufkirchen
Sodium vanadate	Roth, Freiburg
Strep-Tactin Sepharose	IBA, Göttingen
Sulfuric acid	Merck, Darmstadt
Tetramethylethylenediamine (TEMED)	Roth, Freiburg
Tris(hydroxymethyl)-aminomethan (Tris)	Roth, Freiburg
TritonX-100	Roth, Freiburg
Trypan blue	Invitrogen, Carlsbad, USA
Tween 20	Roth, Freiburg
X-tremeGENE HP Transfection Reagent	Roche, Mannheim
^{32}P-α-dATP	Perkin Elmer, Wiesbaden
^{32}P-γ-dATP	Hartmann, Braunschweig
β-Glycerophosphate	Sigma-Aldrich, Taufkirchen

β-Mercaptoethanol   Roth, Freiburg

5.2.2 Cell culture

DMEM   Gibco, Life Technologies, Carlsbad, USA

Fetal calf serum (FCS)   Life Technologies, Carlsbad, USA

L-glutamine   Life Technologies, Carlsbad, USA

Non-essential amino acids (NEAA)   Life Technologies, Carlsbad, USA

Optimem   Life Technologies, Carlsbad, USA

Penicillin/streptomycin (P/S)   Life Technologies, Carlsbad, USA

RPMI 1640   Life Technologies, Carlsbad, USA

Sodium pyruvate   Life Technologies, Carlsbad, USA

Trypsin/EDTA   Life Technologies, Carlsbad, USA

β-Mercaptoethanol   Life Technologies, Carlsbad, USA

5.3 Stimulants

Ionomycin   Calbiochem, Schwalbach

Phorbol 12-myristate 13-acetate (PMA)   Merck Millipore, Darmstadt

Tumor necrosis factor alpha (TNFα)   Biomol, Hamburg

5.4 Enzymes and Kits

CD4 T cell Isolation Kit (mouse)   Miltenyi Biotec, Bergisch Gladbach

CD4 T cell Isolation Kit (human)   Miltenyi Biotec, Bergisch Gladbach

DreamTaq DNA polymerase   Thermo Scientific, Waltham, USA

Gel Extraction Kit   Qiagen, Hilden

Gel Extraction Kit   Macherey & Nagel, Düren

Herculase II DNA Polymerase   Agilent Technologies, Waldbronn

KAPA SYBR FAST qPCR Mastermix   Peqlab, Erlangen

Klenow Polymerase   NEB, Frankfurt

LightCycler 480 SYBR Green I Mastermix   Roche, Mannheim

QIAshredder   Qiagen, Hilden

NucleoSpin PCR & Gel Purification Kit   Macherey & Nagel, Düren

Plasmid Maxi Kit	Qiagen, Hilden
Plasmid Mini Kit	Qiagen, Hilden
NucleoSpin Plasmid Mini Kit	Macherey & Nagel, Düren
Proteinase K	NEB, Frankfurt
Restriction enzymes	NEB, Frankfurt
Restriction buffers	NEB, Frankfurt
RNaseH	Life Technologies, Darmstadt
RNeasy RNA isolation Kit	Qiagen, Hilden
Superscript First Strand Synthesis Kit	Invitrogen, Carlsbad, USA
SuperScript II Reverse Transcriptase	Invitrogen, Carlsbad, USA
T4 DNA ligase	NEB, Frankfurt
Verso cDNA Synthesis Kit	Thermo Fisher Scientific, Waltham, USA

5.5 Mice strains

MALT1$^{tm1a(EUCOMM)Hmgu}$	ES cells obtained from EUCOMM and inoculated into foster mice by IDG, HMGU. MALT1 genome is targeted by homologue recombination. A cassette containing lacZ and neomycin gene flanked by FRT sites was introduced in genome before exon 3. Furthermore, exon 3 is flanked by loxP sites allowing deletion using mating with Cre-expressing mice.
ROSA26::FLPe knock in	C57BL/6N mouse with FLPe knock-in allele, which gene expression is driven by the *Gt(ROSA)26Sor* promoter.
ROSA26::Cre knock in	C57BL/6N mouse with Cre knock-in allele, which gene expression is driven by the *Gt(ROSA)26Sor* promoter.

5.6 Eukaryotic cell lines

HEK293	human embryonic kidney cell line
HEK293T	human embryonic kidney cell line; transformed with SV40 large T antigen
Jurkat T cells	human T cell line; derived from acute T cell leukemia
BCL10$^{-/-}$ Jurkat T cells	human T cell line; exon 1 was deleted by CRISPR/Cas9 (generated by S. Widmann, AG Krappmann)
CARD11$^{-/-}$ Jurkat T cells	human T cell line; exon 3 was deleted by CRISPR/Cas9 (generated by S. Woods, AG Krappmann)

CK1α^{-/-} Jurkat T cells	human T cell line; exon 3 was deleted by CRISPR/Cas9
MALT1^{-/-} Jurkat T cells	human T cell line; exon 2 was deleted by CRISPR/Cas9

5.7 Bacteria

TOP10	*Escherichia coli*, F-mcrA Δ(mrr-hsdRMS-mcrBC) φ80lacZΔM15 ΔlacX74 nupG recA1 araD139 Δ(ara-leu)7697 galE15 galK16 rpsL(StrR) endA1λ-
STBL3	*Escherichia coli*, F⁻mcrB mrrhsdS20(r$_B$⁻, m$_B$⁻) recA13 supE44 ara-14 galK2 lacY1 proA2 rpsL20(Str^R) xyl-5 λ⁻leumtl-1
BL21	*Escherichia coli*, contain extra copies of rare E. coli argU, ileY, leuW, proL tRNA genes

5.8 Vectors and oligonucleotides

5.8.1 Vectors

Table 5-1: List of general vectors.

General vectors	Information
pHAGE-PGK-L1-hΔCD2-T2A-Flag-Strep-Strep (pHAGE-SF; mock)	Lentiviral vector. Obtained from Dr. Marc Schmidt-Supprian. Flag-Strep-Strep-Tag was cloned into pHAGE-PGK-L1-hΔCD2-T2A by *SalI*/*BamHI*.
pMSCV	Retroviral vector; IRES sequence enables simultaneous expression of Thy1.1 (CD90.1) (V. Heissmeyer).
pEF-3x FLAG (3xFL)	Basis vector pEF4HIS-C (Invitrogen). His sequence was replaced by three repeating Flag sequences (*HindIII*/*KpnI*, D. Krappmann).
pEF-HA	Basis vector pEF4HIS-C (Invitrogen). His sequence was replaced by HA sequences (*HindIII*/*BamHI*, A. Eitelhuber)
pX330	A human codon-optimized SpCas9 and chimeric guide RNA expression plasmid (addgene #42230; gifted by F. Zhang).
pX458	Cas9 from S. pyogenes with 2A-EGFP, and cloning backbone for sgRNA (addgene #48138; gifted by F. Zhang)
pGEX-6P-1	Expression vector for protein purification. GST-tag linked with PreScission protease cutting site

Table 5-2: List of additional vectors.

Additional vectors	Information
pX330-MALT1 ex2 sgRNA l#1	sgRNA oligo l#1 was transferred into pX330 plasmid (*BbsI*/*BbsI*)
pX330-MALT1 ex2 sgRNA r#1	sgRNA oligo r#1 was transferred into pX330 plasmid (*BbsI*/*BbsI*)
pX458-CK1α ex3 sgRNA #1	sgRNA oligo #1 was transferred into pX458 plasmid (*BbsI*/*BbsI*)
pEF-HA-CARD11	CARD11 cDNA was transferred into pEF-HA plasmid (*BamHI*/*NotI*, G. Schimmack)
pEF-CARD11-FS	cDNA of CARD11 C-terminally tagged with StrepTagII was transferred into pEF empty plasmid (*BamHI*/*NotI;* M. Bognar)
pEF-HA MALT1	MALT1 cDNA was transferred into pEF-HA plasmid (*BamHI*/*NotI*, A. Oeckinghaus)
pEF-3xFL MALT1	MALT1 cDNA was transferred into pEF-3xFL plasmid (*BamHI*/*NotI*, E. Wegener)
pEF-3xFL BCL10	BCL10 cDNA was transferred into pEF-HA plasmid (*BamHI*/*NotI*, A. Oeckinghaus)
pEF-3xFL CK1α	CK1α cDNA was transferred into pEF-HA plasmid (*BamHI*/*NotI*)
pHAGE-CK1α-Strep	CK1α cDNA was transferred into pHAGE-SF (*NotI*/*SalI*)
pHAGE-CK1α D136N-Strep	Point mutation (D136N) was introduced by PCR-based mutagenesis. MALT1 cDNA was transferred into pHAGE-SF (*NotI*/*SalI*).
pHAGE-CK1α Y292A-Strep	Point mutation (Y292A) was introduced by PCR-based mutagenesis. MALT1 cDNA was transferred into pHAGE-SF (*NotI*/*SalI*).
pHAGE-MALT1B-Strep	MALT1 cDNA was transferred into pHAGE-SF (*NotI*/*SalI*).
pHAGE-MALT1B S559/562A-Strep	Point mutations (S559/562A) were introduced by PCR-based mutagenesis. MALT1 cDNA was transferred into pHAGE-SF (*NotI*/*SalI*).
pHAGE-MALT1B S645/649A-Strep	Point mutations (S645/649A) were introduced by PCR-based mutagenesis. MALT1 cDNA was transferred into pHAGE-SF (*NotI*/*SalI*).

pHAGE-MALT1B S803/805A-Strep	Point mutations (S803/805A) were introduced by PCR-based mutagenesis. MALT1 cDNA was transferred into pHAGE-SF (*Not*I/*Sal*I).
pHAGE-MALT1B-6xSA Strep	Point mutations (S559/562/645/649/803/805A) were introduced by PCR-based mutagenesis. MALT1 cDNA was transferred into pHAGE-SF (*Not*I/*Sal*I).
pMD2.G	Lentiviral envelope plasmid (addgene #12259; gifted by D. Trono)
psPAX2	Lentiviral packaging plasmid (addgene #12260; gifted by D. Trono)
pGEX-GST-MALT1 325-760 aa	cDNA of MALT1 fragment was transferred into pGEX-GST plasmid (*Not*I/*BamHI*, D. Nagel).

5.8.2 Sequences of used sgRNA

Table 5-3: List of used sgRNAs.

Name	Sequence (5' – 3')
MALT1 ex2 sgRNA l#1	CCGTGGTCCAGATATATAGC
MALT1 ex2 sgRNA r#1	GCATTGCATTTGCTTCAACC
CK1α ex3 sgRNA #1	TGTACTTATGTTAGCTGACC

5.8.3 EMSA oligonucleotides

Table 5-4: EMSA oligonucleotide sequence.

Target	Sequence (5' – 3')
NF-κB (H2K) fw	GATCCAGGGCTGGGGATTCCCCATCTCCACAGG
NF-κB (H2K) rev	GATCCCTGTGGAGATGGGGAATCCCCAGCCCTG
OCT1 fw	GATCTGTCGAATGCAAATCACTAGAA
OCT1 rev	GATCTTCTAGTGATTTGCATTCGACA

5.8.4 Primer for RT-PCR

Table 5-5: Human RT-PCR primer sequences.

Target (human)	Sequence (5' – 3')
A20 fw	CTGAAAACGAACGGTGACGG
A20 rev	CGTGTGTCTGTTTCCTTGAGCG
IκBα fw	AGGACGGGGACTCGTTCCTG
IκBα rev	CAAGTGGAGTGGAGTCTGCTG
IL-2 fw	CTCACCAGGATGCTCACATTTA
IL-2 rev	TGTTGTTTCAGATCCCTTTAGTTC
RP2 fw	GCACCACGTCCAATGACAT
RP2 rev	GTGCGGCTGCTTCCATAA

5.9 Antibodies

5.9.1 Antibodies for cell stimulation

Mouse anti-human anti-CD3	BD Pharmigen, Frankfurt am Main
Mouse anti-human anti-CD28	BD Pharmigen, Frankfurt am Main
Rat anti-mouse IgG1	BD Pharmigen, Frankfurt am Main
Rat anti-mouse IgG2	BD Pharmigen, Frankfurt am Main
Hamster anti-mouse anti CD3 (145-2C11)	BD eBioscience, Frankfurt am Main
Hamster anti-mouse anti-CD28 (37.51)	BD eBioscience, Frankfurt am Main
Rabbit anti-hamster IgG (H+L)	JacksonImmunoResearch, Newmarket, UK

5.9.2 FACS antibodies

anti-CD2-APC (RPA-2.10)	eBioscience, Frankfurt am Main
anti-Thy1.1-APC (HIS51)	eBioscience, Frankfurt am Main
anti-B220-PerCP (RA3-6B2)	eBioscience, Frankfurt am Main
anti-CD3-PeCy7 (UCHT1)	eBioscience, Frankfurt am Main
anti-CD4-APC (RM4-5)	eBioscience, Frankfurt am Main
anti-CD4-PerCP (RM4-5)	eBioscience, Frankfurt am Main
anti-CD5-PE (53-7.3)	eBioscience, Frankfurt am Main

anti-CD8-FITC (53-6.7)	eBioscience, Frankfurt am Main
anti-CD19-APC (1D3)	eBioscience, Frankfurt am Main
anti-CD21-FITC (HB5)	eBioscience, Frankfurt am Main
anti-CD23-bio (B3B4)	eBioscience, Frankfurt am Main
anti-CD25-APC (PC61.5)	eBioscience, Frankfurt am Main
anti-CD44-PeCy7 (IM7)	eBioscience, Frankfurt am Main
anti-CD62L-APC (MEL-14)	eBioscience, Frankfurt am Main
anti-CD62L-PE (MEL-14)	eBioscience, Frankfurt am Main
anti-CD69-APC (H1.2F3)	eBioscience, Frankfurt am Main
anti-IL-2-FITC (JES6-5H4)	eBioscience, Frankfurt am Main
anti-PD-1-FITC (J43)	eBioscience, Frankfurt am Main
anti-FoxP3-PE (FJK-16s)	eBioscience, Frankfurt am Main
biotinylated goat anti-rat IgG	Abcam, Cambridge, UK
Streptavidin-APC	BD, Heidelberg
Anti-mouse IgG1-FITC (A85-1)	eBioscience, Frankfurt am Main

5.9.3 Primary antibodies for Western Blot and co-IPs

anti-β-ACTIN-HRP (I-19)	Santa Cruz, Heidelberg
anti-BCL10 (EP606Y)	Abcam, Cambridge, UK
anti-BCL10 (C-17)	Santa Cruz, Heidelberg
anti-CARD11 (1D12)	NEB, Frankfurt am Main
anti-CK1α (C-19)	Santa Cruz, Heidelberg
anti-CK1α (EPR1961)	Abcam, Cambridge, UK
anti-CK1α (H-7)	Santa Cruz, Heidelberg
anti-CYLD (E10)	Santa Cruz, Heidelberg
anti-ERK (442704)	Merck Millipore, Darmstadt
anti-HA (3F1)	Core facility monoclonal antibodies, HMGU (R. Feederle)
anti-HOIL1 (S150D)	MRC PPU Reagents, Dundee
anti-IκBα (L35A5)	NEB, Frankfurt am Main
anti-IKKα/β (H470)	Santa Cruz, Heidelberg
anti-JNK1/2 (9252)	NEB, Frankfurt am Main

anti-MALT1 (human, B12)	Santa Cruz, Heidelberg
anti-MALT1 (mouse, H300)	Santa Cruz, Heidelberg
anti-MALT1B S562	Core facility monoclonal antibodies, HMGU (R. Feederle)
anti-MALT1B S649	Core facility monoclonal antibodies, HMGU (R. Feederle)
anti-MALT1B S803	Core facility monoclonal antibodies, HMGU (R. Feederle)
anti-NEMO (FL-419)	Santa Cruz, Heidelberg
anti-phospho-ERK (9101)	NEB, Frankfurt am Main
anti-phospho-IκBα (5A5)	NEB, Frankfurt am Main
anti-phospho-IKKα/β (2681)	Cell signalling, Frankfurt am Main
anti-phospho-JNK (4668)	NEB, Frankfurt am Main
anti-phospho-p38 (9211)	NEB, Frankfurt am Main
anti-p38 (C-20)	Santa Cruz, Heidelberg
anti-Regnase (604421)	R&D System, Minneapolis
anti-Ubiquitin (P4D1)	Santa Cruz, Heidelberg

5.9.4 Secondary antibodies for Western Blot

HRP-conjugated anti-rabbit	JacksonImmunoResearch, Newmarket, UK
HRP-conjugated anti-mouse	JacksonImmunoResearch, Newmarket, UK
HRP-conjugated anti-goat	JacksonImmunoResearch, Newmarket, UK
HRP-conjugated anti-rat	JacksonImmunoResearch, Newmarket, UK

5.10 Buffers and solutions

Agar plates:	LB (20 g/l), Agar (15 g/l)
Annealing buffer:	Tris-HCl pH 8.0 (50 mM), NaCl (70 mM)
B1 buffer:	PBS (1x), BSA (0.1 % (w/v)), EDTA (2 mM)
Blocking buffer:	BSA in PBS-T (5 % (w/v))

Blotting buffer:	Tris pH 8.3 (48 mM), Glycine (39 mM), Methanol (20 % (v/v)), SDS (0.03 % (w/v))
CB buffer:	PBS (1x), BSA (0.5 % (w/v)), EDTA (2 mM)
Co-IP buffer:	HEPES pH 7.5 (25 mM), NaCl (150 mM), Glycerol (1 mM), NP-40 (0.2 % (v/v)), DTT (1 mM), NaF (10 mM), β-Glycerophosphate (8 mM), NaVanadate (300 µM), Protease inhibitor mix
FACS buffer:	PBS (1x), FCS (2 % (w/v)), NaN_3 (0.01 % (v/v))
High salt buffer:	HEPES pH 7.9 (20 mM), NaCl (350 mM), Glycerol (20 % (v/v)), $MgCl_2$ (1 mM), EDTA (0.5 mM), EGTA (0.1 mM), NP-40 (1 %), DTT (1 mM), NaF (10 mM), β-Glycerophosphate (8 mM), NaVanadate (300 µM), Protease inhibitor mix
IC buffer:	PBS (1x), Saponine (0.5 % (w/v)), NaN_3 (0.01 % (v/v))
Kinase assay buffer:	25 mM MOPS pH 7.2, 12.5 mM glycerol-2-phosphoate, 25 mM $MgCl_2$, 5 mM EGTA and 2 mM EDTA. Just prior to use, add DTT to a final concentration of 0.25 mM
LB medium:	LB (20 g/l)
PBS (1x):	NaCl (137 mM), Na_2HPO_4 (10 mM), KCl (2.7 mM), KH_2PO_4 (1.7 mM)
PBS-T (WB):	PBS, Tween-20 (0.1 % (v/v))
Poly dI-dC:	Poly dI-dC (2 mg/ml), Tris pH 8.0 (10 mM), NaCl (100 mM)
Polyacrylamide gel, native:	TBE buffer (1x), Acrylamide/Bisacrylamide (5 %), APS (0.75 % (v/v)), TEMED (0.075 % (v/v))
SDS electrophoresis buffer (1x):	Tris pH 8.8 (25 mM), Glycine (192 mM), SDS (0.1 % (w/v))
Separation gel:	Tris/HCl pH=8.8 (375 mM), Acrylamide/Bisacrylamide (7.5-11 %), SDS (0.1 %), APS (0.075 %), TEMED (0.05 %)
Shift buffer (2x):	HEPES pH 7.9 (20 mM), KCl (120 mM), Ficoll (4 % (w/v))
Stacking gel:	Tris/HCl pH 6.8 (125 mM), Acrylamide/Bisacrylamide (5 %), SDS (0.1 %), APS (0.1 %), TEMED (0.1 %)
Stripping buffer:	Glycine (0.2 M), SDS (0.1 %), Tween-20 (1 % (v/v)), pH 2.2
TBE buffer:	Tris (50 mM), Boric acid (50 mM), EDTA (1 mM), pH 8.3
TE (Tris EDTA) buffer:	Tris/HCl pH 8.0 (10 mM), EDTA (1 mM)

6 Methods

6.1 Cell culture

6.1.1 Storage of cell lines

For the storage of suspension or adherent cells, 1-2x 10^7 cells were pelleted and resuspended in 1 ml freezing medium (DMEM/RPMI, 20 % FCS, 15 % DMSO). After transfer into cryo tubes, samples were put into an isopropanol-containing freezing chamber over night at -80 °C. For long-term storage, cells were stored in liquid nitrogen.

6.1.2 Cultivation of adherent cells

HEK293 and HEK293T cells were cultured in DMEM medium supplemented with 10 % FCS and 100 U/ml P/S. Cells were splitted after they reached 80 % confluency. To detach cells from dishes, cells were washed with PBS and treated with 1–3 ml 0.05 % trypsin/EDTA solution for approximately 5 min. The reaction was stopped by adding fresh DMEM medium. Finally, cells were diluted in flasks or seeded in appropriate dishes for further experiments.

6.1.3 Cultivation of suspension cells

For cultivation of Jurkat T cells, RPMI medium supplemented with 10 % FCS and 100 U/ml P/S was used. Jurkat T cells were kept at a density between 0.5x and 1.5x 10^6 cells/ml. Before experiment, the cells were kept at a density of approximately 1x 10^6 cells/ml. Primary murine CD4 T cells were cultured in RPMI medium supplemented with 10 % heat-inactivated FCS, 1 % P/S, 1 % NEAA, 1 % HEPES (pH 7,4), 1 % L-glutamine, 1 % sodium pyruvate and 0.1 % β-mercaptoethanol.

6.1.4 Isolation and cultivation of primary murine CD4 T cells

For stimulation and knockdown experiments, primary murine CD4 T cells were isolated from spleen and lymph nodes (axial, inguinal and neck) from MALT1 ko mice by negative magnetic-activated cell sorting (MACS) selection using the murine CD4 T cell isolation kit (Miltenyi Biotec). First, spleen and lymph nodes were put into primary T cell medium (RPMI medium + 10 % heat-inactivated FCS, 1 % P/S, 1 % NEAA, 1 % HEPES, 1 % L-glutamine, 1 % sodium pyruvate and 0.1 % β-mercaptoethanol) and grinded through a cell strainer (100 μM). To separate the cells from residual tissue particles, the homogenate was pelleted by centrifugation (1300 rpm, 5 min). Afterwards, the pellet was re-suspended in 500 μl DMEM and incubated with 5 ml RBC lysis buffer (Miltenyi Biotec) for 2 min on RT to destroy erythrocytes. Samples were washed, centrifuged and re-filtered through a cell strainer to further eliminate residual tissue particles. The remaining cells were resuspended in ice-cold CB buffer (400 μl/mouse) before adding a cocktail of biotin-conjugated antibodies

(100 µl/mouse, Miltenyi Biotec) to deplete non-CD4 T cells. After incubation for 5 min at 4 °C, samples were filled up with 300 µl/mouse of ice-cold CB buffer and incubated with magnetically labeled anti-biotin microbeads (200 µl/mouse, Miltenyi Biotec) for 10 min at 4 °C. Finally, the cell suspension was applied to LS columns (Miltenyi Biotec) in a MACS separator, whereby the magnetically labeled cells were retained in the columns and the unlabeled CD4 T cells were enriched in the flow-through. The separated CD4 T cells were pelleted and re-suspended in an appropriate volume of primary T cell medium (cell density 0.5×10^6 cells/ml). For expansion of primary murine CD4 T cells, 1:5000 recombinant IL-2 (Proleukin®S, Novartis Pharma) was added to the medium.

6.1.5 Isolation and cultivation of primary human CD4 T cells

For isolation of human CD4 T cells, blood was taken from healthy donors into S-Monovette (Sarstadt) columns containing already Lithium-Heparin. Blood was centrifuged (300x g, 10 min, RT, no break) to separate plasma (upper layer), buffy coat (intermediate layer) and erythrocytes (lowest layer). After removal of the plasma fraction, the intermediate buffy coat layer containing leukocytes and platelets was collected (approx. 10-18 ml/50 ml blood) and diluted with PBS up to a volume of 35 ml. To isolate mononuclear cells (MNCs), diluted buffy coat was carefully layered onto 15 ml Lymphoprep density gradient medium (Stemcell Technologies) and centrifuged (160x g, 20 min, RT, no break). About 20 ml supernatant were removed without touching the next layer and the sample was again centrifuged (350x g, 20 min, RT, no break). Finally, the intermediate layer containing the MNCs was collected and washed two times with PBMC buffer B1 (300x g, 8 min, 4 °C). CD4 T cells were isolated by negative MACS selection using the human CD4 T cell isolation kit (Miltenyi Biotec) according to the manufacturer's instructions (see 6.1.4). Purified cells were resuspended in primary T cell medium (RPMI 1640 + 10 % heat-inactivated FCS, 1 % P/S, 1 % NEAA, 1 % HEPES, 1 % L-glutamine, 1 % sodium pyruvate and 0.1 % β-mercaptoethanol) at a density of 2×10^6 cells/ml and used for further stimulations. Written consent and approval by the ethics board of the Medical Faculty at the Technical University Munich was obtained for the use of peripheral blood from healthy donors.

6.2 Cell transfection and transduction

6.2.1 Transfection of Jurkat T cells by electroporation

Transfection of Jurkat T cells with CRISPR/Cas9 and sgRNA constructs was performed by electroporation. Thereby electric pulses are used to induce pores in the cell membrane, which enable the uptake of foreign DNA. 8×10^6 Jurkat T cells in 400 µl Jurkat T cell medium were mixed with 10 µg plasmid DNA and transferred into an electroporation cuvette (0.4 cm). Cells were electroporated at 180 V and 1000 µF using a Gene Pulser (Bio-Rad) and transferred into pre-warmed RPMI medium.

6.2.2 Generation of CK1α- and MALT1-deficient Jurkat T cells

Jurkat T cells were transfected with pX330 (Addgene #42230; gifted by F. Zhang) or pX458 (Addgene #48138; gifted by F. Zhang) plasmids bearing Cas9 and sgRNAs as described in 6.2.1. After 24 h of incubation, the cells were either put under Puromycin selection for 48 h (co-transfection with pX330) or GFP-positive cells were FACS sorted. Using serial dilution selected cells were plated in 96 well plates with a density of 0.5, 2 and 5 cells/well. These plates were then incubated for approximately two weeks at 37 °C and 5 % CO_2 before growing cell clones could be picked, be further expanded and analyzed by PCR and Western blot.

6.2.3 Lentiviral transduction of Jurkat T cells

To generate stable MALT1 expressing cell lines, MALT1-deficient Jurkat T cells were lentivirally transduced with different pHAGE-hΔCD2-T2A-MALT1 constructs. The T2A sequence allows translation of both truncated human surface marker CD2 (hΔCD2) and MALT1 from the same mRNA by a mechanism called ribosomal skipping. Thereby the formation of the glycyl-prolyl peptide bond at the 2A C-terminus is inhibited resulting in a translational stop and the release of the nascent polypeptide from the ribosome [162]. Subsequently, translation of downstream sequences is resumed by the ribosome, which leads to the generation of two distinct proteins [162].

First, lentiviruses were produced by transfecting HEK293T cells with MALT1 expression plasmids and lentiviral packaging vectors. In more detail, 1.5×10^6 HEK293T cells were seeded in a 10 cm^2 dish in 8 ml DMEM medium one day before transfection. The next day, HEK293T cells were transfected with 1 µg of the lentiviral envelope plasmid pMD2.G (Addgene #12259;gifted by D. Trono), 1.5 µg of the packaging vector psPAX2 (Addgene #12260;gifted by D. Trono) and 2 µg MALT1 transfer plasmid (pHAGE-hΔCD2-T2A-MALT1-StrepTagII) using X-tremeGENE HP DNA Transfection Reagent (Roche Diagnostics) according to the manufacturer's instructions. After 3 days, the supernatant containing the virus particles was removed and sterile filtered (0.45 µM). 500 µl, 1000 µl and 1500 µl virus together with 8 µg/ml polybrene was added to 2×10^5 MALT1-deficient Jurkat T cells. 24 h later, cells were washed with PBS and resuspended in 1 ml fresh RPMI medium. After one week in culture, infection efficiency was determined by analyzing hΔCD2 expression using flow cytometry or by checking MALT1 expression levels via Western Blot. When comparing several mutants similar expression levels were used.

6.2.4 Retroviral reconstitution of CD4 T cells from MALT1 KO mice

Retroviruses were produced in Phoenix cells transfected with pMSCV retroviral transfer vectors carrying human MALT1-FlagStrepII constructs and Thy1.1 (separated by internal ribosome entry site (IRES) sequence). Virus supernatants were collected after 48 h and 72 h and combined. Prior to the infection, CD4 T cells were stimulated for 48 h using hamster anti-murine anti-CD3 (0.5 µg/ml) and hamster anti-murine anti-CD28 (1 µg/ml) on anti-

hamster pre-coated plates. For infection, CD4 T cells were incubated for 6 h with retroviral supernatant supplemented with Polybrene (8 µg/ml) and then washed using RPMI medium [40, 66]. Cultivation and expansion of primary murine CD4 T cells was performed as described before.

6.2.5 Overexpressing proteins in HEK293

For overexpression experiments HEK293 cells were transfected using calcium phosphate. Therefore 2.5x 10^6 cells were seeded in a 10 cm dish on the day before. For transfection 50 µl $CaCl_2$ (2.5 M) were mixed with 450 µl H_2O and plasmid were added to this. Per construct 2.5 µg plasmid DNA was used but overall 10 µg DNA. If less constructs were used the approach was filled up using empty vectors. After mixing this solution was added dropwise into 500 µl 2x HBS while vortexing it. The mixture was incubated for 20 min at RT and then added completely dropwise to one cell culture dish. 48 h after transfection the cells were harvested and lysed in 800 µl co-IP buffer containing protease inhibitors (20 min rotating at 4 °C). 30 µl HA antibody (12CA5, Monoclonal Antibody Core Facility, HMGU) was added to the lysate and incubated o/N at 4 °C. Finally 18 µl rec.-Protein G sepharose beads were added, incubated for 1 – 2h at 4 °C on a turning wheel and the resin was washed at least three times with co-IP buffer. The beads were aspirated completely, approx. 20 µl 2x SDS loading buffer (Roti®-Load1, Carl Roth) was added and boiled for 7 min.

6.3 Cell stimulation

6.3.1 Stimulation of Jurkat T cells and primary human CD4 T cells

Jurkat T cells were stimulated with P/I (Phorbol 12-myristate 13-acetate (PMA)/Ionomycin) using a concentration of 200 ng/ml PMA and 300 ng/ml Ionomycin. P/I stimulation acts downstream of TCR/CD28 as PMA directly stimulates PKCθ and Ionomycin triggers Ca^{2+} release from the endoplasmatic reticulum into the cytosol. Stimulation was performed in tubes at 37 °C.

Primary human CD4 T cells were also stimulated with P/I using a concentration of 200 ng/ml PMA and 300 ng/ml Ionomycin.

Anti-CD3/CD28 stimulation was performed in 300 µl medium using 1 µg/ml murine anti-human anti-CD3 antibodies (IgG1) and 3 µg/ml murine anti-human anti-CD28 antibodies (IgG2a). The antibodies were cross linked using each 3 µg/ml anti-mouse IgG1 and anti-mouse IgG2a antibodies. Stimulation was performed in tubes at 37 °C.

6.3.2 Stimulation of primary murine CD4 T cells

Primary murine CD4$^+$ T cells were stimulated with P/I or anti-CD3 and anti-CD28 antibodies in primary T cell medium. For P/I stimulation, 200 ng/ml PMA and 300 ng/ml Ionomycin were used. Anti-CD3/CD28 stimulation was performed on pre-coated plates. Therefor plates were

coated with rabbit anti-hamster IgG (30 µl in 1 ml PBS per 6-well) over night at 4 °C. Afterwards, plates were washed two times with PBS before cells were stimulated with anti-CD3 (0.5 µg/ml) and anti-CD28 (1 µg/ml) and added to the pre-coated wells. Cells were stimulated at a density between 1x 10^6 and 5x 10^6 cells per ml.

6.4 Flow cytometry

6.4.1 Flow cytometry and cell sorting

Cell populations were analyzed regarding their surface protein expression and intracellular cytokine levels either on an Attune Acoustic Focusing Cytometer (Life Technologies). For sorting, the Cytomation MoFlow coupled with a SortMaster DropletControl (Cytomation) was used operating with a 100 µm nozzle.

6.4.2 Staining of surface molecules

To check hΔCD2 surface expression of infected CK1α- or MALT1-deficient Jurkat T cells, around 0.2x 10^6 cells were collected and resuspended in 400 µl FACS buffer. Cells were stained with anti-CD2-APC antibody (human, dilution 1:400) for 15 min at 4 °C in the dark. Afterwards samples were washed with FACS buffer, taken up in ca. 200 µl FACS buffer and acquired on Attune Acoustic Focusing Cytometer.

For staining of Thy1.1 expression in primary murine CD4 T cells, cells (0.2-1x 10^6) were collected after stimulation and were resuspended in FACS buffer. To prevent unspecific antibody binding to Fc receptors, samples were first treated with anti-CD16/32 (mouse, dilution 1:50) for 10 min at 4 °C. Afterwards, staining with anti-Thy1.1-APC (1:200 dilution) was performed for 10-15 min at 4 °C in the dark. Samples were washed, resuspended in FACS buffer and acquired on Attune Cytometer.

6.4.3 Intracellular cytokine staining

For intracellular IL-2 staining, primary murine CD4 T cells (1x 106) were stimulated for 5 h with P/I or anti-CD3/CD28 in the presence of Brefeldin-A (10 ng/ml, Sigma) to prevent exocytosis of signaling molecules. After stimulation, cells were collected, centrifuged (300x g, 5 min, 4 °C) and if needed stained for surface marker. Afterwards, samples were washed and fixed in 2 % PFA for 15 min at RT. Then, cells were washed and permeabilized in IC buffer (0,2 % saponin in PBS) for 15 min at RT. Unspecific antibody binding was blocked with anti-CD16/32 (mouse, dilution 1:50 in saponin buffer, 10 min, 4 °C) before samples were incubated with anti-IL-2-FITC or anti-IκBα antibodies (both mouse, dilution 1:100 in IC buffer) for 30 min on ice. Afterwards, cells were washed (300x g, 5 min, 4 °C) and filled up with FACS buffer to wash out unbound antibodies (> 15 min, RT). Anti-IκBα treated cells had to be stained with a secondary rat anti-mouse-IgG1-FITC antibody (1:300,

20 min at 4 °C in the dark). Samples were again washed (300x g, 5 min, 4 °C), resuspended in FACS buffer and acquired on Attune Cytometer.

6.5 Molecular biology methods

6.5.1 Polymerase chain reaction (PCR)

Amplification of DNA was performed using polymerase chain reaction (PCR).

Table 6-1: PCR standard protocol.

Component	Amount
Template DNA	30 ng
5' primer (10 µM)	1.25 µl
3' primer (10 µM)	1.25 µl
dNTP (10 mM)	1,25 µl
Herculase buffer (10x)	10 µl
DNA polymerase (Herculase)	1 µl
	Add to 50 µl H_2O

Table 6-2: PCR standard program.

Step	Temperature	Time	
Melting	95 °C	10 min	
Melting	95 °C	1 min	
Annealing	Tm primer -5 °C	1 min	30 cycles
Extension	72 °C	30 s/1 kb	
Extension	72 °C	10 min	

PCR program was adapted in times and number of cycles if needed. The products were checked for correct amplification on an agarose gel. Purification of PCR products was performed using PCR Purification Kit (Qiagen). For the generation of MALT1 phospho-mutants, megaprimer PCR was used to introduce serine (S) to alanine (A) point mutations. First, two primers were designed to generate the megaprimer: one primer bears the desired mutation, whereas the other primer flanks the coding sequence. After purification, the generated megaprimert was used in a second PCR round. Thereby, the product was combined with a third primer to amplify the whole gene sequence. Finally, the PCR product can be cloned into the target vector.

6.5.2 DNA restriction digestion, agarose gel electrophoresis and DNA extraction

PCR products or plasmid DNA were digested using endonucleases from NEB and the appropriate buffers. After restriction digest, DNA was mixed with 6x DNA loading buffer and separated on an agarose gel. For gel preparation, agarose was dissolved in TBE buffer and supplemented with ethidium bromide. Agarose gels were run in TBE buffer at 90 to 100 V. To determine DNA fragment size, 3 µl 1 kb plus DNA ladder was loaded. DNA bands were visualized with UV light and were cut out for extraction using the Gel Extraction Kit (Macherey & Nagel) according to the manufacturer's instruction.

6.5.3 DNA ligation and transformation of *Escherichia coli*

For ligation of digested plasmids and PCR products, T4 DNA ligation Kit (NEB) was used according to the manufacturer's protocol. Depending on the size ratio between vector and PCR fragment, ligation was performed using a molar ratio of 1:3 to 1:5 vector to insert. The complete ligation mixture was added to competent *Escherichia coli* (*E. coli*) TOP10 or STBL3 cells and was incubated for 30 min on ice. After a heat-shock at 42 °C for 45 s, competent cells were cooled down on ice for 2 min and subsequently supplemented with 400 µl LB medium. Cells were raised in a shaker at 37 °C for 60 min and afterwards plated on LB agar plates containing the appropriate antibiotic. Plates were incubated over night at 37 °C.

6.5.4 Cultivation of *E. coli* and plasmid preparation

To isolate the generated plasmid DNA, LB medium was prepared and supplemented with the appropriate antibiotic (e.g. ampicillin 100 µg/ml). 3 – 5 ml of LB medium were inoculated with one colony from LB agar plates and cultivated in a shaker (180 rpm) over night at 37 °C. Plasmid DNA was isolated using the Plasmid Mini Kit (Macherey & Nagel) according to the manufacturer's protocol. To generate larger DNA amounts, a small remaining aliquot of mini preps was used or 100-500 ng of the purified plasmid were re-transformed into competent *E. coli* cells. Afterwards, these cells were directly transferred into 150-200 ml LB medium and grown over night at 37 °C. For plasmid isolation, the Plasmid Maxi Kit (Qiagen) was used.

6.5.5 DNA sequencing

Purified DNA and the appropriate sequencing primers were send to Eurofins MWG Operon (Ebersberg) for sequencing.

6.5.6 RNA isolation

For extraction of RNA, 2x 10^6 cells were lysed in 350 µl RLT lysis buffer (Qiagen) or 350 µl Lysis Solution TR (Stratec). Afterwards, RNA was isolated according to the protocol of either the Qiagen RNeasy RNA isolation kit or InviTrap® Spin Universal RNA Mini kit. For the Qiagen kit, lysates had to be transferred onto shredder columns for homogenization (Qiagen) before isolation. In a next step, RNA concentration was measured using NanoDrop and RNA levels were adjusted up to 1 µg/ml. RNA was stored at -80 °C.

6.5.7 Reverse transcription into cDNA

RNA samples were reverse transcribed into cDNA using Verso cDNA Synthesis Kit (Thermo Fisher Scientific) according to the manufacturer's instructions. Thereby, random hexamers were used as primers for the Reverse Transcriptase. Generated cDNA was stored at -80 °C.

6.5.8 Real-time PCR (RT-PCR)

Quantitative real-time PCR (qPCR) is a useful method to quantify RNA amounts, in which DNA amplification can be detected by using a fluorescent dye LightCycler 480 SYBR Green I Mastermix (Roche) that binds double stranded DNA. The fluorescence increases with each cycle of amplification and can be detected with a LightCycler 480 (LC-480, Roche). The following standard protocol was used:

Table 6-3: RT-PCR standard protocol

Component	Amount
Template cDNA	2 µl
5' primer (20 µM)	1 µl
3' primer (20 µM)	1 µl
SYBR Green I Mastermix (2x)	10 µl
	Ad 20 µl H_2O

Table 6-4: RT-PCR standard program.

Step	Temperature	Time	
Melting	95 °C	10 min	
Melting	95 °C	10 s	
Annealing	60 °C	10 s	40–45 cycles
Extension	72 °C	10 s	
Melting curve	65 °C – 95 °C		

To quantify target gene expression, human RNA polymerase II (*RP2*) or was used as internal controls. Relative expression levels were calculated using the ΔΔCp method [163].

6.6 Biochemical and immunological methods

6.6.1 Preparation of whole cell lysates

For analysis of protein expression levels and activation of downstream signaling pathways including NF-κB DNA binding, $1x\ 10^6 - 5x\ 10^6$ cells were harvested (1800 rpm, 5 min, 4 °C), washed with PBS and subsequently lysed in 60–120 µl high salt buffer. Lysates were incubated on a shaker for 20 min at 4 °C before insoluble cellular debris were removed by centrifugation (14 000 rpm, 15 to 30 min, 4 °C). For Western Blot analysis, samples were mixed with 4x SDS loading buffer (Rotiload, Roth) and boiled for 5 min at 95 °C.

6.6.2 Co-immunoprecipitation (co-IP) and Strep-Tactin (ST) pulldown

For protein interaction studies, $1x\ 10^7 - 3x\ 10^7$ cells were lysed in 800 µl co-IP buffer supplemented with protease inhibitors. Lysates were incubated for 20 min at 4 °C in an overhead rotator before samples were cleared by centrifugation (14 000 rpm, 15 min, 4 °C). 30 µl supernatant were collected as lysate controls and were mixed with 4x SDS loading buffer (Rotiload, Roth) and boiled for 5 min at 95 °C. The residual supernatant was used for binding studies. Immunoprecipitations (IPs) were carried out by using antibodies against BCL10 (C-17, 0,5 µg), CK1α (C-19, 1,5 µg or H-7, 2 µg), MALT1 (H300, 1,5 µg or B-12, 1,5 µg) or MALT1 pS803 (50 µl) and samples were incubated in an overhead rotator overnight at 4 °C. After antibody incubation, 18 µl rec Protein G Sepharose 4B (1:1 suspension, life technologies) was added and lysates were rotated for additional 1 – 2 h at 4 °C. For Strep-Tactin pulldowns (ST-PDs), Strep-tagged CK1α or MALT1 proteins were precipitated by using 30 µl Strep-Tactin Sepharose (1:1 suspension, IBA) at 4 °C overnight. After incubation with Protein G Sepharose or StrepTactin Sepharose, beads were washed four times with 500 µl ice-cold co-IP buffer without protease inhibitors (200x g, 5 min, 4 °C). Supernatant was completely removed by aspiration and approx. 15 – 20 µl 2x SDS loading buffer (Roti®-Load1, Carl Roth) was added to the beads. Samples were boiled at 95 °C for 7 min before they were separated by SDS-PAGE.

6.6.3 SDS polyacrylamide gel electrophoresis (SDS-PAGE)

Proteins of cellular lysates were separated by SDS-PAGE, which was performed under reducing conditions. Different concentrations of acrylamide (7 – 12,5 %) were used for the generation of separation gels with different pore sizes. APS (ammonium persulfate) and TEMED were added to the mixture to enable polymerization. After full polymerization of the separation gel, a 5 % polyacrylamide stacking gel containing pockets for the lysate samples was layered on top of the separation gel. When gels were fully polymerized, protein lysates

were loaded. A prestained protein ladder (Thermo Fisher Scientific) was also loaded to estimate the molecular weight of the separated proteins. Electrophoresis was performed in SDS electrophoresis buffer at 90 V for 30 min before voltage was increased to 110 – 130 V for 60 – 90 min.

6.6.4 Western Blot (WB)

To enable detection of proteins separated by SDS-PAGE, proteins were transferred onto PVDF membranes using a semi-dry transfer system. Thereby, PVDF membranes were activated in methanol and Whatman filter papers were soaked in 1x blotting buffer. The SDS gel and the membrane were placed between soaked Whatman filter papers in the blotting apparatus. Proteins are transferred to the PVDF membrane by using an electric field (70 mA per gel for 100 min).

After blotting, membranes were blocked with 5 % BSA/PBS-T or 3 % milk powder/PBS-T for 60 min to avoid unspecific antibody binding. Blocked membranes were incubated with primary antibody (dilution 1:1000 in 1.5 % BSA/PBS-T or milk) overnight at 4 °C. Membranes were washed at least three times with PBS-T for 10 min at RT to remove unspecifically bound antibodies. Afterwards, HRP-coupled secondary antibody (dilution 1:10 000 in 1.5 % BSA/PBS-T) was added for 45 minutes at RT. Membranes were again washed with PBS-T to remove unbound antibodies. HRP activity was detected by using enhanced chemiluminescence (ECL) substrate (Cell Signaling) in a 1:10 – 1:20 dilution in water. HRP catalyses oxidation of the substrate and is accompanied by the emission of light, which was detected by Intas ChemoCam Imager (HR16-3200). For detection of further proteins on the same membrane, membranes were washed with PBS-T and treated with stripping buffer for 30 min at RT to remove all bound primary and secondary antibodies. Membranes were washed at least three times with PBS-T for 5 min, blocked with 5 % BSA or milk solution and incubated with a specific primary and secondary antibody as described before.

6.6.5 MALT1 activity detection using MALT1 activity-based probes

MALT1 activity-based probes (ABPs) can be used to monitor cellular MALT1 activity [80]. The MALT1 ABPs consist of a specific recognition element LRSR, an electrophile (AOMK) that forms a covalent bond with the active cysteine and a certain detection marker. An ABP coupled to biotin was used for pulldown of active MALT1. In this assay, Jurkat T cells (5x 10^7 cells) were lysed in 600 µl co-IP buffer, centrifuged (14 000 rpm, 15 – 20 min, 4 °C) and precleared using 15 µl High Capacity Streptavidin Agarose beads (Thermo Scientific). Afterwards 0.1 µM biotinylated MALT1 ABP was added (1 h at RT) and then again incubated with 15 µl beads (1 h at 4 °C). Beads were washed three times with co-IP buffer without protease inhibitors (200x g, 5 min, 4 °C), then 20 µl 2x SDS loading buffer (Roti®-Load1, Carl Roth) was added and cooked at 90k °C for 7 min.

6.6.6 Electrophoretic mobility shift assay (EMSA)

Electrophoretic mobility shift assays (EMSAs) enable the visualization of transcription factor binding to DNA. Thereby, radioactive labeled oligonucleotides containing specific DNA response elements are incubated with protein lysates, and the mixture is separated on a native polyacrylamide gel, in which protein-DNA complexes migrate more slowly than free unbound DNA. Due to the radioactive labeling, DNA-transcription factor complexes can be detected with X-Ray films.

To produce radioactive labeled DNA probes, single oligonucleotides were annealed resulting in the formation of 5' overhanging dsDNA-oligonucleotides. Overhangs were filled in with radioactive nucleotides by Klenow polymerase according to the following protocol:

Table 6-5: Labeling of DNA probes.

Component	Amount
DNA oligonucleotide	400 ng
Klenow buffer (10x)	2.5 µl
dNTP-A (10 µM)	1.8 µl
[32]P-α-dATP	30 µCi
Klenow Fragment	1 U
	ad 25 µl H_2O

The reaction was incubated for 30 min at 37 °C. Afterwards, samples were purified using QIAQuick Nucleotide Removal Kit (Qiagen). To determine DNA binding activities of NF-κB and OCT1, EMSAs were performed using cells which were lysed in high salt buffer (see 6.6.1) and ^{32}P-α-dATP-labeled NF-κB (H2K) or OCT1 DNA binding site probes. Assays were conducted according to the following protocol:

Table 6-6: EMSA standard protocol.

Component	Amount
Protein extract	~ 5 µg
2x Shift buffer	10 µl
BSA	10 µg
DTT (100 mM)	1 µl
Poly dI-dC (2 µg/µl)	1 µl
[32]P-α-dATP-labeled probe	1 µl (10 000–20 000 cpm)
	ad 20 µl H_2O

Reaction mixture was incubated for 30 min at RT and separated on a native polyacrylamide gel (5 %) in 1x TBE buffer at 26 mA/gel. Gels were dried on a Whatman filter paper at 80 °C for 1 h and exposed to autoradiography films.

6.6.7 Production and purification of recombinant proteins

N-terminally GST-tagged MALT1 325-760 was expressed in *E. coli* BL21-CodonPlus (DE3)-RIPL cells and purified via affinity chromatography using GSTrap™ High Performance columns (GE Healthcare). Bacteria were grown in LB-medium at 37°C with 100 µg/µL ampicillin and 25 µg/mL chloramphenicol to an OD600 of 0.6-0.8, then moved to 18°C and rotated for an additional 30 min before induction with 50 µM IPTG. Protein was produced overnight (18°C, 150 rpm). Cells were harvested and resuspended in 7 mL of lysis buffer (50 mM HEPES pH 7.5, 10% (v/v) glycerin, 0.1 % (v/v) Triton X100, 150 mM NaCl, 2 mM MgCl$_2$ x 6H$_2$O, 1 mM DTT, protease inhibitor cocktail (Roche)). Cell suspension was lysed by sonication and centrifuged for 30 min (16,500 rpm, 4°C). Supernatant was transferred to a new tube, and centrifugation was repeated for 60 min. Supernatant containing recombinant Malt1 protein was applied to the ÄKTA and unspecifically bound proteins were washed through the column with wash buffer (50 mM Tris, 150 mM NaCl, pH 8.0). Malt1 was eluted with elution buffer (wash buffer with 15 mM glutathione). Eluate was concentrated to 600-800 µL using Amicon cellulose membrane filters (Merck) and protein concentration was determined using a NanoDrop (Thermo Fisher).

6.6.8 Generation of MALT1 protein using the baculoviral expression system

His$_6$-tagged MALT1 (aa 334-824)-HA were expressed in Sf9 cells using the baculovirus expression system [39]. The protein was purified using a nickel affinity chromatography according to the manufacturer's instructions (Qiagen).

6.6.9 *In vitro* kinase assay

Recombinant CK1α (Sigma-Aldrich) was incubated with of several bacterial produced and purified MALT1 protein constructs in the presence of radioactive γ-32P-ATP (Hartmann). Therefore 150 ng CK1α and 5 µg of each MALT1 proteins were used in 20 µl kinase assay buffer. In parallel a γ-32P-ATP-containing assay cocktail was prepared according to the manufacturer's guide. When Western blot samples were produced, the in vitro kinase assay was performed without radioactivity and therefore the γ-32P-ATP was replaced with non-radioactive ATP. The mix was incubated for 2 h at 30 °C, then 4x SDS loading buffer was added and the samples cooked for 5 min. 10 µl sample were loaded to 12,5 % SDS-PAGE. The gel was either dried and exposed to a X-ray film or a Western blot was performed (see 6.6.4 and 6.6.6).

6.6.10 NF-κB reporter assay

Co-transfection of 8x 10^6 Jurkat T cells with 5 µg plasmid of interest and 2 µg 6x NF-κB reporter plasmid (expressing Firefly luciferase) as well as 1 µg pTKluc plasmid (expressing Renilla luciferase) using electroporation. 48 h after transfection, cells were stimulated for 4 h with either P/I or anti-CD3/CD28 antibodies and lysed in 100 µl passive lysis buffer (PLB, Promega). A dual luciferase assay (Promega) was performed according to the manufacturer's protocol and luciferase activity was determined using a luminometer (LB 960, Berthold). Renilla luciferase activity was independent of NF-κB activation and could be used to normalize measured stimulations.

6.6.11 Generation of phospho-specific antibodies

Monoclonal antibodies were generated in cooperation with the Monoclonal Antibody Core Facility, HMGU. Therefore, C57BL/6 mice and Lou/c rats were immunized by injection of ovalbumin-coupled peptides comprising phosphorylated serine S562, S649 and S803 (S562: EYSAEpSLVRNL, S649: GSYLVpSKDLPK, S803: DEIPFpSFSDRL). Animals were injected subcutaneously and intraperitoneally with a mixture of 40 ug peptides, 5 nmol CpG (Tib Molbiol, Berlin, Germany) and an equal volume of incomplete Freund's adjuvant. Boost was performed 6 weeks later without Freund's adjuvant and spleen cells were fused with P3X63Ag8.653 myeloma cells using standard procedures. Hybriodma supernatants were screened in a solid-phase enzyme-linked immunosorbent assay (ELISA) for binding to the respective phospho-peptides. Specificity was confirmed by negative screening on respective non-phosphorylated peptides. Positive supernatants were further validated by Western blot analysis. Hybridoma cells from selected supernatants were subcloned at least twice by limiting dilution to obtain stable monoclonal cell clones recognizing phosphorylated serines pS562 (clone 24E9; rat IgG2b/k), pS649 (clone 29E12; mouse IgG2a/k) and pS803 (clone 24A4; rat IgG2c/k). Experiments were performed with hybridoma supernatant.

6.6.12 Sample preparation for phospho-peptide analysis of MALT1

For mass spectrometric analyses, Jurkat T cells were stimulated and MALT1 was enriched by ST-PD against MALT1 as described earlier. The eluates were diluted to 200 µl with ABC buffer (50 mM ammonium bicarbonate) and digested by a modified filter aided sample preparation (FASP) method [164] as described in [165]. Briefly, samples were reduced with 20 µl DTT (100 mM) for 30 min at RT (shaking), followed by alkylation of cysteine residues with 50 µl Iodoacetamide (300 mM) for 30 min at RT in the dark. Urea buffer (8 M Urea/0.1 M Tris/HCl (pH 8.5)) was added to a final concentration of ≥ 4 M and samples were loaded on a 30 kDa cut-off filter (Nanosep 30k OMEGA, Pall Life Sciences, Ann Arbor) previously equilibrated with 200 µl UA buffer and centrifuged at 14,000 g for 15-30 min. After sample loading, filters were washed three times with 200 µl urea buffer and twice with 100 µl ABC buffer. Digestion was performed with 2 µg Lys-C (Wako Chemicals, Neuss) in 70 µl ABC buffer containing phosphatase inhibitors (Phosphatase Inhibitor Cocktails 2 & 3,

1:100 (v/v), Sigma-Aldrich) for 2 h at RT followed by tryptic (5 µg, Sigma-Aldrich) digest at 37° C for 16 h. Digested peptides were collected by centrifugation at 16,000 g for 15 min and residual peptides were eluted from the filters with 20 µl 50 mM ABC/2 % ACN. Combined eluates were concentrated to 40 - 50 µl in a vacuum centrifuge (Univapo 150 ECH, UniEquip, Martinsried).

For phospho-peptide enrichment, TiO_2 beads (Sachtopore NP, 5 µm, 300 Å (SNX030S005), Sachtleben Chemie, Duisburg) were suspended in water at 125 µg/µl and 20 µl per sample were washed sequentially with 400 µl water, 400 µl ACN and equilibrated in 400 µl washing buffer (60 % ACN/4 % TFA) by centrifugation at 15,000 g for 1 min. The peptide eluates were diluted with 160 µl loading buffer (80 % ACN/5 % TFA) and incubated with the bead preparation for 90 min at RT (shaking). The supernatant containing unbound peptides was discarded after centrifugation and the beads were washed three times for 2 min at RT with 200 µl 50 % ACN/0.1 % TFA. Enriched phospho-peptides were then eluted twice with 20 µl NH_4OH (10 %) for 10 min at RT (shaking) by centrifugation (21,000 g, 3 min) and the combined eluates were acidified with TFA to pH 2.

6.6.13   LC-MS/MS data acquisition

Enriched phospho-peptides were analyzed on an Ultimate 3000 nano HPLC system (Dionex, Sunnyvale, CA) coupled to a LTQ Orbitrap XL mass spectrometer (Thermo Fisher Scientific), equipped with a nano-ESI source.

20 µl of each enriched sample were injected automatically and peptides were loaded on a nano trap column (5 mm x 300 µm i.d., packed with 5 µm Acclaim PepMap100 C18 resin, 100 Å pore size (LC Packings, Sunnyvale)) at a flow rate of 30 µl/min using 7 % ACN/0.1 % FA (v/v) in HPLC-grade water for 5 min. Separation of peptides was performed on a reversed-phase analytical column (15 cm x 75 µm i.d., Acclaim PepMap C18 resin, 3 µm, 100 Å pore size (Dionex)) at a constant temperature of 40° C and peptides were eluted using the following gradient conditions at a flow rate of 300 nl/min: linear from 7 % ACN to 32 % ACN over 60 min, linear from 32 % ACN to 93 % ACN in 1 min and isocratic at 93 % ACN for 5 min, followed by an equilibration step for 15 min at starting conditions (all ACN buffers included 0.1 % (v/v) FA).

Ionisation of peptides was performed in a nano-ESI source using 1.51 kV spray voltage and a capillary temperature of 200° C. The mass spectrometer was operated in data-dependent acquisition mode, in which up to ten most intense precursor ions were selected for fragmentation. The signal of polysiloxan (m/z = 445.12002) was used as lock mass for internal calibration. Full scan MS spectra were acquired in the Orbitrap mass analyser within a m/z range from 300 to 1500 with a resolution of 60,000 at m/z 400. The AGC target value for precursor ions was set to 1e6 and ions were collected for maximally 500 ms. Up to ten precursors with charge state ≥ 2 were isolated in a window of 2 Th and selected for fragmentation by CID in the linear ion trap if a minimal ion count of 200 was exceeded. Precursor ions were fragmented with 35 % normalized collision energy and an activation time of 30 ms. MS/MS scans were acquired with a resolution of 15,000 at m/z 400 and an

AGC target value of 1e4 with a maximal injection time of 100 ms. After MS/MS analysis, precursor ions were dynamically excluded for 30 s.

6.6.14 Raw data processing and analysis

Mass spectrometric raw data were analyzed with Proteome Discoverer Software (Version 1.4.1.14, Thermo Fisher Scientific) using Mascot (Version 2.5.1, Matrix Science, London) as search engine. MS/MS spectra were searched against Ensembl Human database (Release 80, May 2015) with a precursor mass tolerance of 7 ppm and fragment mass tolerance of 0.7 Da, carbamidomethylation (C) as static modification and deamidation (N,Q), oxidation (M) and phosphorylation (S, T, Y) as dynamic modifications. Enzyme specificity was set to trypsin and up to two missed cleavages were allowed. For the confident localization of phosphosites, phosphoRS (Version 3.0) node was included in the Proteome Discoverer workflow. MALT1 identifications were adjusted to < 1 % FDR at PSM level based on Percolator q-Value.

6.7 Statistical analysis

All experiments were performed at least three times unless otherwise indicated. Values represent the mean ± standard deviation (SD). Experiments were analyzed by using unpaired Student's *t*-test. Statistical significance values are *p < 0.05; **p < 0.01; ***p < 0.001.

7 Abbreviations

° C	° Celsius
A/Ala	alanine
Å	Ångström
aa	amino acid
ABC	activated B cell-like (DLBCL)
ABP	activity based probe
AgR	antigen-receptor
AP-1	activator protein-1
APC	antigen presenting cell
APC	allophycocyanin
APS	ammonium persulfate
ATP	adenosine triphosphate
BCL10	B cell chronic lymphocytic leukemia/lymphoma 10
BCR	B cell receptor
BM	bone marrow
bp	base pair
BSA	bovine serum albumin
BTK	Bruton's tyrosine kinase
C/Cys	cysteine
Ca^{2+}	calcium
CaMKII	calmodulin-dependent protein kinase II
CARD	caspase-recruitment domain
CARMA1	CARD-containing MAGUK 1 (also known as CARD11)
CARD11	Caspase recruitment domain-containing protein 11
Cas9	CRISPR-associated protein-9
CBM	CARMA1-BCL10-MALT1
CC	coiled-coil
CD	cluster of differentiation
CD62L	CD62 ligand
cDNA	complementary DNA
CK1α	Casein kinase 1 alpha
Co-IP	Co-immunoprecipitation
cpm	counts per minute

CRISPR	Clustered Regularly Interspaced Short Palindromic Repeats
Cryo-EM	cryo-electron microscopy
C-Terminus	Carboxyl-terminus
CYLD	cylindromatosis
D/Asp	aspartate
DAG	diacylglycerol
dATP	desoxyadenosine triphosphate
DD	death domain
DLBCL	diffuse large B cell lymphoma
DMEM	Dulbecco's Modified Eagle Medium
DMSO	dimethyl sulfoxide
DNA	deoxyribonucleic acid
dNTP	deoxyribonucleotide triphosphate
ds	double-stranded
DTT	dithiothreitol
DUB	deubiquitinase
E/Glu	glutamate
EAE	experimentally induced autoimmune encephalomyelitis
ECL	enhanced chemiluminescence
EDTA	ethylenediaminetetraacetic acid
EGFP	enhanced green fluorescent protein
EGTA	Ethyleneglycol-bis(2-aminoethylether)-N,N,N′,N′-tetraacetic acid
EMSA	electrophoretic mobility shift assay
ERK	extracellular signal-regulated kinase
ES	embryonal stem cell
EUCOMM	European Conditional Mouse Mutagenesis Program
FACS	fluorescence-activated cell sorting
FCS	fetal calf serum
FITC	fluorescein isothiocyanate
FO B cell	follicular B cell
FOXP3	forkhead box p3
FRT	binding site for recombinase Flippase (Flp)
FS	Flag-StrepII
g	gravity
GADS	GRB2-related adapter downstream of Shc

GCB	germinal center B cell-like (DLBCL)
GRB2	growth factor receptor-bound protein 2
GSK3	glycogen synthase kinase
GUK	guanylate kinase
H/His	histidine
h	human
h	hour
HEK	human embryonic kidney
HEPES	2-[4-(2-Hydroxyethyl)-1-piperazino]-ethansulfonic acid
HSC	hematopoietic stem cells
HMBS	hydroxymethylbilane synthase
HOIL1	heme-oxidized IRP2 ubiquitin ligase 1
HPK1	hematopoietic progenitor kinase 1
HRP	horseradish peroxidase
I	Ionomycin
ICOS	inducible T cell co-stimulator
IFNγ	interferon gamma
Ig	immunoglobulin
IKK	IκB kinase
IL	interleukin
IP	immunoprecipitation
IP3	inositol 1,4,5-trisphosphate
IRES	internal ribosome entry site
IS	immunological synapse
ITAM	immunoreceptor tyrosine-based activation motif
ITCH	E3 ubiquitin-protein ligase Itchy homolog
IκB	inhibitor of κB
IKK	IκB kinase
JNK	c-Jun N-terminal kinase
K/Lys	lysine
kb	kilo base
kDa	kilo Dalton
KH2PO4	potassium hydrogen phosphate
KO	knockout
LAT	linker for activation of T cells

LB	Luria-Bertani (medium)
Lck	lymphocyte-specific protein tyrosine kinase
LEF	lymphoid enhancer binding factor 1
LN	lymph node
LPS	lipopolysaccharide
LUBAC	linear ubiquitin chain assembly complex
MACS	magnetic-activated cell sorting
MAGUK	membrane associated guanylate kinase
MALT1	mucosa associated lymphoid tissue lymphoma translocation protein 1
MAPK	mitogen activated protein kinase
MFI	mean fluorescence intensity
MFI	median fluorescence intensity
mg	milligram
$MgCl_2$	magnesium chloride
MHC	major histocompatibility complex
min	minute
ml	milliliter
mRNA	messenger RNA
MZ B cell	marginal zone B cell
Na_2HPO_4	disodium hydrogen phosphate
NaCl	sodium chloride
NaF	sodium fluoride
NaN_3	sodium azide
NEAA	non-essential amino acids
NEDD	neural precursor cell expressed developmentally down-regulated protein
NEMO	NF-κB essential modulator
NFAT	nuclear factor of activated T cells
NF-κB	nuclear factor kappa B
ng	nanogram
NH_4Cl	ammonium chloride
nm	nanometer
NP-40	nonidet P40 substitude
nt	nucleotide
N-terminus	amino-terminus

OVA	ovalbumin
P/S	penicillin/streptomycin
PAMP	pathogen-associated molecular pattern
PBMC	peripheral blood mononuclear cells
PBS	phosphate buffered saline
PBS-T	PBS-Tween 20
PCASP	paracaspase
PCR	polymerase chain reaction
PD-1	programmed cell death protein-1
PDK1	phosphoinositide-dependent kinase 1
PDZ	PSD-95/DLG/ZO1 homology
PE	phycoerythrin
PFA	paraformaldehyde
PH	pleckstrin homology
PI3K	phosphoinositide 3 kinase
PIP2	phosphatidyl inositol 4,5-bisphosphate
PIP3	phosphatidyl inositol 3,4,5-trisphosphate
PKC	protein kinase C
PLCγ1	phospholipase C gamma 1
PM	paracaspase mutant
PMA	phorbol 12-myristate 13-acetate
PP2A	protein phosphatase 2A
PPR	pattern-recognition receptor
R	arginine
Ras	rat sarcoma
RasGRP	Ras guanyl nucleotide-releasing protein
RHD	Rel homology domain
RNA	ribonucleic acid
RPII	RNA polymerase II
rpm	rounds per minute
RT	room temperature
RT-PCR	Real-time PCR
S	serine
s	second
SD	standard deviation

SDS	Sodium dodecyl sulfate
SDS-PAGE	SDS polyacrylamide gel electrophoresis
Ser/Thr-rich	serine/threonine-rich
SH2	Src homology 2
SH3	Src homology 3
shRNA	small hairpin RNA
SLP76	SH2-domain containing leukocyte protein of 76 kDa
ST-PD	Strep-Tactin pulldown
SV40	simian virus 40
T/Thr	threonine
T6BM	TRAF6 binding motif
TAB	TAK1 binding protein
TAC	tris ammonium cloride
TAK	transforming growth factor beta activated kinase
TBE	Tris borate EDTA
TCR	T cell receptor
TE	Tris EDTA
TEMED	Tetramethylethylenediamine
TH	T helper cells
TLR	toll like receptor
Tm	melting temperature
TNF	tumour necrosis factor
TRAF	tumor-necrosis factor associated receptor-associated factor
T_{reg}	regulatory T cell
Tris	Tris(hydroxymethyl)-aminomethan
U	Unit
UTR	untranslated region
UV	ultraviolet radiation
V	volt
WB	Western Blot
WT	wildtype
ZAP70	zeta-chain-associated protein 70 kDa
β-TrCP	beta-transducin repeat containing protein
µg	microgram
µl	microliter

8 References

1. Parkin, J. and B. Cohen, *An overview of the immune system.* Lancet, 2001. **357**(9270): p. 1777-89.
2. Garred, P., et al., *Increased frequency of homozygosity of abnormal mannan-binding-protein alleles in patients with suspected immunodeficiency.* Lancet, 1995. **346**(8980): p. 941-3.
3. Medzhitov, R. and C. Janeway, Jr., *Innate immunity.* N Engl J Med, 2000. **343**(5): p. 338-44.
4. Muzio, M., et al., *Toll-like receptors: a growing family of immune receptors that are differentially expressed and regulated by different leukocytes.* J Leukoc Biol, 2000. **67**(4): p. 450-6.
5. Aplin, A.E., A.K. Howe, and R.L. Juliano, *Cell adhesion molecules, signal transduction and cell growth.* Curr Opin Cell Biol, 1999. **11**(6): p. 737-44.
6. Cyster, J.G., *Chemokines and cell migration in secondary lymphoid organs.* Science, 1999. **286**(5447): p. 2098-102.
7. K. Abbas, A., A. Lichtmabn, and S. Pillai, *Cellular Molecular Immunology.* 2007.
8. Janeway, C.A., Jr., *How the immune system protects the host from infection.* Microbes Infect, 2001. **3**(13): p. 1167-71.
9. Alberts, B.J., A.; Lewis, J., *T Cells and MHC Proteins*, in *Molecular Biology of the Cell*. 2002.
10. Medzhitov, R. and C.A. Janeway, Jr., *Innate immune recognition and control of adaptive immune responses.* Semin Immunol, 1998. **10**(5): p. 351-3.
11. Murphy, K., P. Travers, and M. Walport, *Janeway's Immuno Biology.* Vol. 7. 2008.
12. Benson, M.J., et al., *Cutting edge: the dependence of plasma cells and independence of memory B cells on BAFF and APRIL.* J Immunol, 2008. **180**(6): p. 3655-9.
13. MacLennan, I.C., *Germinal centers.* Annu Rev Immunol, 1994. **12**: p. 117-39.
14. MacLennan, I.C., et al., *Extrafollicular antibody responses.* Immunol Rev, 2003. **194**: p. 8-18.
15. Hardy, R.R., et al., *Murine B cell differentiation lineages.* J Exp Med, 1984. **159**(4): p. 1169-88.
16. Hayakawa, K., et al., *Progenitors for Ly-1 B cells are distinct from progenitors for other B cells.* J Exp Med, 1985. **161**(6): p. 1554-68.
17. Baumgarth, N., J.W. Tung, and L.A. Herzenberg, *Inherent specificities in natural antibodies: a key to immune defense against pathogen invasion.* Springer Semin Immunopathol, 2005. **26**(4): p. 347-62.
18. Martin, F. and J.F. Kearney, *B1 cells: similarities and differences with other B cell subsets.* Curr Opin Immunol, 2001. **13**(2): p. 195-201.
19. Montecino-Rodriguez, E. and K. Dorshkind, *B-1 B cell development in the fetus and adult.* Immunity, 2012. **36**(1): p. 13-21.
20. Germain, R.N., *T-cell development and the CD4-CD8 lineage decision.* Nat Rev Immunol, 2002. **2**(5): p. 309-22.
21. Chaplin, D.D., *Overview of the immune response.* J Allergy Clin Immunol, 2010. **125**(2 Suppl 2): p. S3-23.
22. Pitcher, L.A. and N.S. van Oers, *T-cell receptor signal transmission: who gives an ITAM?* Trends Immunol, 2003. **24**(10): p. 554-60.
23. Warrington, R., et al., *An introduction to immunology and immunopathology.* Allergy Asthma Clin Immunol, 2011. **7 Suppl 1**: p. S1.
24. Vyas, J.M., A.G. Van der Veen, and H.L. Ploegh, *The known unknowns of antigen processing and presentation.* Nat Rev Immunol, 2008. **8**(8): p. 607-18.
25. Chan, A.C., et al., *ZAP-70: a 70 kd protein-tyrosine kinase that associates with the TCR zeta chain.* Cell, 1992. **71**(4): p. 649-62.
26. Irving, B.A., A.C. Chan, and A. Weiss, *Functional characterization of a signal transducing motif present in the T cell antigen receptor zeta chain.* J Exp Med, 1993. **177**(4): p. 1093-103.
27. Bubeck Wardenburg, J., et al., *Phosphorylation of SLP-76 by the ZAP-70 protein-tyrosine kinase is required for T-cell receptor function.* J Biol Chem, 1996. **271**(33): p. 19641-4.

28. Zhang, W., et al., *LAT: the ZAP-70 tyrosine kinase substrate that links T cell receptor to cellular activation.* Cell, 1998. **92**(1): p. 83-92.

29. Wang, H., et al., *ZAP-70: an essential kinase in T-cell signaling.* Cold Spring Harb Perspect Biol, 2010. **2**(5): p. a002279.

30. Liu, S.K., et al., *The hematopoietic-specific adaptor protein gads functions in T-cell signaling via interactions with the SLP-76 and LAT adaptors.* Curr Biol, 1999. **9**(2): p. 67-75.

31. Zhong, X.P., et al., *Diacylglycerol kinases in immune cell function and self-tolerance.* Immunol Rev, 2008. **224**: p. 249-64.

32. Oh-hora, M. and A. Rao, *Calcium signaling in lymphocytes.* Curr Opin Immunol, 2008. **20**(3): p. 250-8.

33. Macian, F., *NFAT proteins: key regulators of T-cell development and function.* Nat Rev Immunol, 2005. **5**(6): p. 472-84.

34. Zha, Y., et al., *T cell anergy is reversed by active Ras and is regulated by diacylglycerol kinase-alpha.* Nat Immunol, 2006. **7**(11): p. 1166-73.

35. Olenchock, B.A., et al., *Disruption of diacylglycerol metabolism impairs the induction of T cell anergy.* Nat Immunol, 2006. **7**(11): p. 1174-81.

36. Schulze-Luehrmann, J. and S. Ghosh, *Antigen-receptor signaling to nuclear factor kappa B.* Immunity, 2006. **25**(5): p. 701-15.

37. Matsumoto, R., et al., *Phosphorylation of CARMA1 plays a critical role in T Cell receptor-mediated NF-kappaB activation.* Immunity, 2005. **23**(6): p. 575-85.

38. Sommer, K., et al., *Phosphorylation of the CARMA1 linker controls NF-kappaB activation.* Immunity, 2005. **23**(6): p. 561-74.

39. Sun, L., et al., *The TRAF6 ubiquitin ligase and TAK1 kinase mediate IKK activation by BCL10 and MALT1 in T lymphocytes.* Mol Cell, 2004. **14**(3): p. 289-301.

40. Oeckinghaus, A., et al., *Malt1 ubiquitination triggers NF-kappaB signaling upon T-cell activation.* Embo j, 2007. **26**(22): p. 4634-45.

41. Wu, C.J. and J.D. Ashwell, *NEMO recognition of ubiquitinated Bcl10 is required for T cell receptor-mediated NF-kappaB activation.* Proc Natl Acad Sci U S A, 2008. **105**(8): p. 3023-8.

42. Kang, S.M., et al., *NF-kappa B subunit regulation in nontransformed CD4+ T lymphocytes.* Science, 1992. **256**(5062): p. 1452-6.

43. Oeckinghaus, A. and S. Ghosh, *The NF-kappaB family of transcription factors and its regulation.* Cold Spring Harb Perspect Biol, 2009. **1**(4): p. a000034.

44. Vu, D., et al., *A structural basis for selective dimerization by NF-kappaB RelB.* J Mol Biol, 2013. **425**(11): p. 1934-1945.

45. Siggers, T., et al., *Principles of dimer-specific gene regulation revealed by a comprehensive characterization of NF-kappaB family DNA binding.* Nat Immunol, 2011. **13**(1): p. 95-102.

46. Smale, S.T., *Dimer-specific regulatory mechanisms within the NF-kappaB family of transcription factors.* Immunol Rev, 2012. **246**(1): p. 193-204.

47. Lin, X. and D. Wang, *The roles of CARMA1, Bcl10, and MALT1 in antigen receptor signaling.* Semin Immunol, 2004. **16**(6): p. 429-35.

48. Blonska, M. and X. Lin, *NF-kappaB signaling pathways regulated by CARMA family of scaffold proteins.* Cell Res, 2011. **21**(1): p. 55-70.

49. Bertin, J., et al., *CARD11 and CARD14 are novel caspase recruitment domain (CARD)/membrane-associated guanylate kinase (MAGUK) family members that interact with BCL10 and activate NF-kappa B.* J Biol Chem, 2001. **276**(15): p. 11877-82.

50. Gaide, O., et al., *Carma1, a CARD-containing binding partner of Bcl10, induces Bcl10 phosphorylation and NF-kappaB activation.* FEBS Lett, 2001. **496**(2-3): p. 121-7.

51. Funke, L., S. Dakoji, and D.S. Bredt, *Membrane-associated guanylate kinases regulate adhesion and plasticity at cell junctions.* Annu Rev Biochem, 2005. **74**: p. 219-45.

52. Kao, W.P., et al., *The versatile roles of CARDs in regulating apoptosis, inflammation, and NF-kappaB signaling.* Apoptosis, 2015. **20**(2): p. 174-95.

53.   Tanner, M.J., et al., *CARMA1 coiled-coil domain is involved in the oligomerization and subcellular localization of CARMA1 and is required for T cell receptor-induced NF-kappaB activation.* J Biol Chem, 2007. **282**(23): p. 17141-7.

54.   McCully, R.R. and J.L. Pomerantz, *The protein kinase C-responsive inhibitory domain of CARD11 functions in NF-kappaB activation to regulate the association of multiple signaling cofactors that differentially depend on Bcl10 and MALT1 for association.* Mol Cell Biol, 2008. **28**(18): p. 5668-86.

55.   Qiao, Q., et al., *Structural architecture of the CARMA1/Bcl10/MALT1 signalosome: nucleation-induced filamentous assembly.* Mol Cell, 2013. **51**(6): p. 766-79.

56.   Hara, H., et al., *The molecular adapter Carma1 controls entry of IkappaB kinase into the central immune synapse.* J Exp Med, 2004. **200**(9): p. 1167-77.

57.   Wang, D., et al., *CD3/CD28 costimulation-induced NF-kappaB activation is mediated by recruitment of protein kinase C-theta, Bcl10, and IkappaB kinase beta to the immunological synapse through CARMA1.* Mol Cell Biol, 2004. **24**(1): p. 164-71.

58.   Hara, H., et al., *Clustering of CARMA1 through SH3-GUK domain interactions is required for its activation of NF-kappaB signalling.* Nat Commun, 2015. **6**: p. 5555.

59.   Langel, F.D., et al., *Multiple protein domains mediate interaction between Bcl10 and MALT1.* J Biol Chem, 2008. **283**(47): p. 32419-31.

60.   Gehring, T., T. Seeholzer, and D. Krappmann, *BCL10 - Bridging CARDs to Immune Activation.* Front Immunol, 2018. **9**: p. 1539.

61.   Wegener, E., et al., *Essential role for IkappaB kinase beta in remodeling Carma1-Bcl10-Malt1 complexes upon T cell activation.* Mol Cell, 2006. **23**(1): p. 13-23.

62.   David, L., et al., *Assembly mechanism of the CARMA1-BCL10-MALT1-TRAF6 signalosome.* Proc Natl Acad Sci U S A, 2018.

63.   Schlauderer, F., et al., *Molecular architecture and regulation of BCL10-MALT1 filaments.* Nat Commun, 2018. **9**(1): p. 4041.

64.   Li, S., et al., *Structural insights into the assembly of CARMA1 and BCL10.* PLoS One, 2012. **7**(8): p. e42775.

65.   Lucas, P.C., et al., *Bcl10 and MALT1, independent targets of chromosomal translocation in malt lymphoma, cooperate in a novel NF-kappa B signaling pathway.* J Biol Chem, 2001. **276**(22): p. 19012-9.

66.   Meininger, I., et al., *Alternative splicing of MALT1 controls signalling and activation of CD4(+) T cells.* Nat Commun, 2016. **7**: p. 11292.

67.   Noels, H., et al., *A Novel TRAF6 binding site in MALT1 defines distinct mechanisms of NF-kappaB activation by API2middle dotMALT1 fusions.* J Biol Chem, 2007. **282**(14): p. 10180-9.

68.   Coornaert, B., et al., *T cell antigen receptor stimulation induces MALT1 paracaspase-mediated cleavage of the NF-kappaB inhibitor A20.* Nat Immunol, 2008. **9**(3): p. 263-71.

69.   Rebeaud, F., et al., *The proteolytic activity of the paracaspase MALT1 is key in T cell activation.* Nat Immunol, 2008. **9**(3): p. 272-81.

70.   Uren, A.G., et al., *Identification of paracaspases and metacaspases: two ancient families of caspase-like proteins, one of which plays a key role in MALT lymphoma.* Mol Cell, 2000. **6**(4): p. 961-7.

71.   Yu, J.W., et al., *Crystal structure of the mucosa-associated lymphoid tissue lymphoma translocation 1 (MALT1) paracaspase region.* Proc Natl Acad Sci U S A, 2011. **108**(52): p. 21004-9.

72.   Wiesmann, C., et al., *Structural determinants of MALT1 protease activity.* J Mol Biol, 2012. **419**(1-2): p. 4-21.

73.   Hulpiau, P., et al., *MALT1 is not alone after all: identification of novel paracaspases.* Cell Mol Life Sci, 2016. **73**(5): p. 1103-16.

74.   Hachmann, J., et al., *Mechanism and specificity of the human paracaspase MALT1.* Biochem J, 2012. **443**(1): p. 287-95.

75. Pelzer, C., et al., *The protease activity of the paracaspase MALT1 is controlled by monoubiquitination.* Nat Immunol, 2013. **14**(4): p. 337-45.

76. Cabalzar, K., et al., *Monoubiquitination and activity of the paracaspase MALT1 requires glutamate 549 in the dimerization interface.* PLoS One, 2013. **8**(8): p. e72051.

77. Lee, K.Y., et al., *PDK1 nucleates T cell receptor-induced signaling complex for NF-kappaB activation.* Science, 2005. **308**(5718): p. 114-8.

78. Park, S.G., et al., *The kinase PDK1 integrates T cell antigen receptor and CD28 coreceptor signaling to induce NF-kappaB and activate T cells.* Nat Immunol, 2009. **10**(2): p. 158-66.

79. Moreno-Garcia, M.E., et al., *Serine 649 phosphorylation within the protein kinase C-regulated domain down-regulates CARMA1 activity in lymphocytes.* J Immunol, 2009. **183**(11): p. 7362-70.

80. Eitelhuber, A.C., et al., *Dephosphorylation of Carma1 by PP2A negatively regulates T-cell activation.* Embo j, 2011. **30**(3): p. 594-605.

81. Shinohara, H., et al., *IkappaB kinase beta-induced phosphorylation of CARMA1 contributes to CARMA1 Bcl10 MALT1 complex formation in B cells.* J Exp Med, 2007. **204**(13): p. 3285-93.

82. Ishiguro, K., et al., *Ca2+/calmodulin-dependent protein kinase II is a modulator of CARMA1-mediated NF-kappaB activation.* Mol Cell Biol, 2006. **26**(14): p. 5497-508.

83. Brenner, D., et al., *Phosphorylation of CARMA1 by HPK1 is critical for NF-kappaB activation in T cells.* Proc Natl Acad Sci U S A, 2009. **106**(34): p. 14508-13.

84. Cheng, J., K.S. Hamilton, and L.P. Kane, *Phosphorylation of Carma1, but not Bcl10, by Akt regulates TCR/CD28-mediated NF-kappaB induction and cytokine production.* Mol Immunol, 2014. **59**(1): p. 110-6.

85. Bidere, N., et al., *Casein kinase 1alpha governs antigen-receptor-induced NF-kappaB activation and human lymphoma cell survival.* Nature, 2009. **458**(7234): p. 92-6.

86. Gaide, O., et al., *CARMA1 is a critical lipid raft-associated regulator of TCR-induced NF-kappa B activation.* Nat Immunol, 2002. **3**(9): p. 836-43.

87. Cannons, J.L., et al., *SAP regulates T(H)2 differentiation and PKC-theta-mediated activation of NF-kappaB1.* Immunity, 2004. **21**(5): p. 693-706.

88. Oruganti, S.R., et al., *CaMKII targets Bcl10 in T-cell receptor induced activation of NF-kappaB.* Mol Immunol, 2011. **48**(12-13): p. 1448-60.

89. Abd-Ellah, A., et al., *GSK3beta modulates NF-kappaB activation and RelB degradation through site-specific phosphorylation of BCL10.* Sci Rep, 2018. **8**(1): p. 1352.

90. Ishiguro, K., et al., *Bcl10 is phosphorylated on Ser138 by Ca2+/calmodulin-dependent protein kinase II.* Mol Immunol, 2007. **44**(8): p. 2095-100.

91. Lobry, C., et al., *Negative feedback loop in T cell activation through IkappaB kinase-induced phosphorylation and degradation of Bcl10.* Proc Natl Acad Sci U S A, 2007. **104**(3): p. 908-13.

92. Zeng, H., et al., *Phosphorylation of Bcl10 negatively regulates T-cell receptor-mediated NF-kappaB activation.* Mol Cell Biol, 2007. **27**(14): p. 5235-45.

93. Moreno-Garcia, M.E., et al., *Kinase-independent feedback of the TAK1/TAB1 complex on BCL10 turnover and NF-kappaB activation.* Mol Cell Biol, 2013. **33**(6): p. 1149-63.

94. Palkowitsch, L., et al., *The Ca2+-dependent phosphatase calcineurin controls the formation of the Carma1-Bcl10-Malt1 complex during T cell receptor-induced NF-kappaB activation.* J Biol Chem, 2011. **286**(9): p. 7522-34.

95. Frischbutter, S., et al., *Dephosphorylation of Bcl-10 by calcineurin is essential for canonical NF-kappaB activation in Th cells.* Eur J Immunol, 2011. **41**(8): p. 2349-57.

96. Yang, Y.K., et al., *Molecular Determinants of Scaffold-induced Linear Ubiquitinylation of B cell lymphoma/leukemia 10 (Bcl10) During T Cell receptor and Oncogenic Caspase Recruitment Domain-Containing Protein 11 (CARD11) Signaling.* J Biol Chem, 2016.

97. Paul, S. and B.C. Schaefer, *Selective autophagy regulates T cell activation.* Autophagy, 2012. **8**(11): p. 1690-2.

98. Scharschmidt, E., et al., *Degradation of Bcl10 induced by T-cell activation negatively regulates NF-kappa B signaling.* Mol Cell Biol, 2004. **24**(9): p. 3860-73.

99. Deng, L., et al., *Activation of the IkappaB kinase complex by TRAF6 requires a dimeric ubiquitin-conjugating enzyme complex and a unique polyubiquitin chain.* Cell, 2000. **103**(2): p. 351-61.

100. Shambharkar, P.B., et al., *Phosphorylation and ubiquitination of the IkappaB kinase complex by two distinct signaling pathways.* Embo j, 2007. **26**(7): p. 1794-805.

101. Hinz, M. and C. Scheidereit, *The IkappaB kinase complex in NF-kappaB regulation and beyond.* EMBO Rep, 2014. **15**(1): p. 46-61.

102. Israel, A., *The IKK complex, a central regulator of NF-kappaB activation.* Cold Spring Harb Perspect Biol, 2010. **2**(3): p. a000158.

103. Hayden, M.S. and S. Ghosh, *NF-kappaB, the first quarter-century: remarkable progress and outstanding questions.* Genes Dev, 2012. **26**(3): p. 203-34.

104. Blonska, M., et al., *The CARMA1-Bcl10 signaling complex selectively regulates JNK2 kinase in the T cell receptor-signaling pathway.* Immunity, 2007. **26**(1): p. 55-66.

105. Blonska, M. and X. Lin, *CARMA1-mediated NF-kappaB and JNK activation in lymphocytes.* Immunol Rev, 2009. **228**(1): p. 199-211.

106. Hara, H., et al., *The MAGUK family protein CARD11 is essential for lymphocyte activation.* Immunity, 2003. **18**(6): p. 763-75.

107. Gewies, A., et al., *Uncoupling Malt1 threshold function from paracaspase activity results in destructive autoimmune inflammation.* Cell Rep, 2014. **9**(4): p. 1292-305.

108. Jaworski, M., et al., *Malt1 protease inactivation efficiently dampens immune responses but causes spontaneous autoimmunity.* EMBO J, 2014. **33**(23): p. 2765-81.

109. Bornancin, F., et al., *Deficiency of MALT1 paracaspase activity results in unbalanced regulatory and effector T and B cell responses leading to multiorgan inflammation.* J Immunol, 2015. **194**(8): p. 3723-34.

110. Ruefli-Brasse, A.A., D.M. French, and V.M. Dixit, *Regulation of NF-kappaB-dependent lymphocyte activation and development by paracaspase.* Science, 2003. **302**(5650): p. 1581-4.

111. Ruland, J., et al., *Differential requirement for Malt1 in T and B cell antigen receptor signaling.* Immunity, 2003. **19**(5): p. 749-58.

112. Staal, J., et al., *T-cell receptor-induced JNK activation requires proteolytic inactivation of CYLD by MALT1.* Embo j, 2011. **30**(9): p. 1742-52.

113. Hailfinger, S., et al., *Malt1-dependent RelB cleavage promotes canonical NF-kappaB activation in lymphocytes and lymphoma cell lines.* Proc Natl Acad Sci U S A, 2011. **108**(35): p. 14596-601.

114. Uehata, T., et al., *Malt1-induced cleavage of regnase-1 in CD4(+) helper T cells regulates immune activation.* Cell, 2013. **153**(5): p. 1036-49.

115. Jeltsch, K.M., et al., *Cleavage of roquin and regnase-1 by the paracaspase MALT1 releases their cooperatively repressed targets to promote T(H)17 differentiation.* Nat Immunol, 2014. **15**(11): p. 1079-89.

116. Douanne, T., J. Gavard, and N. Bidere, *The paracaspase MALT1 cleaves the LUBAC subunit HOIL1 during antigen receptor signaling.* J Cell Sci, 2016. **129**(9): p. 1775-80.

117. Elton, L., et al., *MALT1 cleaves the E3 ubiquitin ligase HOIL-1 in activated T cells, generating a dominant negative inhibitor of LUBAC-induced NF-kappaB signaling.* FEBS J, 2016. **283**(3): p. 403-12.

118. Klein, T., et al., *The paracaspase MALT1 cleaves HOIL1 reducing linear ubiquitination by LUBAC to dampen lymphocyte NF-kappaB signalling.* Nat Commun, 2015. **6**: p. 8777.

119. Graves, P.R., et al., *Molecular cloning, expression, and characterization of a 49-kilodalton casein kinase I isoform from rat testis.* J Biol Chem, 1993. **268**(9): p. 6394-401.

120. Gross, S.D. and R.A. Anderson, *Casein kinase I: spatial organization and positioning of a multifunctional protein kinase family.* Cell Signal, 1998. **10**(10): p. 699-711.

121. Knippschild, U., et al., *The CK1 Family: Contribution to Cellular Stress Response and Its Role in Carcinogenesis.* Front Oncol, 2014. **4**: p. 96.

122. Xu, R.M., et al., *Crystal structure of casein kinase-1, a phosphate-directed protein kinase.* Embo j, 1995. **14**(5): p. 1015-23.

123. Longenecker, K.L., P.J. Roach, and T.D. Hurley, *Crystallographic studies of casein kinase I delta toward a structural understanding of auto-inhibition.* Acta Crystallogr D Biol Crystallogr, 1998. **54**(Pt 3): p. 473-5.

124. Budini, M., et al., *Autophosphorylation of carboxy-terminal residues inhibits the activity of protein kinase CK1alpha.* J Cell Biochem, 2009. **106**(3): p. 399-408.

125. Bustos, V.H., et al., *Generation of protein kinase Ck1alpha mutants which discriminate between canonical and non-canonical substrates.* Biochem J, 2005. **391**(Pt 2): p. 417-24.

126. Venerando, A., M. Ruzzene, and L.A. Pinna, *Casein kinase: the triple meaning of a misnomer.* Biochem J, 2014. **460**(2): p. 141-56.

127. Cruciat, C.M., *Casein kinase 1 and Wnt/beta-catenin signaling.* Curr Opin Cell Biol, 2014. **31**: p. 46-55.

128. Cheong, J.K. and D.M. Virshup, *Casein kinase 1: Complexity in the family.* Int J Biochem Cell Biol, 2011. **43**(4): p. 465-9.

129. Logan, C.Y. and R. Nusse, *The Wnt signaling pathway in development and disease.* Annu Rev Cell Dev Biol, 2004. **20**: p. 781-810.

130. Peters, J.M., et al., *Casein kinase I transduces Wnt signals.* Nature, 1999. **401**(6751): p. 345-50.

131. Krappmann, D. and M. Vincendeau, *Mechanisms of NF-kappaB deregulation in lymphoid malignancies.* Semin Cancer Biol, 2016. **39**: p. 3-14.

132. Staudt, L.M. and S. Dave, *The biology of human lymphoid malignancies revealed by gene expression profiling.* Adv Immunol, 2005. **87**: p. 163-208.

133. Davis, R.E., et al., *Chronic active B-cell-receptor signalling in diffuse large B-cell lymphoma.* Nature, 2010. **463**(7277): p. 88-92.

134. Lenz, G., et al., *Oncogenic CARD11 mutations in human diffuse large B cell lymphoma.* Science, 2008. **319**(5870): p. 1676-9.

135. Wilson, W.H., et al., *Targeting B cell receptor signaling with ibrutinib in diffuse large B cell lymphoma.* Nat Med, 2015. **21**(8): p. 922-6.

136. Ngo, V.N., et al., *A loss-of-function RNA interference screen for molecular targets in cancer.* Nature, 2006. **441**(7089): p. 106-10.

137. Ferch, U., et al., *Inhibition of MALT1 protease activity is selectively toxic for activated B cell-like diffuse large B cell lymphoma cells.* J Exp Med, 2009. **206**(11): p. 2313-20.

138. Nagel, D., et al., *Pharmacologic inhibition of MALT1 protease by phenothiazines as a therapeutic approach for the treatment of aggressive ABC-DLBCL.* Cancer Cell, 2012. **22**(6): p. 825-37.

139. Nagel, D., et al., *Combinatorial BTK and MALT1 inhibition augments killing of CD79 mutant diffuse large B cell lymphoma.* Oncotarget, 2015. **6**(39): p. 42232-42.

140. Jeelall, Y.S., et al., *Human lymphoma mutations reveal CARD11 as the switch between self-antigen-induced B cell death or proliferation and autoantibody production.* J Exp Med, 2012. **209**(11): p. 1907-17.

141. Calado, D.P., et al., *Constitutive canonical NF-kappaB activation cooperates with disruption of BLIMP1 in the pathogenesis of activated B cell-like diffuse large cell lymphoma.* Cancer Cell, 2010. **18**(6): p. 580-9.

142. Knies, N., et al., *Lymphomagenic CARD11/BCL10/MALT1 signaling drives malignant B-cell proliferation via cooperative NF-kappaB and JNK activation.* Proc Natl Acad Sci U S A, 2015. **112**(52): p. E7230-8.

143. Bognar, M.K., et al., *Oncogenic CARMA1 couples NF-kappaB and beta-catenin signaling in diffuse large B-cell lymphomas.* Oncogene, 2016. **35**(32): p. 4269-81.

144. Sakurai, H., et al., *Tumor necrosis factor-alpha-induced IKK phosphorylation of NF-kappaB p65 on serine 536 is mediated through the TRAF2, TRAF5, and TAK1 signaling pathway.* J Biol Chem, 2003. **278**(38): p. 36916-23.

145. Eitelhuber, A.C., et al., *Activity-based probes for detection of active MALT1 paracaspase in immune cells and lymphomas.* Chem Biol, 2015. **22**(1): p. 129-38.

146. Seeholzer, T., Kurz, S., Schlauderer, F., Woods, S., Gehring, T., Widmann, S., Lammens, K. and Krappmann, D., *BCL10-CARD11 fusion mimics an active CARD11 seed that triggers constitutive BCL10 oligomerization and lymphocyte activation.* submitted.

147. Duwel, M., et al., *A20 negatively regulates T cell receptor signaling to NF-kappaB by cleaving Malt1 ubiquitin chains.* J Immunol, 2009. **182**(12): p. 7718-28.

148. Bian, Y., et al., *An enzyme assisted RP-RPLC approach for in-depth analysis of human liver phosphoproteome.* J Proteomics, 2014. **96**: p. 253-62.

149. Mertins, P., et al., *Proteogenomics connects somatic mutations to signalling in breast cancer.* Nature, 2016. **534**(7605): p. 55-62.

150. Sharma, K., et al., *Ultradeep human phosphoproteome reveals a distinct regulatory nature of Tyr and Ser/Thr-based signaling.* Cell Rep, 2014. **8**(5): p. 1583-94.

151. Satpathy, S., et al., *Systems-wide analysis of BCR signalosomes and downstream phosphorylation and ubiquitylation.* Mol Syst Biol, 2015. **11**(6): p. 810.

152. Paul, S., et al., *Selective autophagy of the adaptor protein Bcl10 modulates T cell receptor activation of NF-kappaB.* Immunity, 2012. **36**(6): p. 947-58.

153. Hailfinger, S., et al., *Essential role of MALT1 protease activity in activated B cell-like diffuse large B-cell lymphoma.* Proc Natl Acad Sci U S A, 2009. **106**(47): p. 19946-51.

154. Hailfinger, S., F. Rebeaud, and M. Thome, *Adapter and enzymatic functions of proteases in T-cell activation.* Immunol Rev, 2009. **232**(1): p. 334-47.

155. Shinohara, H., et al., *Positive feedback within a kinase signaling complex functions as a switch mechanism for NF-kappaB activation.* Science, 2014. **344**(6185): p. 760-4.

156. Carvalho, G., et al., *Interplay between BCL10, MALT1 and IkappaBalpha during T-cell-receptor-mediated NFkappaB activation.* J Cell Sci, 2010. **123**(Pt 14): p. 2375-80.

157. Phelan, J.D., et al., *A multiprotein supercomplex controlling oncogenic signalling in lymphoma.* Nature, 2018. **560**(7718): p. 387-391.

158. Nagel, D., et al., *Mechanisms and consequences of constitutive NF-κB activation in B-cell lymphoid malignancies.* Oncogene, 2014. **33**: p. 5655.

159. Kloo, B., et al., *Critical role of PI3K signaling for NF-kappaB-dependent survival in a subset of activated B-cell-like diffuse large B-cell lymphoma cells.* Proc Natl Acad Sci U S A, 2011. **108**(1): p. 272-7.

160. Manicassamy, S., et al., *Protein kinase C-theta-mediated signals enhance CD4+ T cell survival by up-regulating Bcl-xL.* J Immunol, 2006. **176**(11): p. 6709-16.

161. Cesaro, L. and L.A. Pinna, *The generation of phosphoserine stretches in phosphoproteins: mechanism and significance.* Mol Biosyst, 2015. **11**(10): p. 2666-79.

162. Szymczak, A.L., et al., *Correction of multi-gene deficiency in vivo using a single 'self-cleaving' 2A peptide-based retroviral vector.* Nature biotechnology, 2004. **22**(5): p. 589-94.

163. Pfaffl, M.W., *A new mathematical model for relative quantification in real-time RT-PCR.* Nucleic Acids Res, 2001. **29**(9): p. e45.

164. Wisniewski, J.R., et al., *Universal sample preparation method for proteome analysis.* Nat Methods, 2009. **6**(5): p. 359-62.

165. Grosche, A., et al., *The Proteome of Native Adult Muller Glial Cells From Murine Retina.* Mol Cell Proteomics, 2016. **15**(2): p. 462-80.

9 Appendix

9.1 Publications

<u>Research articles:</u>

Gehring, T., Erdmann, T., Rahm, M., Graß, C., Flatley, A., O'Neill, T.J., Woods, S., Meininger, I., Karayel, O., Kutzner, K., Grau, M., Shinohara, H., Lammens, K., Feederle, R., Hauck, S.M., Lenz, G. and Krappmann, D. MALT1 phosphorylation controls activation of T lymphocytes and survival of ABC DLBCL tumor cells., Cell Rep., in revision

Seeholzer, T., Kurz, S., Schlauderer, F., Woods, S., **Gehring, T.**, Widmann, S., Lammens, K. and Krappmann, D. (2018). BCL10-CARD11 fusion mimics an active CARD11 seed that triggers constitutive BCL10 oligomerization and lymphocytes activation. Front Immunol. 9, 2695

Schlauderer, F., Seeholzer, T., Desfosses, A., **Gehring, T.**, Strauss, M., Hopfner, K.P., Gutsche, I., Krappmann, D. and Lammens, K. (2018). Molecular architecture and regulation of BCL10-MALT1 filaments. Nat Commun. 9, 4041.

Schimmack, G., Schorpp, K., Kutzner, K., **Gehring, T.**, Brenke, J.K., Hadian, K. and Krappmann, D. (2017). YOD1/TRAF6 association balances p62-dependent IL-1 signaling to NF-kB. Elife. 6. pii: e22416

Meininger, I., Griesbach, R.A., Hu, D., **Gehring, T.**, Seeholzer, T., Bertossi, A., Kranich, J., Oeckinghaus, A., Eitelhuber, A.C., Greczmiel, U., Gewies, A., Schmidt-Supprian, M., Ruland, J., Brocker, T., Heissmeyer, V., Heyd, F., and Krappmann, D. (2016). Alternative splicing of MALT1 controls signalling and activation of CD4(+) T cells. Nat Commun. 7, 11292.

<u>Review:</u>

Gehring, T., Seeholzer, T. and Krappmann, D. (2018). BCL10 – Bridging CARDs to Immune Activation. Front Immunol. 9:1539

9.2 Curriculum Vitae

Persönliche Daten

Geburtsdatum:	07.10.1987
Geburtsort:	Krefeld
Familienstand:	ledig
Nationalität:	Deutsch

Ausbildung

Seit 04/2014	**Promotion am Helmholtz Zentrum München, Institut für Molekulare Toxikologie und Pharmakologie, Abteilung Zelluläre Signalintegration** Titel der Arbeit: "MALT1 phosphorylation controls activation of T lymphocytes" Leitung: Prof. Dr. Daniel Krappmann
10/2011 – 04/2014	**Masterstudium Biochemie, Technische Universität München** Studienschwerpunkte: Immunologie, molekulare Onkologie, Klinische Chemie und molekulare Pathologie
06/2013 – 12/2013	Master's Thesis: Institut für klinische Chemie und Pathobiochemie, Prof. Dr. J. Ruland, TU München Titel der Arbeit: "Role of RANK mutations in B cell function and disease" (Note 1,3) Abschluss: Master of Science (Note 1,6)
10/2008 – 09/2011	**Bachelorstudium Biochemie, Technische Universität München** Studieninhalte: Grundlagen der Biochemie, Zellbiologie, Immunologie, organischen und anorganischen Chemie
06/2011 – 07/2011	Bachelor's Thesis: Lehrstuhl für Biotechnologie, Prof. Dr. J. Buchner, TU München Titel der Arbeit: "Analysis of HSP90 mutants regarding of their ATPase activity and the influence of the N-terminal" (Note 1,3) Abschluss: Bachelor of Science (Note 2,5)
07/2007 – 03/2008	**Malteser Hilfsdienst Oldenburg** Zivildienst; Ausbildung zum Rettungshelfer
08/2000 – 07/2007	**Altes Gymnasium Oldenburg** Leistungskurse: Biologie, Chemie Abschluss: Allgemeine Hochschulreife (Note 2,4)

9.3 Acknowledgments

There are many people I would like to thank for helping and supporting me within the last four and a half years.

First, I am deeply grateful to my supervisor and doctor father Daniel Krappmann for my project, his constant support and advice, and the excellent working conditions that he provided.

I also want to thank the members of the thesis committee for the time and effort they offered in reviewing my thesis: Prof. Dr. Michael Boshart, Prof. Dr. Dirk Eick, Prof. Dr. Wolfgang Frank, Prof. Dr. Angelika Böttger and Prof. Dr. Bettina Kempkes.

Special thanks go to the members of my HELENA thesis committee, PD Dr. Ursula Zimber-Strobl and PD Dr. Reinhard Obst.

I am very thankful to the present and former members of the Krappmann lab and other groups in the Institute for Molecular Toxicology and Pharmacology for their precious help, scientific and non-scientific input and their companionship: Arianna Bertossi, Miriam Bognar, Stefanie Brandner, Jara Brenke, Katrin Demski, Scarlett Dornauer, Andrea Eitelhuber, Andreas Gewies, Martin Göttlicher, Carina Graß, Kamyar Hadian, Johanna Kössl, Vera Kühne, Kerstin Kutzner, Zhoulei Li, Moritz Ludwig, Isabel Meininger, Thomas J. O'Neill, Susanne Pfeiffer, Larissa Ringelstetter, Anna Schaub, Joel Schick, Gisela Schimmack, Kenji Schorpp, Thomas Seeholzer, Michelle Vincendeau, Aurelia Weber, Elisabeth Weber, Simone Woods, Hongli Yin and Hans Zischka. Special thanks to Simone Woods for proofreading my thesis.

Finally, I am also deeply grateful to my family and friends without their support, love and encouragement this thesis would not have been possible. I want to especially thank Geli, who always supported and motivated me as well as patiently endured my moods and extra hours.

Eidesstattliche Erklärung

Ich versichere hiermit an Eides statt, dass die vorgelegte Dissertation von mir selbständig und ohne unerlaubte Hilfe angefertigt ist.

München, den ....*05.07.2019*........   *Torben Gehring*
....

<div align="center">(Unterschrift)</div>

Erklärung

Hiermit erkläre ich, *

☐   dass die Dissertation nicht ganz oder in wesentlichen Teilen einer anderen Prüfungskommission vorgelegt worden ist.

☐   dass ich mich anderweitig einer Doktorprüfung ohne Erfolg **nicht** unterzogen habe.

☐   ~~dass ich mich mit Erfolg der Doktorprüfung im Hauptfach~~ ....

      ~~und in den Nebenfächern~~ ....

      ~~bei der Fakultät für~~ .... ~~der~~ ....

<div align="right">~~(Hochschule/Universität)~~</div>

      ~~unterzogen habe.~~

☐   ~~dass ich ohne Erfolg versucht habe, eine Dissertation einzureichen oder mich der Doktorprüfung zu unterziehen.~~

München, den........*05.07.2019*........   *Torben Gehring*
....

<div align="center">(Unterschrift)</div>

*) Nichtzutreffendes streichen